How do climate, ozone and crops interact to impact on health and nutrition?

Ioannis Droutsas

Submitted in accordance with the requirements for the degree of
Doctor of Philosophy

The University of Leeds
School of Earth and Environment

May 2020

The candidate confirms that the work submitted is his own, except where work which has formed part of jointly authored publications has been included. The contribution of the candidate and the other authors to this work has been explicitly indicated below. The candidate confirms that appropriate credit has been given within the thesis where reference has been made to the work of others.

The work in Chapter 2 of the thesis has appeared in publication as follows: Droutsas, I., Challinor, A.J., Swiderski, M. and Semenov, M.A., 2019. *New modelling technique for improving crop model performance - application to the GLAM model.* Environmental Modelling and Software, 118, pp.187-200. The candidate developed the SEMAC approach and the GLAM-Parti crop model, designed and performed the analysis, produced the figures and wrote the manuscript with comments from all co-authors. The candidate performed all GLAM and GLAM-Parti simulations and M.A. Semenov provided with the experimental dataset.

The work in Chapter 3 of the thesis has been accepted for publication as follows: Droutsas, I., Challinor, A.J., Arnold, S.R., Mikkelsen, T.N., Hansen E.M.Ø., 2020. *A new model of ozone stress in wheat including grain yield loss and plant acclimation to the pollutant*, European Journal of Agronomy. The candidate developed the GLAM-ROC crop model, designed and performed the analysis, produced the figures and wrote the manuscript with comments from all co-authors. The candidate performed all GLAM-ROC simulations with T.N. Mikkelsen, and E.M.Ø. Hansen providing with the experimental dataset.

The work in Chapter 4 of the thesis is a manuscript prepared to be submitted for publication as follows: Droutsas, I., Challinor, A.J., Arnold, S.R., Turnock, S.T., Deva, C., 2020. *Use of a crop model to estimate the effect of ozone pollution on wheat in India.* The candidate designed and performed the analysis, produced the figures and wrote the manuscript with comments from all co-authors. The candidate performed all GLAM-ROC simulations. S.T. Turnock provided with the ozone mixing ratios from the simulations of the UKESM1 model. C. Deva provided with the district-level wheat yield data for India.

Acknowledgements

First and foremost I would like to thank God for giving the blessing of this study to me the sinner. Without Him, nothing would have been possible. I'm also grateful to my supervisors Andy Challinor, Steve Arnold and Caroline Orfila for giving me the opportunity to undertake this PhD and for their excellent guidance and support through the years. I'm very happy to be part of the Climate Impacts group of the University of Leeds - led by the incredible Professor and man Andy Challinor - and having shared so many beautiful experiences with my nice colleagues. You are all unique and we form a nice group all together. I would also like to thank Richard Rigby for his significant technical support and his beautiful personality which teaches us valuable life lessons without even speaking. I'm also thankful to Andreas Chrysanthou and Andreas Andreou for sharing this PhD journey with me from the beginning and the rest of the Greek group for having lunches and fun together. I thank my parents and my brother for standing always next to me. It is a blessing to have such a beautiful family. Finally, I'm extremely grateful to my wife Sinead for sharing her love and being united with me. She contributed to every part of this study through her presence in my life, in happy as well as in difficult times.

Abstract

Ozone pollution is negatively affecting human nutrition and health due to its adverse effects on crops. The effect of ozone on crop performance can be significant and has causal links to climate. The climatic conditions interact with ozone and modify the impact of the pollutant on crop productivity. Atmospheric composition models simulate surface ozone concentrations and can be used by crop models to assess the crop ozone damage. However, crop models exhibit limited skill in simulations of crop growth and yield under stress conditions, thus improvement in model performance is previously required to enhance the model skill.

In this thesis, a new dynamic crop modelling technique is introduced, SEMAC (Simultaneous Equation Modelling for Annual Crops), which uses simultaneous solution of the model equations to improve the model structure, ensure internal model consistency and reduce the parameterization requirements. SEMAC was implemented into an existing crop model, GLAM (General Large Area Model for annual crops), resulting in a new model version, GLAM-Parti. GLAM and GLAM-Parti were compared against observed data with wheat exposed to different levels of water stress and GLAM-Parti exhibited higher skill in all drought experiments. The RMSE of GLAM-Parti was reduced by at least 44, 66 and 41% for LAI, biomass and grain yield respectively in comparison with GLAM in the early, late and full drought treatments.

GLAM-Parti was further extended to incorporate the effect of ozone pollution on wheat performance. The derived model, GLAM-ROC (GLAM-Relative Ozone Concentrations) was successfully evaluated against experiments with wheat exposed to elevated ozone concentrations in variable duration of exposure to the pollutant. GLAM-ROC was then applied to determine the effect of ozone pollution on historical wheat productivity in India. Large damage to crop yield was found, ranging from 9.8% in Punjab to 18.9% in Bihar. Reduction in the levels of ozone pollution of 25, 50 and 75% decrease wheat yield loss by 27.2, 70 and 92% respectively. Thus, ground-level ozone pollution poses a considerable threat to food production in India and reduction in the levels of the pollutant can act as an effective mechanism for increasing wheat productivity.

In conclusion, SEMAC demonstrated high skill in simulating ozone and drought and shows promise for the addition of more stresses in the future, such as heat and nitrogen.

Contents

List of Figures

List of Tables

Chapter 1

Introduction

1.1 Background

Food is an essential element of all heterotrophs on Earth, since it provides the energy and nutrients needed for survival and growth. Humans are not an exception and our existence is intimately acquainted to the consumption of food. Thus, providing adequate food supply has always been a major concern of human societies across the world. The cultivation of land started around 12,000 years ago (*Larson et al.*, 2014) and continually evolves in the present day.

On the last two centuries, the rapid expansion of biological and mechanical technology have completely transformed the agricultural processes (*Binswanger*, 1986). Farming has become more efficient and productive over time, primarily in industrialized and some developing countries, where the yields of staple crops have dramatically increased (*Reilly and Fuglie*, 1998; *Jain*, 2012). Agriculture is also significantly less labour-intensive and today less than 1% of the UK population is occupied in the agricultural sector (*Devlin and Foundation*, 2016).

Despite the improvement in the quality of life, technological progress has come with considerable environmental trade-offs. Serious environmental challenges are climate change and air pollution, stemming mainly from anthropogenic activities which emit greenhouse gasses (GHGs) and air pollutants into the atmosphere (*Solomon et al.*, 2007). The main sources of GHG emissions are the combustion of fossil fuels for energy production, the industrial activities, transportation, deforestation and agriculture (Fig. 1.1).

As a result of GHG emissions, the global surface temperature has increased by around 1 °C in comparison with the pre-industrial level (*Stocker et al.*, 2013). This rise in temperature is projected to continue on the next decades with a rate depending upon the change of anthropogenic emissions of GHGs, air pollutants as well as land use changes. By the end of the 21st century, the global mean surface temperature is likely to have raised by up to 4.8 °C in comparison with the current level (i.e. under RCP8.5

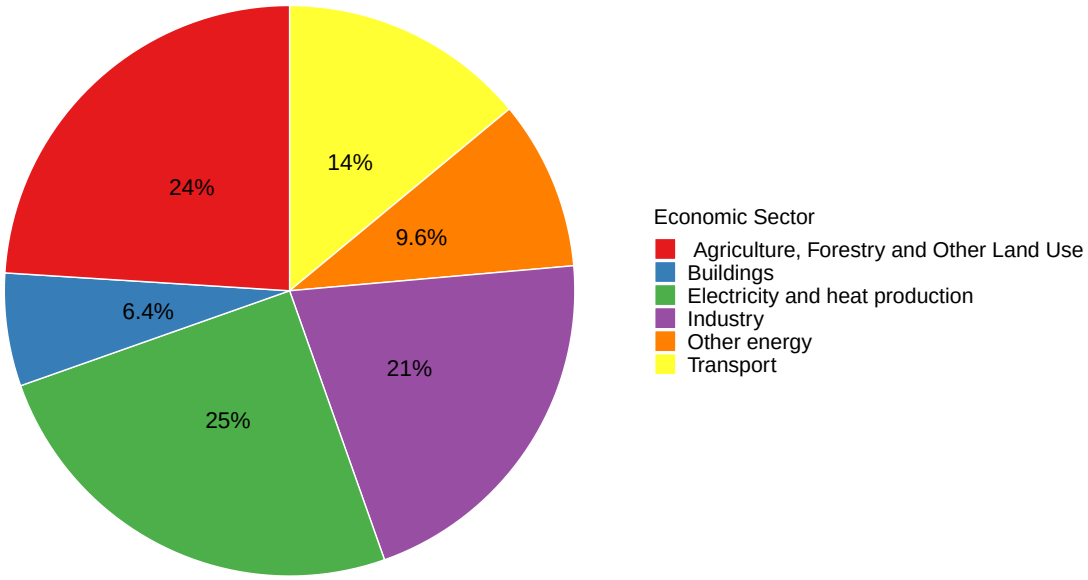

Figure 1.1: Global anthropogenic GHG emissions listed by economic sectors (Extracted from *IPCC* (2014)).

scenario and using 1980 - 2005 period as baseline) (*Pachauri et al.*, 2014). In addition, the severity and frequency of heat waves are projected to increase (*Meehl and Tebaldi*, 2004; *Coumou and Robinson*, 2013) and changes in precipitation patterns may lead to more frequent drought and flood events (*Sillmann et al.*, 2013).

Crop simulation models can be used to estimate the risks on food production from climate change and air pollution in the present and future years. These models are agricultural tools describing the plant performance and yield in any given environment at local, regional or even global scale (*Chenu et al.*, 2017). Their role is significant for food security applications, especially in regions affected by both climate change and air pollution. One such country is India where the increase in temperature as well as the rise in concentrations of air pollutants have deteriorated the environmental conditions for crop growth and development (*Burney and Ramanathan*, 2014). At the same time, the increasing population in the country brings higher demand for food (*Ritchie et al.*, 2018). Thus, ensuring adequate food supply is a major concern for the Indian agricultural sector in the present and future years (*Agoramoorthy*, 2008).

1.2 Crop productivity under climate change

Increasing average temperatures can have significant impact on crop productivity and yield. Crops growing below their optimal temperature can benefit from increased tem-

peratures (e.g., *Tian et al.*, 2012), whilst crops exceeding their optimal conditions will be negatively affected (*Lobell et al.*, 2011). Overall, for maize, wheat and rice, average yield losses of 4.9% per °C are projected under climate change, with wheat and maize being mainly affected in tropical and rice in temperate regions (*Challinor et al.*, 2014). In addition, extreme temperatures can cause significant yield declines. Heat stress around flowering can reduce plant fertility and reproduction with subsequent decreases in harvest index and grain yield (*Wollenweber et al.*, 2003; *Challinor et al.*, 2005; *Fábián et al.*, 2019). For example, in the Southwestern US, the large number of extreme temperature days ($>$ 35 °C) projected by mid-century is estimated to reduce maize and cotton yields by 27 and 37% respectively (*Elias et al.*, 2018).

Drought is another significant environmental stress lowering crop productivity. Under limiting water conditions, plants close their stomata (Fig. 1.2) to avoid leaf water loss through transpiration, thus decreasing their CO_2 uptake and photosynthesis level (*Chaves*, 1991). Depending on the severity of the water stress event, metabolic impairment may also lower photosynthetic CO_2 assimilation (i.e. non-stomatal limitation) (*Flexas and Medrano*, 2002). As a result, crop growth and productivity decreases with negative effect on the partitioning of biomass to grain yield (*Boutraa and Sanders*, 2001).

During the past four decades, drought events are estimated to have caused 1820 Mt losses globally in the production of maize, wheat and rice (*Lesk et al.*, 2016). In addition, water stress interacts with high temperature and exacerbates the effects of heat stress on crop yield. This is especially true in rainfed agricultural systems when reduction in rainfall occurs during sensitive crop growth stages (*Roudier et al.*, 2011).

1.3 Ozone

Air pollutants interact with humans, animals and plants and when found in sufficient concentrations, they can cause significant damage and decrease the lifetime of living organisms (*Loomis et al.*, 2013). Air pollution is a mixture of solid particles, liquid droplets and gases derived either from natural or anthropogenic sources. Solid particles and liquid droplets (aerosol) can be divided into two categories, those with a diameter greater or smaller than 10 µm (*Hocking*, 1993). The former group consists of heavier particles which tend to deposit onto surfaces quickly due to the gravitational force, whilst the particles in the latter group stay in the air for longer (such as fine particulate matter ($PM_{2.5}$)). The third category of air pollutants are gases found either in gaseous or vapour state (*Hocking*, 1993).

Human activities dominate the emission of air pollutants into the atmosphere with the major sources being the combustion of fuels for energy production, the industrial activities, transportation, agriculture and biomass burning (*Unger et al.*, 2010). Major air pollutants are particulate matter (PM), NO_x, Ozone (O_3), sulphur oxides (SO_x),

black carbon (BC) and carbon monoxide (CO).

O_3 is the most important air pollutant for damage to crop yield at global scale (*Mauzerall and Wang*, 2001). Staple crops such as wheat, maize, soybean and rice are all sensitive to ozone stress (*Mills et al.*, 2007). In the future, O_3 pollution is estimated to either dominate or exacerbate the effects of climate change on the above-mentioned crops, depending on the region and the scenario considered (i.e. the highest ozone damage to crop yield is projected under the RCP8.5 scenario) (*Tai et al.*, 2014).

1.3.1 Ozone in the atmosphere

O_3 is a gas made up by three atoms of oxygen and is present both in the troposphere and the stratosphere (i.e. up to 50 kilometres above Earth's surface). Stratospheric O_3 consists of about 90% of the total atmospheric O_3, whilst the rest 10% is present in the troposphere (*Lelieveld and Dentener*, 2000). Stratospheric O_3 is beneficial to life as it protects our planet from the biologically harmful ultraviolet radiation (*Krupa and Manning*, 1988). On the contrary, tropospheric O_3 is harmful to living organisms and has been recognised as a significant air quality issue due to its adverse effects on both humans (*Conibear et al.*, 2018) and the vegetation (*Yunus and Iqbal*, 1996).

O_3 in the troposphere is not directly emitted into the air, but produced through photochemical oxidation of precursor gasses such as carbon monoxide (CO), methane (CH_4) and volatile organic compounds (VOC) in the presence of NO_x (*Arnold et al.*, 2018). O_3 can also be transferred into the troposphere through the stratosphere-troposphere exchange, however this source is small relative to its chemical production in-situ in the troposphere (*Monks et al.*, 2015).

Surface O_3 concentrations exhibit an increasing trend in major air pollution - emitting countries such as China and India (*Oksanen et al.*, 2013; *Silver et al.*, 2018; *Fleming et al.*, 2018) and are projected to remain enhanced in many regions of the world in the future (*Sicard et al.*, 2017). In addition, O_3 and its precursors can travel long distances and lead to enhanced background concentrations in various parts of the world. For instance, increasing air pollution emissions in China during the years 2005 - 2010 have counterbalanced more than 40% of the decrease in O_3 pollution in the western US (*Verstraeten et al.*, 2015). Thus, the high O_3 phytotoxicity (*Krupa et al.*, 2001) as well as the enhanced concentrations of the pollutant pose a major threat to food production at global scale.

1.3.2 Ozone effects on crops

O_3 enters the plants through the stomata, which are pores on the plant epidermis used for gas exchange (Fig. 1.2). Since most of the stomata are present in the leaves (*Kirkham*, 2014), this is the primary route of O_3 into the plants.

Inside the leaves, O_3 can react with volatile compounds (e.g. isoprene) in the inter-

cellular air space, or move further to react with water in the apoplast and form reactive oxygen species (ROS) (*Fiscus et al.*, 2005). Enhanced ROS levels cause oxidative plant stress and lead to cell destruction (*Mittler*, 2002). Plants use various enzymic and non-enzymic antioxidants as defensive mechanisms to scavenge ROS (*Dusart et al.*, 2019). ROS that remain unscavenged lead to cell death through oxidative processes such as the peroxidation of lipids, oxidation of proteins, inhibition of enzymes, damage to DNA and RNA (*Mittler*, 2002; *Sharma et al.*, 2012).

Acute exposure to high O_3 concentration (above 150 ppbv) can lead to visible symptoms, such as leaf chlorosis or necrosis (*Fiscus et al.*, 2005; *Fumagalli et al.*, 2001). Nevertheless, plants may exhibit considerable O_3 damage without visible effects. Chronic exposure to moderate O_3 concentration accelerates the decline of Rubisco activity and quantity and decreases photosynthesis (*Pell et al.*, 1992). Stomatal conductance is also reduced with subsequent effect on leaf transpiration (*Temple*, 1986; *Lombardozzi et al.*, 2013). In addition, the rate of leaf senescence accelerates (*Pell et al.*, 1997) and the root:shoot carbon allocation ratio declines (*Andersen*, 2003). O_3 can also inhibit the activity of phloem loading which lowers the ability of the plant to transport sugars from the leaves to the grains (*Grantz*, 2003).

Overall, exposure to O_3 decreases crop growth as well as the allocation of carbon to the grain, leading to lower productivity and loss in grain yield. The magnitude of the effects of O_3 on plants depends upon the concentration level of the pollutant, the time and duration of exposure (*Heath et al.*, 2009), the plant sensitivity (*Van Goethem et al.*, 2013) and the stage of plant development (*Tiedemann and Pfähler*, 1994; *Mulholland et al.*, 1998).

Water stress can also interact with O_3 and cause stomatal closure which decreases the uptake of the pollutant by the leaves (*Khan and Soja*, 2003). Moreover, future increases in atmospheric CO_2 can protect against O_3 pollution, since elevated CO_2 causes stomatal closure and similarly decreases the uptake of O_3 by the leaves (*Fiscus et al.*, 1997; *Hudak et al.*, 1999). Thus, the interaction between O_3, CO_2 and drought on crop growth and productivity is significant and should be taken into account for estimations of future food production under climate change and air pollution.

1.3.3 Experimental studies of ozone and wheat

Various experimental studies have demonstrated the deleterious effect of O_3 on wheat growth, development and productivity. *McKee and Long* (2001) exposed spring wheat plants to peak O_3 concentration of 60 ppb from plant emergence to maturity and reported decreased Rubisco content and activity, leading to lower photosynthesis and biomass accumulation. Nevertheless, the most significant factor for damage to grain yield was the alteration in crop development, where chronic exposure to O_3 accelerated the rate of plant senescence (i.e. the time from flag leaf emergence to panicle emergence was reduced by 8%) and reduced the allocation of carbon to the grains (i.e. the grain

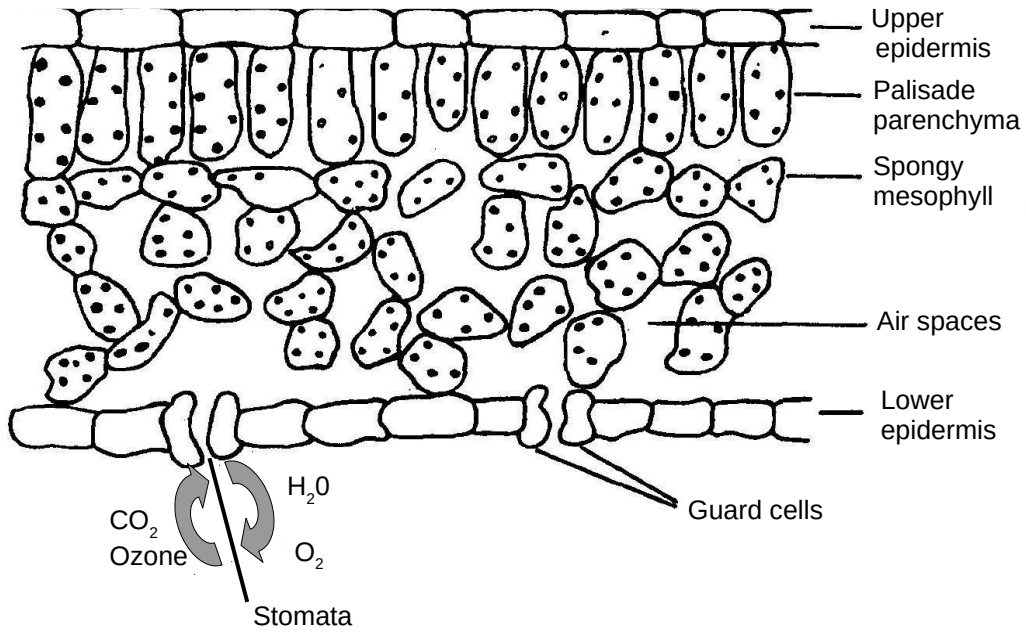

Figure 1.2: Cross-section of a leaf of a dicotyledonous plant with CO_2 and O_3 uptake and O_2 and water loss through stomata (Adopted from *Krupa and Manning* (1988)).

mass was decreased by 17%). *Osborne et al.* (2019) reached to the same finding after analyzing experiments with two European wheat cultivars exposed to chronic O_3 stress. The study showed that the major driver of the O_3-induced reduction to grain yield was the acceleration of leaf senescence as well as an earlier onset of senescence. The photosynthetic leaf response to O_3 was less significant and dependent on the leaf age.

The meta-analysis of *Feng et al.* (2008) considered various experiments with wheat plants fumigated with different O_3 levels for at least 10 days. The study found that the aboveground biomass decreases by an average of 18% at 72 ppb of O_3 in comparison with carbon-filtered treatments. Grain yield is more affected than biomass and is reduced by 29%, whilst harvest index decreases by 9% on average at the same O_3 level. This is consistent with the above findings regarding that the O_3 damage to wheat yield is greater than the effect of the pollutant on crop biomass due to the larger effect of O_3 on plant developmental than growth processes.

Wheat exposure to chronic O_3 stress alters the nutritional properties of the grains, however this area is less explored. The meta-analysis of *Broberg et al.* (2015) considered 19 wheat cultivars exposed to elevated O_3 for at least 14 days. The study showed that enhanced O_3 levels increase the concentration of grain protein and important minerals, such as P, K, Mg, Ca, Zn and Mn, but decrease their yield. This means that under

O_3 exposure, wheat produces grains with higher concentration of the above elements, but reduced total amount per cultivated area. In addition, the baking properties of the grains were positively affected by O_3 (e.g. Zeleny value, Hagberg falling number) and the concentration as well as the yield of the potentially toxic element Cd was reduced. These findings show that the effect of O_3 on the quality of the grains in wheat is significant with both positive and negative influence.

1.4 Wheat in India

Before 1960, India was suffering from low wheat yields and was reliant on food imports to meet the population demand. In the mid-1960s, the development of high-yielding crop varieties introduced a new era in agriculture, the Green Revolution. The newly developed varieties were semi-dwarf plants with thicker stems, which were highly more efficient in partitioning biomass to the grains, in favour of their straw and leaf parts (*Evenson and Gollin*, 2003). In India, the adoption of these varieties in agriculture together with the improvement in management practices, the increased use of fertilizers and pesticides as well as the agricultural mechanization significantly boosted the production of cereals (*Larson et al.*, 2004). As a result, today, the annual wheat production is almost nine times higher than in 1961 and the grain yield has more than tripled (Fig. 1.3). Thus, India has become the second largest producer of wheat globally (*Singh et al.*, 2007) and is self-sufficient despite the increase in human population.

1.4.1 Effect of ozone pollution on wheat in India

India is a country with some of the highest air pollution levels in the world. Several of its cities hold global records of air pollution and together with China, they are attributable to more than 50% of the deaths globally due to ambient air pollution (for year 2015) (*Landrigan et al.*, 2018). One of the regions with severe air quality issues, the Indo-Gangetic plain is a densely populated zone, where human activities lead to high emissions of air pollutants (*Ghude et al.*, 2008). At the same time, this region is the breadbasket of India, contributing with a large proportion of the total wheat production in the country. The states of Utter Pradesh, Punjab, Haryana, and Bihar provide with 34.97, 13.09, 7.88, and 7.56% respectively of the total wheat grain production (i.e. for years 1966 - 2011) (*ICRISAT*, 2015). Together with Madhya Pradesh and Rajastan, these six states contribute with around 88% of the total wheat production in India (Fig. 1.4).

During the months from February to June, high temperatures and increased solar radiation favour the photochemical production of O_3 (*Deb Roy et al.*, 2009). This period also coincides with the later stages of wheat development, which are the most O_3-sensitive for damage to grain yield. Unsurprisingly, studies have demonstrated the deleterious effect of O_3 on wheat productivity in India. *Mills et al.* (2018) estimated

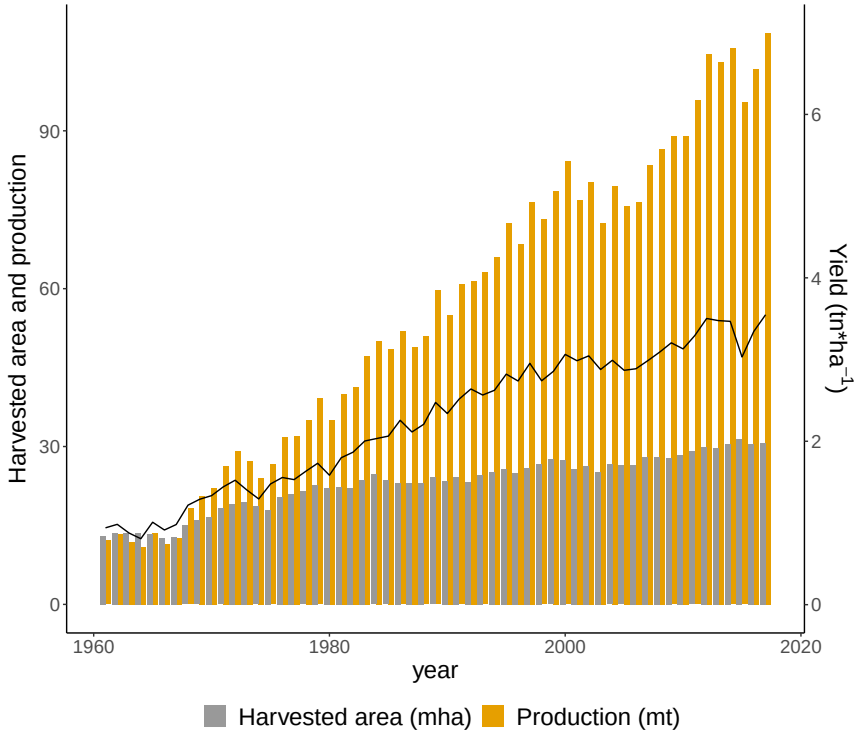

Figure 1.3: Harvested area (yellow bars; in million hectares) and annual production (grey bars; in million tonnes) of wheat as well as grain yield (black line) for years 1961 - 2017 (data downloaded from: http://www.fao.org/faostat/).

that the O_3-induced damage to wheat yield in large areas of North India has exceeded 15% on average for the years 2010 - 2012. *Ghude et al.* (2014) estimated that present-day O_3 levels lower total wheat production by about 3.5 Mt. Given that India is one of the largest producers of wheat globally and the second most populated country in the world, the effect of O_3 pollution on wheat yield is a crucial issue of food security in the country.

1.5 Crop models

The agricultural cropping systems are complex and interactive environments (*Bouman et al.*, 1996). Crop models attempt to simulate these systems in a simplified way by using a set of mathematical equations (*Marcelis et al.*, 1998). The models of explanatory, dynamic nature describe plant processes in short time intervals (e.g. one day) such as the accumulation of biomass, the growth of leaf area and the soil water and nutrient content (*de Vries*, 1980). These models rely on the principle that the state of a system can be quantified at any time using suitable mathematical equations (*De Wit*, 1982). The first models of this kind were introduced around 50 years ago and their main purpose was to explain the physiological mechanisms driving the crop performance both in terms of growth and development (*Bouman et al.*, 1996).

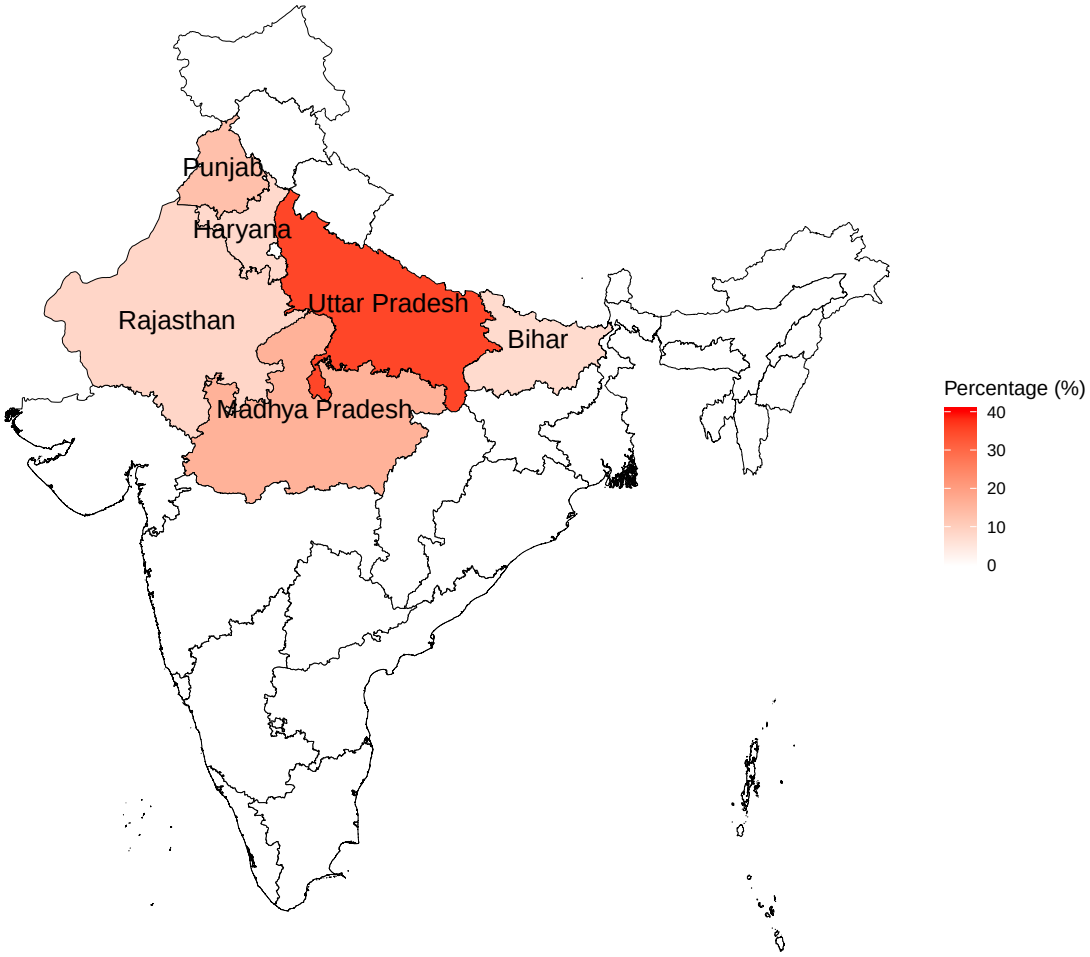

Figure 1.4: The six highest wheat-producing states in India and their percentage contribution to annual wheat production in the country (Data extracted from *ICRISAT* (2015)).

Today, various crop models have been developed according to the plant species of interest as well as the temporal and spatial resolution. Most of them were initially designed for operation with single crops at field scale (*Ewert et al.*, 2015). Recently, the advancement in the understanding of plant physiology supported the evolution of models capable of wider application. As a result, the state-of-the-art crop models do not only target the improvement of scientific knowledge but also the involvement in decision-making for policy shaping (*Jones et al.*, 2017). One category of such tools are the combined crop-climate models which use seasonal weather information to forecast crop productivity at regional or even global scale (*Challinor et al.*, 2009). These large-area models rely upon the principle that there is a significant relationship between weather and crop yield (*Challinor et al.*, 2003). Their advantage is the ability to project future food production, to inform the risks of climate change and suggest opportunities for adaptation in the agricultural sector (*Challinor et al.*, 2013).

1.5.1 Crop model structure

Crop models are designed upon different levels of complexity, according to the scope and the scientific questions that they seek to address (*Challinor et al.*, 2018). Usually, the models designed for large-area applications tend to be simpler with less site-specific information and reduced parameterization requirements. On the contrary, field-based crop models require more detailed information and include a larger set of parameters. The expectation is that complex modelling approaches can lead to improved performance by including more processes and interactions of the real world. However, it is often impossible to describe with mathematical equations all factors affecting the crop performance, due to the complexity of the biological processes involved (*Affholder et al.*, 2012). Thus, in some cases, an increase in model complexity may lead to unwarranted complexity and to a system that is not well understood (*Challinor et al.*, 2018). *Passioura* (1996) showed that in such systems, the total error stemming from the model structure and the parameters cannot be decreased below a certain level (Fig. 1.5). In contrast, in well understood systems, there is an appropriate level of complexity which minimizes the total model error.

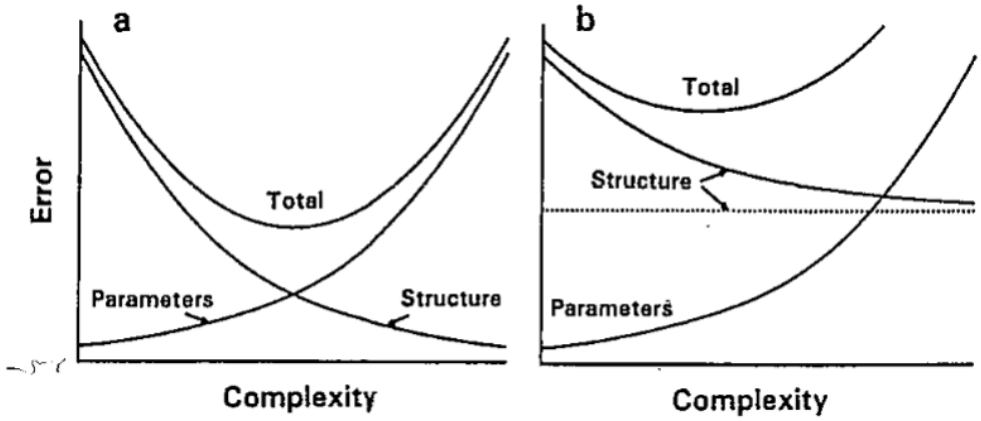

Figure 1.5: Structural, parameter and total model error against complexity in a system where a) the structure is well-understood, b) the structure is wrong (taken from *Passioura* (1996)).

Based on the above, the simple and complex crop models may both be affected by problematic model structures which limit their performance. Simple crop models may oversimplify the simulated processes and not provide sufficient detail in the representation of real-world conditions. On the contrary, complex crop models may introduce large numbers of parameters and equations and increase the risk of over-parameterization, leading to internal model inconsistencies (*Tremblay and Wallach*, 2004). In both cases, a sub-optimal model structure decreases the model skill and limits the benefit of further model development. Thus, all models should target for a robust model structure which represents the modelled processes in sufficient detail, includes the correct number of parameters and processes and leads to an optimal level of complexity, minimizing the

model error (*Passioura*, 1996; *Challinor et al.*, 2018).

1.5.2 GLAM crop model

The General Large Area Model for annual crops (GLAM) is a process-based crop model which simulates the impact of climate on crop growth, development and yield (*Challinor et al.*, 2004). It is a relatively simple model which runs in daily time step and is designed to operate at large spatial scales. The model requires incoming solar radiation, minimum and maximum temperature and rainfall as input weather information. The output consists of growth variables such as biomass and yield as well as other variables such as the crop water consumption and the soil water content. GLAM was originally developed for groundnut (i.e. peanut: Arachis hypogaea L.) (*Challinor et al.*, 2004), whilst other crops were later introduced including wheat (*Sanai et al.*, 2010), maize (*Bergamaschi et al.*, 2013), sorghum (*Nicklin*, 2013), soybean (*Osborne et al.*, 2013) and potato (*Jennings*, 2018).

Regarding the model structure, GLAM uses a maximum daily growth rate of leaf area index which can be decreased by water stress. The daily potential evapotranspiration is calculated by the Priestley-Taylor equation and is partitioned into potential evaporation and potential transpiration. The actual transpiration is calculated from the potential transpiration rate by taking into account the soil water content. The transpiration is multiplied by the transpiration efficiency to return the daily biomass growth. The grain yield is estimated by partitioning the above-ground biomass to the grains using the harvest index.

GLAM has been extensively used for large-scale applications. *Challinor et al.* (2007) used the model to examine the importance of temperature on the productivity of the groundnut crop in India. The study showed that increases in mean temperature have significant effect on groundnut yield in the current climate, whilst extreme temperature days become an important driver of yield under climate change projections. The authors demonstrated that the adaptation of suitable genotypes provides an effective mechanism to limit the negative impact of increasing temperature on groundnut yield in the future.

Challinor et al. (2010) used GLAM to show that climate change threatens the production of spring wheat in Northeast China. The study found that the increases in water and heat stress suggested by future climate projections enhance the rates of crop failure in the region. The authors recommended that possible adaptation options for increasing the resilience of the cropping system are the use of suitable crop varieties, the development of crop insurance programs designed for climate variability, the necessity of research focused on plant breeding and the importance of informing the farmers regarding forthcoming extreme weather events.

1.5.3 Crop model limitations

The role of crop models is significant in decision-making due to their ability to connect the climate information to agricultural impacts at large spatial scale. *Rosenzweig et al.* (2014) used seven global gridded crop models to show that maize and wheat are in risk of significant yield losses in low-latitude areas by the end of the century according to the RCP8.5 climate scenario. *Cammarano et al.* (2019) used the CERES-Barley model of DSSAT v4.7 (Decision Support System for Agrotechnology Transfer) to estimate an average 9% loss in barley yield in the Mediterranean region by 2050 (under the RCP4.5 climate scenario). *Traore et al.* (2017) applied the APSIM (Agricultural Production Systems sIMulator) model in southern Mali to assess potential food security issues due to climate change. The study showed that projected increases in temperature under both the RCP4.5 and RCP8.5 climate scenario can decrease the crop productivity of maize and millet significantly. As a consequence, all farm types in the region are expected to experience lower food availability with small-scale farms being in high risk of not reaching self-sufficiency by mid-century.

The above studies consist of significant steps toward disseminating the risks of climate change on agricultural production and assist in preparation of adaptation. However, the use of the above information requires a crop model with high skill to allow confidence in the projections. Thus, studies have been implemented to evaluate the performance of crop models under environmental stress conditions as expected by climate change. *Asseng et al.* (2013) tested 27 crop models in the response of wheat to climate change and concluded that no single model could adequately simulate the expected reality. Especially when the input information was limited, the model error was increased. The authors also demonstrated that a crop model ensemble was needed to increase the confidence in the output. In a following study, *Asseng et al.* (2015) examined the performance of 30 crop models in the simulation of wheat under various temperature environments. The study showed that when the average growing-season temperature increased above 22 °C, the simulation of grain yield consistently deviated from the observations. Detailed information on physiological aspects of the cultivars improved the performance of some models, however this level of information is almost never achieved in large-scale applications. Again, the multi-model ensemble performed better than any individual crop model.

Based on the above information there is an definite need for improvement in the performance of crop models in simulations of plant response to environmental stress conditions. One of the ways to do this is by reforming the model structure. *Tao et al.* (2018) used 7 crop models to compare the uncertainty in the output stemming from the model structure, the model parameters and the climate projections. The barley crop was used as case study and the model simulations consisted of two sites with contrasting climates, Jokioinen (Finland) and Lleida (Spain). The study showed

that the largest source of uncertainty in the crop model ensemble output was due to the model structure. Especially when one set of calibrated parameters was used, the contribution of the crop model structure to the total variance was at least 60% in each site (Fig. 1.6). The authors concluded that the model structure exhibits a vital role on the performance and output. Thus, the Chapter 2 of this thesis focuses on improving the crop model structure as a means of increasing the model skill in the simulations.

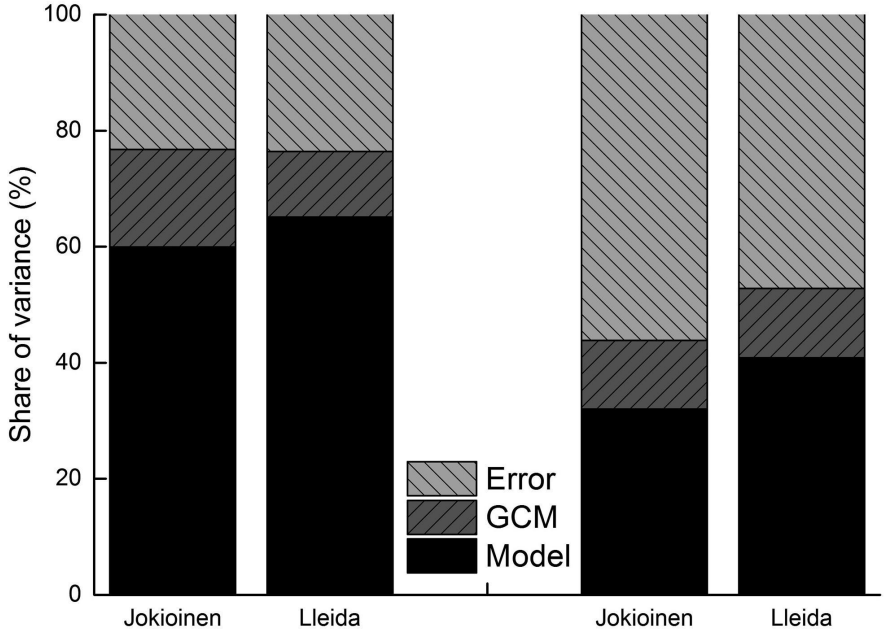

Figure 1.6: Share of variance by crop model structure and climate projections in the simulated barley yield changes. Left barplots are with single set of calibrated parameters and right barplots are with 3^n sets of parameters for Jokioinen and Lleida respectively. The error variance is that which is neither due to crop model structure nor climate projections; hence, in the right two columns (with 3^n sets of parameters), the error variance includes the share of crop model parameters (taken from *Tao et al.* (2018)).

1.6 Simulation of plant ozone damage in crop models

Current O_3 pollution levels decrease the yields of staple crops at global scale (e.g., *Van Dingenen et al.*, 2009; *Avnery et al.*, 2011; *Hollaway et al.*, 2012), however most crop models have thus far overlooked the effect of this stressor in their simulations. Thus, limited parametrization schemes exist which explicitly account for the impact of O_3 on crop growth and development.

Ewert and Porter (2000) introduced an O_3 damage subroutine to the AFRCWHEAT2 crop model. The derived model (AFRCWHEAT2-O3) simulates both the short-term effects of O_3 (i.e. reduced leaf photosynthesis) as well as the chronic O_3 damage (i.e. acceleration of leaf senescence). The algorithm initially calculates the daily O_3 uptake

rate by using information on stomatal conductance and the O_3 concentration at the surface of the leaf. The O_3 uptake is then used to compute the reduction of photosynthesis, which starts above an empirical threshold to account for the plant detoxification capacity. The O_3 damage to photosynthesis can be further reduced due to the repair ability of the leaf, which is estimated according to the leaf age. Regarding the long-term effects, the O_3-induced acceleration of leaf senescence decreases photosynthesis and is simulated as function of the accumulated O_3 uptake during the crop growing season. The evaluation of the model revealed relative success and the authors emphasized the need of more research designed on the response of leaf area dynamics to O_3.

Guarin et al. (2019) introduced equations of O_3 damage into the DSSAT-NWheat model to simulate the effect of the pollutant on wheat photosynthesis and leaf senescence. In their modelling study, the effect of O_3 pollution on crop growth was not simulated via a leaf uptake mechanism (i.e. through stomatal conductance). Instead, the damage to plant growth and the acceleration of leaf senescence were set as linear functions of the O_3 concentration at the leaf level. Both equations were empirical and had variable slope and intercept values to account for different sensitivities between the cultivars (i.e. sensitive, intermediate, tolerant). The model was evaluated against limited observed data and the authors indicated the need of testing the model against a larger range of plant exposures to O_3 as well as in combination with other stresses.

Plants can enhance their defence in response to an abiotic stress in a process called acclimation (*Bruce et al.*, 2007). A limitation of the above modelling studies is the lack of incorporating a plant acclimation mechanism under chronic exposure to O_3 pollution. *Gillespie et al.* (2011) showed that soybean plants grown under chronic O_3 exposure exhibited significantly higher antioxidant capacity in comparison with the same plants grown under elevated CO_2. The authors reported that the primed antioxidant system of the O_3-treated plants was less affected by an acute O_3 pollution event later in the season than the plants grown in high CO_2 environment. Similarly, *Held et al.* (1991) exposed radish plants to high O_3 concentration either six days after germination or three days later and found that the plants which were exposed to the pollutant for the longer time period exhibited higher dry mass than the plants exposed to O_3 later, implying an acclimation mechanism.

In Chapter 3 of the present thesis a new parametrization of O_3 stress is introduced. The focus of the new approach is to develop a model capable of simulating the O_3 damage to crop growth and productivity at different durations of exposure to the pollutant (i.e. from episodic to chronic exposure). In order to do this, the plant acclimation mechanism should be incorporated to account for reduced crop sensitivity to O_3 stress over time. To my knowledge, this is the first time that the mechanism of plant acclimation to O_3 is considered in a crop model.

1.7 Research aims and objectives

This thesis aims to provide an existing crop model, GLAM, with the ability to simulate the interactive effects of climate and air pollution on wheat growth, development and productivity. Initially, a new modelling framework is developed to improve upon the previous approach in the simulation of crop performance under abiotic stress conditions. The effect of O_3 stress is then incorporated into the new modelling methodology and the derived model is applied to estimate the effect of O_3 pollution on wheat productivity in India.

The aims of the study will be achieved through the objectives listed below:

1. In Chapter 2, the Simultaneous Equation Modelling for Annual Crops (SEMAC) is introduced, a new crop modelling methodology which relies on a simultaneous solution of the model equations. SEMAC is implemented into GLAM and a new model version is formed called GLAM-Parti (i.e. GLAM-Partitioning). The new model is designed to improve the simulations of crop response to environmental variability and extreme weather conditions, without increasing the model complexity or the parameterization requirements. In addition to the improvement in skill, SEMAC also equips GLAM-Parti with the ability to integrate multiple stresses in the model simulations. This is a significant step toward incorporating the effect of O_3 pollution on crop productivity into the model on the next chapter.

2. In Chapter 3, GLAM-Parti is extended to simulate the effect of O_3 stress on wheat performance and yield. A new parameterization of O_3 damage is introduced into the model, resulting in a model version called GLAM-ROC (i.e. GLAM-Relative Ozone Concentrations). Unlike previous crop modelling approaches, the simulation of O_3 pollution includes a parameterization of plant acclimation to chronic O_3 stress. This is necessary for capturing the O_3 damage to wheat biomass and yield when O_3 fumigation increases from episodic to chronic exposure. The error introduced by the omission of the acclimation process into the model is also estimated.

3. Chapter 4 examines the impact of O_3 pollution on historical wheat yield in India. GLAM-ROC is used for the simulations which cover a long time period (years 1980-2009). The model is also used to estimate the reduction in yield loss due to 25, 50 and 75% decrease in ground-level O_3 pollution.

4. Chapter 5 summarises the enhancement in model performance due to the addition of the SEMAC methodology into GLAM. It discusses the overall usefulness of GLAM-Parti and GLAM-ROC, the current model limitations and provides

recommendations for further model development which will allow the model application to a larger domain.

References

Affholder, F., P. Tittonell, M. Corbeels, S. Roux, N. Motisi, P. Tixier, and J. Wery (2012), Ad hoc modeling in agronomy: what have we learned in the last 15 years?, *Agronomy Journal*, *104*(3), 735–748. 1.5.1

Agoramoorthy, G. (2008), Can india meet the increasing food demand by 2020?, *Futures*, *40*(5), 503–506. 1.1

Andersen, C. P. (2003), Source–sink balance and carbon allocation below ground in plants exposed to ozone, *New Phytologist*, *157*(2), 213–228. 1.3.2

Arnold, S., D. Lombardozzi, J.-F. Lamarque, T. Richardson, L. Emmons, S. Tilmes, S. Sitch, G. Folberth, M. Hollaway, and M. Val Martin (2018), Simulated global climate response to tropospheric ozone-induced changes in plant transpiration, *Geophysical Research Letters*, *45*(23), 13–070. 1.3.1

Asseng, S., F. Ewert, C. Rosenzweig, J. W. Jones, J. L. Hatfield, A. C. Ruane, K. J. Boote, P. J. Thorburn, R. P. Rötter, D. Cammarano, et al. (2013), Uncertainty in simulating wheat yields under climate change, *Nature climate change*, *3*(9), 827–832. 1.5.3

Asseng, S., F. Ewert, P. Martre, R. P. Rötter, D. B. Lobell, D. Cammarano, B. Kimball, M. J. Ottman, G. Wall, J. W. White, et al. (2015), Rising temperatures reduce global wheat production, *Nature climate change*, *5*(2), 143. 1.5.3

Avnery, S., D. L. Mauzerall, J. Liu, and L. W. Horowitz (2011), Global crop yield reductions due to surface ozone exposure: 1. year 2000 crop production losses and economic damage, *Atmospheric Environment*, *45*(13), 2284–2296. 1.6

Bergamaschi, H., S. M. S. d. Costa, T. R. Wheeler, and A. J. Challinor (2013), Simulating maize yield in sub-tropical conditions of southern brazil using glam model, *Pesquisa Agropecuária Brasileira*, *48*(2), 132–140. 1.5.2

Binswanger, H. (1986), Agricultural mechanization: a comparative historical perspective, *The World Bank Research Observer*, *1*(1), 27–56. 1.1

Bouman, B., H. Van Keulen, H. Van Laar, and R. Rabbinge (1996), The school of de witcrop growth simulation models: a pedigree and historical overview, *Agricultural systems*, *52*(2-3), 171–198. 1.5

Boutraa, T., and F. Sanders (2001), Influence of water stress on grain yield and vegetative growth of two cultivars of bean (phaseolus vulgaris l.), *Journal of Agronomy and Crop Science*, *187*(4), 251–257. 1.2

Broberg, M. C., Z. Feng, Y. Xin, and H. Pleijel (2015), Ozone effects on wheat grain quality–a summary, *Environmental Pollution*, *197*, 203–213. 1.3.3

Bruce, T. J., M. C. Matthes, J. A. Napier, and J. A. Pickett (2007), Stressful memories of plants: evidence and possible mechanisms, *Plant Science*, *173*(6), 603–608. 1.6

Burney, J., and V. Ramanathan (2014), Recent climate and air pollution impacts on indian agriculture, *Proceedings of the National Academy of Sciences*, *111*(46), 16,319–16,324. 1.1

Cammarano, D., S. Ceccarelli, S. Grando, I. Romagosa, A. Benbelkacem, T. Akar, A. Al-Yassin, N. Pecchioni, E. Francia, and D. Ronga (2019), The impact of climate change on barley yield in the mediterranean basin, *European Journal of Agronomy*, *106*, 1–11. 1.5.3

Challinor, A., J. Slingo, T. Wheeler, P. Craufurd, and D. Grimes (2003), Toward a combined seasonal weather and crop productivity forecasting system: determination of the working spatial scale, *Journal of Applied Meteorology*, *42*(2), 175–192. 1.5

Challinor, A., T. Wheeler, P. Craufurd, J. Slingo, and D. Grimes (2004), Design and optimisation of a large-area process-based model for annual crops, *Agricultural and forest meteorology*, *124*(1-2), 99–120. 1.5.2

Challinor, A., T. Wheeler, P. Craufurd, and J. Slingo (2005), Simulation of the impact of high temperature stress on annual crop yields, *Agricultural and Forest Meteorology*, *135*(1-4), 180–189. 1.2

Challinor, A., T. Wheeler, P. Craufurd, C. Ferro, and D. Stephenson (2007), Adaptation of crops to climate change through genotypic responses to mean and extreme temperatures, *Agriculture, ecosystems & environment*, *119*(1-2), 190–204. 1.5.2

Challinor, A. J., F. Ewert, S. Arnold, E. Simelton, and E. Fraser (2009), Crops and climate change: progress, trends, and challenges in simulating impacts and informing adaptation, *Journal of experimental botany*, *60*(10), 2775–2789. 1.5

Challinor, A. J., E. S. Simelton, E. D. Fraser, D. Hemming, and M. Collins (2010), Increased crop failure due to climate change: assessing adaptation options using

models and socio-economic data for wheat in china, *Environmental Research Letters*, *5*(3), 034,012. 1.5.2

Challinor, A. J., M. S. Smith, and P. Thornton (2013), Use of agro-climate ensembles for quantifying uncertainty and informing adaptation, *Agricultural and Forest Meteorology*, *170*, 2–7. 1.5

Challinor, A. J., J. Watson, D. B. Lobell, S. Howden, D. Smith, and N. Chhetri (2014), A meta-analysis of crop yield under climate change and adaptation, *Nature Climate Change*, *4*(4), 287. 1.2

Challinor, A. J., C. Müller, S. Asseng, C. Deva, K. J. Nicklin, D. Wallach, E. Vanuytrecht, S. Whitfield, J. Ramirez-Villegas, and A.-K. Koehler (2018), Improving the use of crop models for risk assessment and climate change adaptation, *Agricultural systems*, *159*, 296–306. 1.5.1, 1.5.1

Chaves, M. (1991), Effects of water deficits on carbon assimilation, *Journal of experimental Botany*, *42*(1), 1–16. 1.2

Chenu, K., J. R. Porter, P. Martre, B. Basso, S. C. Chapman, F. Ewert, M. Bindi, and S. Asseng (2017), Contribution of crop models to adaptation in wheat, *Trends in plant science*, *22*(6), 472–490. 1.1

Conibear, L., E. W. Butt, C. Knote, D. V. Spracklen, and S. R. Arnold (2018), Current and future disease burden from ambient ozone exposure in india, *GeoHealth*, *2*(11), 334–355. 1.3.1

Coumou, D., and A. Robinson (2013), Historic and future increase in the global land area affected by monthly heat extremes, *Environmental Research Letters*, *8*(3), 034,018. 1.1

de Vries, F. P. (1980), Simulation models of growth of crops, particularly under nutrient stress, in *Physiological aspects of crop productivity, Proc. 15th Coll. Int. Potash Inst., Wageningen*, pp. 213–226. 1.5

De Wit, C. (1982), Simulation of living systems, in *Simulation of plant growth and crop production*, pp. 3–8, Pudoc. 1.5

Deb Roy, S., G. Beig, and S. D. Ghude (2009), Exposure-plant response of ambient ozone over the tropical indian region, *Atmospheric Chemistry and Physics*, *9*(14), 5253–5260. 1.4.1

Devlin, S., and N. E. Foundation (2016), Agricultural labour in the uk, *London: Food Research Collaboration*. 1.1

Dusart, N., A. Gandin, M.-N. Vaultier, R. Joffe, M. Cabané, P. Dizengremel, and Y. Jolivet (2019), Importance of detoxification processes in ozone risk assessment: need to integrate the cellular compartmentation of antioxidants?, *Frontiers in Forests and Global Change*, *2*, 45. 1.3.2

Elias, E., A. Marklein, J. T. Abatzoglou, J. Dialesandro, J. Brown, C. Steele, A. Rango, and K. Steenwerth (2018), Vulnerability of field crops to midcentury temperature changes and yield effects in the southwestern usa, *Climatic Change*, *148*(3), 403–417. 1.2

Evenson, R. E., and D. Gollin (2003), Assessing the impact of the green revolution, 1960 to 2000, *science*, *300*(5620), 758–762. 1.4

Ewert, F., and J. R. Porter (2000), Ozone effects on wheat in relation to co2: modelling short-term and long-term responses of leaf photosynthesis and leaf duration, *Global Change Biology*, *6*(7), 735–750. 1.6

Ewert, F., R. P. Rötter, M. Bindi, H. Webber, M. Trnka, K. C. Kersebaum, J. E. Olesen, M. K. van Ittersum, S. Janssen, M. Rivington, et al. (2015), Crop modelling for integrated assessment of risk to food production from climate change, *Environmental Modelling & Software*, *72*, 287–303. 1.5

Fábián, A., E. Sáfrán, G. Szabó-Eitel, B. Barnabás, and K. Jäger (2019), Stigma functionality and fertility are reduced by heat and drought co-stress in wheat, *Frontiers in plant science*, *10*, 244. 1.2

Feng, Z., K. Kobayashi, and E. A. Ainsworth (2008), Impact of elevated ozone concentration on growth, physiology, and yield of wheat (triticum aestivum l.): a meta-analysis, *Global Change Biology*, *14*(11), 2696–2708. 1.3.3

Fiscus, E., C. Reid, J. Miller, and A. Heagle (1997), Elevated co2 reduces o3 flux and o3-induced yield losses in soybeans: possible implications for elevated co2 studies, *Journal of Experimental Botany*, *48*(2), 307–313. 1.3.2

Fiscus, E. L., F. L. Booker, and K. O. Burkey (2005), Crop responses to ozone: uptake, modes of action, carbon assimilation and partitioning, *Plant, Cell & Environment*, *28*(8), 997–1011. 1.3.2

Fleming, Z. L., R. M. Doherty, E. Von Schneidemesser, C. Malley, O. R. Cooper, J. P. Pinto, A. Colette, X. Xu, D. Simpson, M. G. Schultz, et al. (2018), Tropospheric ozone assessment report: Present-day ozone distribution and trends relevant to human health, *Elementa: Science of the Anthropocene*. 1.3.1

Flexas, J., and H. Medrano (2002), Drought-inhibition of photosynthesis in c3 plants: stomatal and non-stomatal limitations revisited, *Annals of botany*, *89*(2), 183–189. 1.2

Fumagalli, I., B. S. Gimeno, D. Velissariou, L. De Temmerman, and G. Mills (2001), Evidence of ozone-induced adverse effects on crops in the mediterranean region, *Atmospheric Environment*, *35*(14), 2583–2587. 1.3.2

Ghude, S. D., S. Fadnavis, G. Beig, S. Polade, and R. Van Der A (2008), Detection of surface emission hot spots, trends, and seasonal cycle from satellite-retrieved no2 over india, *Journal of Geophysical Research: Atmospheres*, *113*(D20). 1.4.1

Ghude, S. D., C. Jena, D. Chate, G. Beig, G. Pfister, R. Kumar, and V. Ramanathan (2014), Reductions in india's crop yield due to ozone, *Geophysical Research Letters*, *41*(15), 5685–5691. 1.4.1

Gillespie, K. M., A. Rogers, and E. A. Ainsworth (2011), Growth at elevated ozone or elevated carbon dioxide concentration alters antioxidant capacity and response to acute oxidative stress in soybean (glycine max), *Journal of Experimental Botany*, *62*(8), 2667–2678. 1.6

Grantz, D. (2003), Ozone impacts on cotton: towards an integrated mechanism, *Environmental Pollution*, *126*(3), 331–344. 1.3.2

Guarin, J. R., B. Kassie, A. M. Mashaheet, K. Burkey, and S. Asseng (2019), Modeling the effects of tropospheric ozone on wheat growth and yield, *European Journal of Agronomy*, *105*, 13–23. 1.6

Heath, R. L., A. S. Lefohn, and R. C. Musselman (2009), Temporal processes that contribute to nonlinearity in vegetation responses to ozone exposure and dose, *Atmospheric Environment*, *43*(18), 2919–2928. 1.3.2

Held, A., H. Mooney, and J. N. Gorham (1991), Acclimation to ozone stress in radish: leaf demography and photosynthesis, *New phytologist*, *118*(3), 417–423. 1.6

Hocking, M. B. (1993), *Handbook of chemical technology and pollution control*, Academic Press, San Diego. 1.3

Hollaway, M. J., S. Arnold, A. J. Challinor, and L. Emberson (2012), Intercontinental trans-boundary contributions to ozone-induced crop yield losses in the northern hemisphere, *Biogeosciences*, *9*(1), 271–292. 1.6

Hudak, C., J. Bender, H.-J. Weigel, and J. Miller (1999), Interactive effects of elevated co2, o3, and soil water deficit on spring wheat (triticum aestivum l. cv. nandu). 1.3.2

ICRISAT (2015), Meso level data for India: 1966-2011, collected and compiled under the project on Village Dynamics in South Asia. (document), 1.4.1, 1.4

IPCC, . (2014), Mitigation of climate change, *Contribution of Working Group III to the Fifth Assessment Report of the Intergovernmental Panel on Climate Change*, *1454*. (document), 1.1

Jain, H. (2012), Transition to twenty-first century agriculture: change of direction, *Agricultural Research*, *1*(1), 12–17. 1.1

Jennings, S. A. (2018), The impacts of climate change on global potato agriculture, Ph.D. thesis, University of Leeds. 1.5.2

Jones, J. W., J. M. Antle, B. Basso, K. J. Boote, R. T. Conant, I. Foster, H. C. J. Godfray, M. Herrero, R. E. Howitt, S. Janssen, et al. (2017), Brief history of agricultural systems modeling, *Agricultural systems*, *155*, 240–254. 1.5

Khan, S., and G. Soja (2003), Yield responses of wheat to ozone exposure as modified by drought-induced differences in ozone uptake, *Water, Air, and Soil Pollution*, *147*(1-4), 299–315. 1.3.2

Kirkham, M. B. (2014), *Principles of soil and plant water relations*, Academic Press. 1.3.2

Krupa, S., M. T. McGrath, C. P. Andersen, F. L. Booker, K. O. Burkey, A. H. Chappelka, B. I. Chevone, E. J. Pell, and B. A. Zilinskas (2001), Ambient ozone and plant health, *Plant Disease*, *85*(1), 4–12. 1.3.1

Krupa, S. V., and W. J. Manning (1988), Atmospheric ozone: formation and effects on vegetation, *Environmental Pollution*, *50*(1-2), 101–137. (document), 1.3.1, 1.2

Landrigan, P. J., R. Fuller, N. J. Acosta, O. Adeyi, R. Arnold, A. B. Baldé, R. Bertollini, S. Bose-O'Reilly, J. I. Boufford, P. N. Breysse, et al. (2018), The lancet commission on pollution and health, *The Lancet*, *391*(10119), 462–512. 1.4.1

Larson, D. W., E. Jones, R. Pannu, and R. Sheokand (2004), Instability in indian agriculturea challenge to the green revolution technology, *Food Policy*, *29*(3), 257–273. 1.4

Larson, G., D. R. Piperno, R. G. Allaby, M. D. Purugganan, L. Andersson, M. Arroyo-Kalin, L. Barton, C. C. Vigueira, T. Denham, K. Dobney, et al. (2014), Current perspectives and the future of domestication studies, *Proceedings of the National Academy of Sciences*, *111*(17), 6139–6146. 1.1

Lelieveld, J., and F. J. Dentener (2000), What controls tropospheric ozone?, *Journal of Geophysical Research: Atmospheres*, *105*(D3), 3531–3551. 1.3.1

Lesk, C., P. Rowhani, and N. Ramankutty (2016), Influence of extreme weather disasters on global crop production, *Nature*, *529*(7584), 84. 1.2

Lobell, D. B., W. Schlenker, and J. Costa-Roberts (2011), Climate trends and global crop production since 1980, *Science*, *333*(6042), 616–620. 1.2

Lombardozzi, D., J. Sparks, and G. Bonan (2013), Integrating o 3 influences on terrestrial processes: photosynthetic and stomatal response data available for regional and global modeling, *Biogeosciences*, *10*(11), 6815–6831. 1.3.2

Loomis, D., Y. Grosse, B. Lauby-Secretan, F. El Ghissassi, V. Bouvard, L. Benbrahim-Tallaa, N. Guha, R. Baan, H. Mattock, and K. Straif (2013), The carcinogenicity of outdoor air pollution, *The lancet oncology*, *14*(13), 1262–1263. 1.3

Marcelis, L., E. Heuvelink, and J. Goudriaan (1998), Modelling biomass production and yield of horticultural crops: a review, *Scientia Horticulturae*, *74*(1-2), 83–111. 1.5

Mauzerall, D. L., and X. Wang (2001), Protecting agricultural crops from the effects of tropospheric ozone exposure: reconciling science and standard setting in the united states, europe, and asia, *Annual Review of energy and the environment*, *26*(1), 237–268. 1.3

McKee, I., and S. P. Long (2001), Plant growth regulators control ozone damage to wheat yield, *New Phytologist*, *152*(1), 41–51. 1.3.3

Meehl, G. A., and C. Tebaldi (2004), More intense, more frequent, and longer lasting heat waves in the 21st century, *Science*, *305*(5686), 994–997. 1.1

Mills, G., A. Buse, B. Gimeno, V. Bermejo, M. Holland, L. Emberson, and H. Pleijel (2007), A synthesis of aot40-based response functions and critical levels of ozone for agricultural and horticultural crops, *Atmospheric Environment*, *41*(12), 2630–2643. 1.3

Mills, G., K. Sharps, D. Simpson, H. Pleijel, M. Frei, K. Burkey, L. Emberson, J. Uddling, M. Broberg, Z. Feng, et al. (2018), Closing the global ozone yield gap: Quantification and cobenefits for multistress tolerance, *Global change biology*, *24*(10), 4869–4893. 1.4.1

Mittler, R. (2002), Oxidative stress, antioxidants and stress tolerance, *Trends in plant science*, *7*(9), 405–410. 1.3.2

Monks, P. S., A. Archibald, A. Colette, O. Cooper, M. Coyle, R. Derwent, D. Fowler, C. Granier, K. S. Law, G. Mills, et al. (2015), Tropospheric ozone and its precursors from the urban to the global scale from air quality to short-lived climate forcer. 1.3.1

Mulholland, B., J. Craigon, C. Black, J. Colls, J. Atherton, and G. Landon (1998), Effects of elevated co2 and o3 on the rate and duration of grain growth and harvest index in spring wheat (triticum aestivum l.), *Global Change Biology*, *4*(6), 627–635. 1.3.2

Nicklin, K. J. (2013), Seasonal crop yield forecasting in semi-arid west africa., Ph.D. thesis, University of Leeds. 1.5.2

Oksanen, E., V. Pandey, A. Pandey, S. Keski-Saari, S. Kontunen-Soppela, and C. Sharma (2013), Impacts of increasing ozone on indian plants, *Environmental pollution*, *177*, 189–200. 1.3.1

Osborne, S., D. Pandey, G. Mills, F. Hayes, H. Harmens, D. Gillies, P. Büker, and L. Emberson (2019), New insights into leaf physiological responses to ozone for use in crop modelling, *Plants*, *8*(4), 84. 1.3.3

Osborne, T., G. Rose, and T. Wheeler (2013), Variation in the global-scale impacts of climate change on crop productivity due to climate model uncertainty and adaptation, *Agricultural and Forest Meteorology*, *170*, 183–194. 1.5.2

Pachauri, R. K., M. R. Allen, V. R. Barros, J. Broome, W. Cramer, R. Christ, J. A. Church, L. Clarke, Q. Dahe, P. Dasgupta, et al. (2014), *Climate change 2014: synthesis report. Contribution of Working Groups I, II and III to the fifth assessment report of the Intergovernmental Panel on Climate Change*, Ipcc. 1.1

Passioura, J. B. (1996), Simulation models: science, snake oil, education, or engineering?, *Agronomy Journal*, *88*(5), 690–694. (document), 1.5.1, 1.5, 1.5.1

Pell, E., N. Eckardt, and A. Enyedi (1992), Timing of ozone stress and resulting status of ribulose bisphosphate carboxylase/oxygenase and associated net photosynthesis, *New Phytologist*, *120*(3), 397–405. 1.3.2

Pell, E. J., C. D. Schlagnhaufer, and R. N. Arteca (1997), Ozone-induced oxidative stress: mechanisms of action and reaction, *Physiologia Plantarum*, *100*(2), 264–273. 1.3.2

Reilly, J. M., and K. O. Fuglie (1998), Future yield growth in field crops: what evidence exists?, *Soil and Tillage Research*, *47*(3-4), 275–290. 1.1

Ritchie, H., D. Reay, and P. Higgins (2018), Sustainable food security in indiadomestic production and macronutrient availability, *PloS one*, *13*(3), e0193,766. 1.1

Rosenzweig, C., J. Elliott, D. Deryng, A. C. Ruane, C. Müller, A. Arneth, K. J. Boote, C. Folberth, M. Glotter, N. Khabarov, et al. (2014), Assessing agricultural risks of climate change in the 21st century in a global gridded crop model intercomparison, *Proceedings of the National Academy of Sciences*, *111*(9), 3268–3273. 1.5.3

Roudier, P., B. Sultan, P. Quirion, and A. Berg (2011), The impact of future climate change on west african crop yields: What does the recent literature say?, *Global Environmental Change*, *21*(3), 1073–1083. 1.2

Sanai, L., T. Wheeler, A. Challinor, L. Erda, X. Yinlong, and J. Hui (2010), Simulating the impacts of global warming on wheat in china using a large area crop model, *Journal of Meteorological Research*, *24*(1), 123–135. 1.5.2

Sharma, P., A. B. Jha, R. S. Dubey, and M. Pessarakli (2012), Reactive oxygen species, oxidative damage, and antioxidative defense mechanism in plants under stressful conditions, *Journal of botany*, *2012*. 1.3.2

Sicard, P., A. Anav, A. D. Marco, and E. Paoletti (2017), Projected global ground-level ozone impacts on vegetation under different emission and climate scenarios, *Atmospheric Chemistry and Physics*, *17*(19), 12,177–12,196. 1.3.1

Sillmann, J., V. V. Kharin, F. Zwiers, X. Zhang, and D. Bronaugh (2013), Climate extremes indices in the cmip5 multimodel ensemble: Part 2. future climate projections, *Journal of geophysical research: atmospheres*, *118*(6), 2473–2493. 1.1

Silver, B., C. Reddington, S. Arnold, and D. Spracklen (2018), Substantial changes in air pollution across china during 2015–2017, *Environmental Research Letters*, *13*(11), 114,012. 1.3.1

Singh, H., A. Singh, H. Kushwaha, and A. Singh (2007), Energy consumption pattern of wheat production in india, *Energy*, *32*(10), 1848–1854. 1.4

Solomon, S., M. Manning, M. Marquis, D. Qin, et al. (2007), *Climate change 2007-the physical science basis: Working group I contribution to the fourth assessment report of the IPCC*, vol. 4, Cambridge university press. 1.1

Stocker, T., D. Qin, G. Plattner, M. Tignor, S. Allen, J. Boschung, A. Nauels, Y. Xia, V. Bex, and P. Midgley (2013), Ipcc, 2013: summary for policymakers in climate change 2013, *The Physical Science Basis. Contribution of Working Group I to the Fifth Assessment Report of the Intergovernmental Panel on Climate Change*. 1.1

Tai, A. P., M. V. Martin, and C. L. Heald (2014), Threat to future global food security from climate change and ozone air pollution, *Nature Climate Change*, *4*(9), 817–821. 1.3

Tao, F., R. P. Rötter, T. Palosuo, C. Gregorio Hernández Díaz-Ambrona, M. I. Mínguez, M. A. Semenov, K. C. Kersebaum, C. Nendel, X. Specka, H. Hoffmann, et al. (2018), Contribution of crop model structure, parameters and climate projections to uncertainty in climate change impact assessments, *Global change biology*, *24*(3), 1291–1307. (document), 1.5.3, 1.6

Temple, P. (1986), Stomatal conductance and transpirational responses of field-grown cotton to ozone, *Plant, Cell & Environment*, *9*(4), 315–321. 1.3.2

Tian, Y., J. Chen, C. Chen, A. Deng, Z. Song, C. Zheng, W. Hoogmoed, and W. Zhang (2012), Warming impacts on winter wheat phenophase and grain yield under field conditions in yangtze delta plain, china, *Field Crops Research*, *134*, 193–199. 1.2

Tiedemann, A., and B. Pfähler (1994), Growth stage-dependent effects of ozone on the permeability for ions and non-electrolytes of wheat leaves in relation to the susceptibility to septoria nodorum berk., *Physiological and molecular plant pathology*, *45*(2), 153–167. 1.3.2

Traore, B., K. Descheemaeker, M. T. Van Wijk, M. Corbeels, I. Supit, and K. E. Giller (2017), Modelling cereal crops to assess future climate risk for family food self-sufficiency in southern mali, *Field Crops Research*, *201*, 133–145. 1.5.3

Tremblay, M., and D. Wallach (2004), Comparison of parameter estimation methods for crop models. 1.5.1

Unger, N., T. C. Bond, J. S. Wang, D. M. Koch, S. Menon, D. T. Shindell, and S. Bauer (2010), Attribution of climate forcing to economic sectors, *Proceedings of the National Academy of Sciences*, *107*(8), 3382–3387. 1.3

Van Dingenen, R., F. J. Dentener, F. Raes, M. C. Krol, L. Emberson, and J. Cofala (2009), The global impact of ozone on agricultural crop yields under current and future air quality legislation, *Atmospheric Environment*, *43*(3), 604–618. 1.6

Van Goethem, T., L. Azevedo, R. Van Zelm, F. Hayes, M. Ashmore, and M. Huijbregts (2013), Plant species sensitivity distributions for ozone exposure, *Environmental pollution*, *178*, 1–6. 1.3.2

Verstraeten, W. W., J. L. Neu, J. E. Williams, K. W. Bowman, J. R. Worden, and K. F. Boersma (2015), Rapid increases in tropospheric ozone production and export from china, *Nature geoscience*, *8*(9), 690. 1.3.1

Wollenweber, B., J. Porter, and J. Schellberg (2003), Lack of interaction between extreme high-temperature events at vegetative and reproductive growth stages in wheat, *Journal of Agronomy and Crop Science*, *189*(3), 142–150. 1.2

Yunus, M., and M. Iqbal (1996), *Plant response to air pollution*, Wiley Chichester. 1.3.1

Chapter 2

New modelling technique for improving crop model performance - application to the GLAM model

I. Droutsas[1,2], A. J. Challinor[1,2], M. Swiderski[1] and M. A. Semenov[1]

[1] *Institute for Climate and Atmospheric Science, School of Earth and Environment, University of Leeds, LS2 9JT Leeds, UK*

[2] *Priestley International Centre for Climate, University of Leeds, LS2 9JT Leeds, UK*

[3] *Collaborative Research Program from CGIAR and Future Earth on Climate Change, Agriculture and Food Security (CCAFS), International Centre for Tropical Agriculture (CIAT), A.A. 6713, Cali, Colombia*

[4] *Rothamsted Research, Harpenden, Herts, AL5 2JQ, UK*

Abstract

Crop models simulate growth and development and they are often used for climate change applications. However, they have a variable skill in the simulation of crop responses to extreme climatic events. Here, we present a new dynamic crop modelling method for simulating the impact of abiotic stresses. The Simultaneous Equation Modelling for Annual Crops (SEMAC) uses simultaneous solution of the model equations to ensure internal model consistency within daily time steps; something that is not always guaranteed in the usual sequential method. The SEMAC approach is implemented in GLAM, resulting in a new model version (GLAM-Parti). The new model shows a clear improvement in skill under water stress conditions and it successfully simulates the acceleration of leaf senescence in response to drought. We conclude that SEMAC is a

promising crop modelling technique that might be applied to a range of models.

2.1 Introduction

The plant growth and development are influenced by a wide range of biotic and abiotic factors. Understanding the complex interactions between plants and their surrounding environments is important for prediction under environmental change. In this context, crop models are developed as systems for describing the growth and development of a crop in any given environment at local, regional or even global scale (*Chenu et al.*, 2017). Crop models simulate the plant growth and development by using a set of mathematical equations and they often include complex functions and modelling techniques for their simulations (*Marcelis et al.*, 1998). They are widely used as agricultural tools to describe the plant performance and to predict the final production and yield.

Climate change brings a higher frequency of extreme weather events and more complex interactions which can damage the crops, limit their yield (*Howden et al.*, 2007; *Porter et al.*, 2014; *Zhao et al.*, 2017), and alter their nutritional properties (*Myers et al.*, 2014; *Jones et al.*, 2017). Crop modelling has a long history in simulating these complex interactions. However significant challenges remain if the risks posed by climate change are to be reliably quantified (*Challinor et al.*, 2014). Extreme events, and the abiotic stresses that result, are particularly challenging, especially considering the wide range of environments across which crops are cultivated. The simulation of crop performance in these extreme climatic conditions can be significantly uncertain (*Zhang and Tao*, 2013; *Asseng et al.*, 2013, 2015). *Tao et al.* (2018) showed that for climate change impact assessment, the largest source of uncertainty in their crop model ensemble was due to the model structure. *Rivington and Koo* (2010) suggests that one of the ways to improve the crop model performance is by better simulating the various processes through an improved connection between them. Thus, improving the crop model structure is a significant step towards reducing the uncertainty in the model output for climate change impact studies (*Challinor et al.*, 2013).

A common practice to improve the performance of a crop model is to add new processes and interactions (*Affholder et al.*, 2012). It is expected that this practice will lead to an improvement in skill, while at the same time the model will be able to simulate more processes of the real world. Nevertheless, adding complexity in a crop model may not always lead to an improvement in skill, especially in large scale applications. This can partially occur from the inclusion of site-specific parameters and processes that are difficult to generalize in larger regions (*Challinor et al.*, 2009). This is a common problem in crop modelling and in some cases modellers tend to develop simplified versions of models that are already very complex (e.g., *Stella et al.*, 2014). According to *Passioura* (1996) there is an optimal level of complexity in which the total model error is minimized. At this point, there is a balance between a robust

model structure and the number of parameters included. In accordance with that, crop modellers should design their models upon an appropriate level of complexity (*Sinclair and Seligman*, 2000). This level is defined by the scope of the model and the scientific questions that it seeks to address (*Challinor et al.*, 2018).

Simultaneous equation modelling approaches are commonly used to provide a robust way of simulating the interdependence between processes that are jointly determined in the real world (e.g., *Oldroyd*, 1950; *Chou and Kamel*, 1988; *Zeng and Cai*, 2005; *Lefcheck*, 2016). Agricultural environments consist of complex systems with many interactions and the interdependence between various processes makes modelling difficult. The aim of this paper is to introduce a new crop modelling method which uses simultaneous solution of all model equations for crop growth and development. The new approach is called SEMAC (Simultaneous Equations Modelling for Annual Crops). The solution of the system of equations returns the values of the state variables for growth and development of the crop. This is done twice for each time step, initially for optimal conditions, where the impact of any stresses is ignored, and then again after considering of the environmental limitations. Applying the new modelling technique results in a dynamic crop model with reduced parameterization requirements, robust structure, and improved internal consistency.

SEMAC is implemented here in the GLAM crop model and a new model version is formed. The new model is called GLAM-Parti as it introduces partitioning of biomass based on allometric relationships; a necessary step for the application of SEMAC. GLAM-Parti advantages over GLAM since it has improved model structure, it gives a better connection between the model processes and finally, it increases the ability of the model to capture the impact of water stress on crop growth and development.

2.2 Rationale and methodology

2.2.1 Methodology and internal consistency in SEMAC

The simultaneous solution of model equations is not a new concept in crop modelling. For instance, simultaneous modelling approaches have been developed to couple leaf photosynthesis to stomatal conductance (e.g., *Baldocchi*, 1994; *Yin and Struik*, 2009). In addition, *Goudriaan and Van Laar* (1994) combined the rate of formation of new leaf area and the growth of biomass to develop an equation which explains the evolution of the total biomass during the season. Nevertheless, in order to avoid a very complicated system, they made simplifications, such as that the relative growth rates of biomass and leaf area are identical and constant over time.

SEMAC develops a system of simultaneous equations which accounts for all above-ground crop growth and development processes. This differentiates SEMAC from the prevailing crop modelling techniques. Otherwise, the modelling process follows the

methodology described in *van Ittersum et al.* (2003). At the first step (i.e. the potential production level) the crop growth is defined by the given environmental conditions and the crop properties without considering of any limitations from stresses. At this step, the system of equations is solved to return the potential crop production level. At the second step (i.e. the attainable production level) the impact of stresses is taken into account - in this case water stress - which reduces transpiration and growth, decreases the specific leaf area (SLA), and alters the allocation of dry matter between leaves and stems. These modifications are incorporated into the model equations, which are solved to return the values of the state variables. This step ensures consistency between the prognostic variables of the system and it outputs the attainable production level. At the third step, the growth reducing factors are taken into account (i.e. weeds, pests, diseases, pollutants). In SEMAC, the steps 1-3 are always carried out in order as necessary (Fig. 2.1).

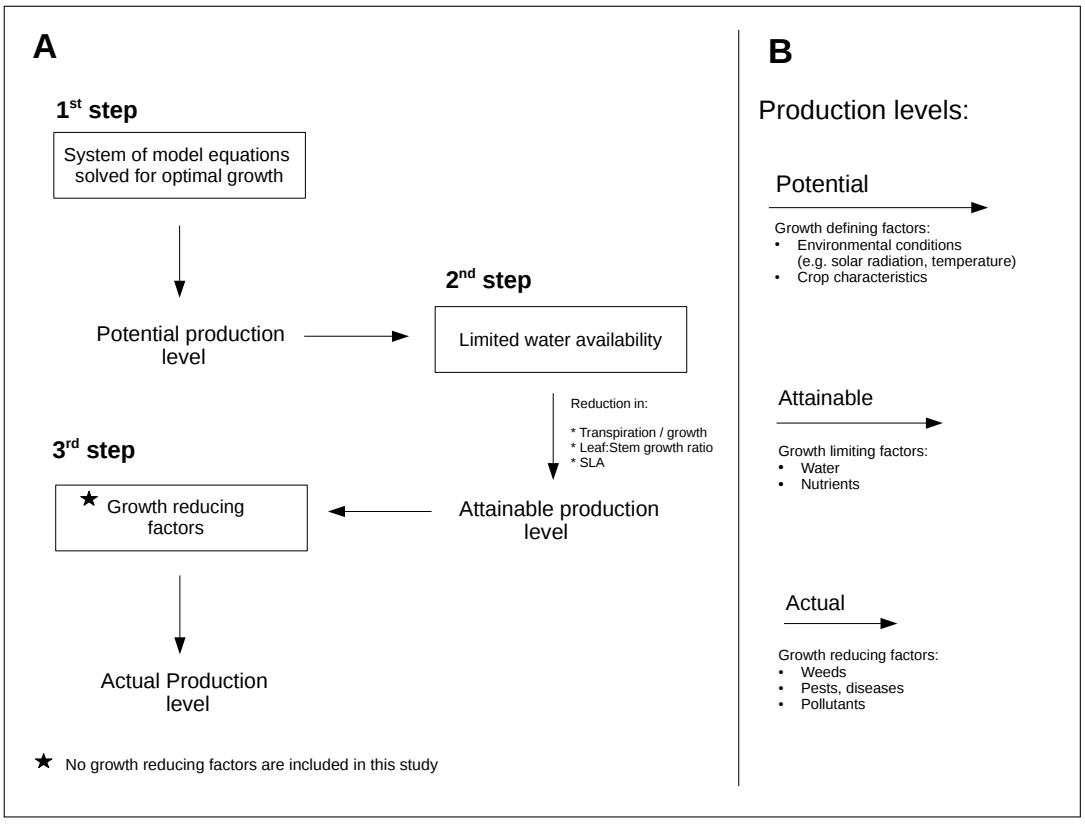

Figure 2.1: A. SEMAC methodology for crop production; B. Production levels in Wageningen crop models (*Van Ittersum and Rabbinge*, 1997; *van Ittersum et al.*, 2003)

Applying SEMAC to a crop model involves the following steps:

i) Introduction of allometric relationships to relate state variables: There are various modelling techniques for simulating the carbon allocation among the plant organs. Common approaches are the use of partitioning coefficients that are dependent on the development stage or modelling the source to sink carbon dynamics (*Marcelis and*

Heuvelink, 2007). In SEMAC, the concept of allometric growth is implemented, which expands upon the principle that the growth of the different plant compartments is jointly determined through allometric relationships. Based on these relationships, the total biomass (W) can be expressed as function of LAI, following the modifications shown in Section 2.3.4.2.

ii) Expression of any remaining state variables as functions of other state variables: In crop models, the daily increase in biomass (dW/dt) is estimated either from intercepted radiation, transpiration or photosynthesis. At the canopy level, the biomass growth can be expressed as function of LAI (i.e. this is especially true for radiation or transpiration driven models). For instance, in water-based crop models, the production of new biomass depends on canopy transpiration. The transpiration is a function of evapotranspiration, which is in turn dependent on the environmental conditions and LAI. After calculating the environmental influence (i.e. based on the weather conditions), the growth of biomass can be expressed as function of LAI (see Section 2.3.4.3 and Appendix A).

iii) Substitution of the relationships from i and ii into the simple mass balance equation W_n - W_{n-1} - dW/dt = 0. The W_n and dW/dt terms of the equation are explained in steps i, ii, where they are expressed as function of LAI. W_{n-1} is the biomass value of the previous time step. The solution of the mass balance equation returns the value of LAI which is then used to solve all other equations that participate into the system. This is done twice, initially for optimal conditions, where the stress impact is ignored, and then again, after incorporating the stress effects. In this study water stress is considered, however SEMAC can be similarly applied to various stress conditions. A schematic representation of the implementation of SEMAC in crop models is given in Fig. 2.2.

2.2.2 Use of SEMAC to model stress conditions

The implementation of SEMAC leads to three main potential sources of error in the simulation of crop growth and development at each time step. These are: the production of new biomass, the allocation of biomass to the different plant compartments and the canopy SLA. The first two aspects affect the accuracy of the model to simulate the above-ground biomass and the masses of the different organs (e.g. leaves, stems, grains). The third aspect (i.e. the SLA) affects both the simulation of leaf mass and the estimation of LAI. This accounts for all climatic conditions and abiotic stresses. More specifically, various stresses and management practices can significantly affect the plant growth (*Cramer et al.*, 2011) and alter the dry matter allocation patterns (*Weiner*, 2004; *Sieling et al.*, 2016; *Poorter et al.*, 2012). In crop models, the biomass accumulation rate may be modified and the SLA as well as the carbon partitioning between different organs may be adjusted to the environmental conditions (i.e. through modifications in the allometric relationships). SEMAC provides a simple modelling

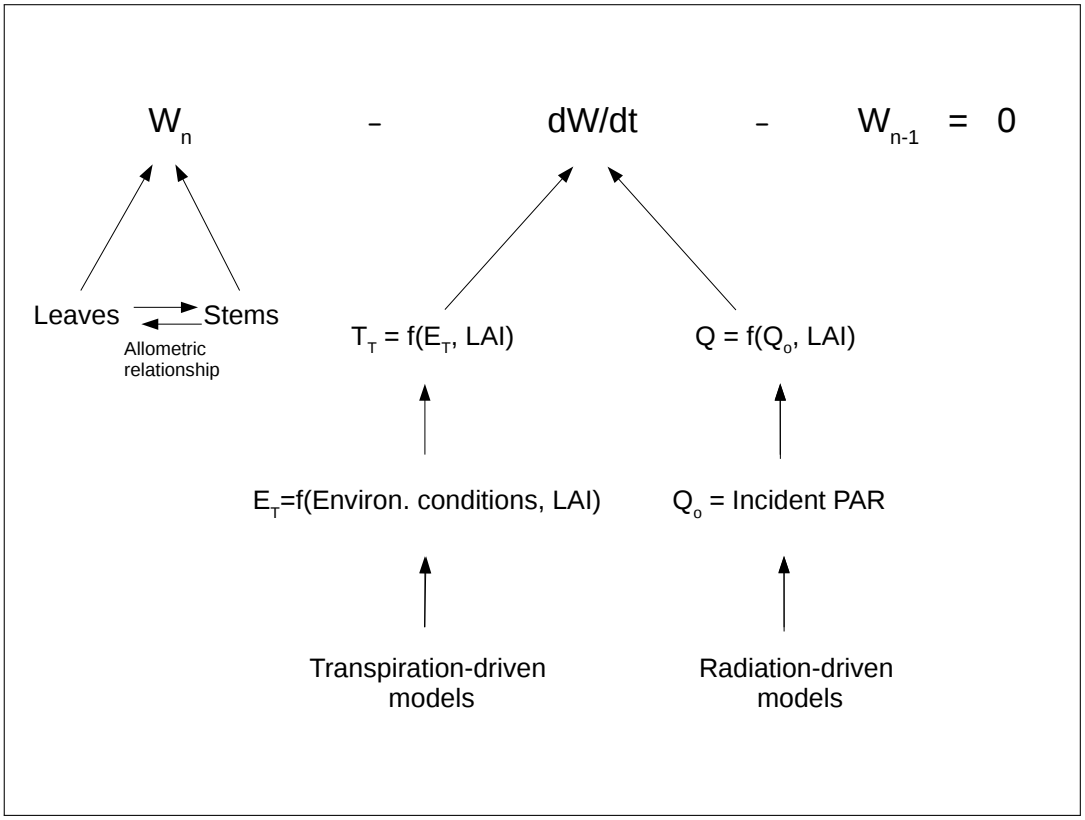

Figure 2.2: Implementation of SEMAC in radiation and transpiration driven crop models. T_T=Transpiration, E^T=Evapotranspiration, Q=Intercepted PAR, W=total above-ground biomass, dW/dt=daily increase in biomass, n=time step. W_n and dW/dt are expressed as function of LAI and the solution of the mass balance equation returns the value of LAI.

framework for simulating these growth and development processes and ensures internal model consistency with the use of the simultaneous equation modelling. This secures that there are no missing interactions between processes that are interconnected in the field, which is particularly important under stress conditions where the system becomes more complex. Crop modelling techniques based on sequential approaches may face issues in capturing the plant / environment interactions at the same time step.

2.2.3 Modelling water stress effects in SEMAC

Most crop models use a water stress factor to simulate the impact of water shortage on crops (e.g., *Jamieson et al.*, 1998; *Asseng et al.*, 2004). This factor is usually calculated as the rate of the available water in the soil to the total water demand by the plant. If this rate is below a pre-determined threshold then the plant is affected by the water deficit. The water stress factor takes values from zero to one and it is usually applied to modify LAI or accelerate leaf senescence (*Raes et al.*, 2009; *Ewert et al.*, 2015).

Nevertheless, the leaf development is affected by various factors under limited water in the field. Most importantly, drought conditions may alter the leaf:stem mass ratio

(*Ratjen et al.*, 2016) and decrease the SLA (*Fernández and Reynolds*, 2000; *Brisson and Casals*, 2005; *Zhang et al.*, 2010). If these effects are omitted in a crop model, a bias may be introduced in the simulation of leaf dynamics (*Ratjen et al.*, 2016). For this reason, in SEMAC, LAI is not directly effected by the water stress effects. Instead, the water stress factor is used to apply modifications on the leaf:stem dry matter production and the canopy SLA under drought. LAI is then altered both due to decreased carbon allocation to the leaves and to lower SLA. Simultaneously, the biomass production is affected by the LAI reduction. These effects are captured at the same time step due to the robust model structure and the simultaneous solution of the model equations. Through this method, both the LAI takes into account the water stress effects on leaf growth and development, and all state variables (including biomass growth) are consistent with the value of LAI, since they are updated by the same system of equations.

2.2.4 Modelling of stress interactions

Climate change brings a higher frequency of extreme weather conditions and more stress interactions acting on crops (*Gray and Brady*, 2016). When multiple stresses affect the crop performance, the response of plants cannot be addressed only by taking into account of each stress individually (*Mittler*, 2006). In crop modelling studies, the simulation of crop growth and development in these environments can be very complex. For instance, in drought prone regions with high air pollution levels, the use of multiple factors to simulate the leaf expansion or accelerate leaf senescence may result to an unrealistic model output. SEMAC attempts to increase the model predictability in these situations by introducing an improved connection between the various model processes. LAI is computed by the system of equations which decreases the parameterization requirements, as it removes the need of using stress factors to modify the LAI growth. It also improves the LAI simulation since it takes into account all equations in the system for the estimation of LAI. The use of allometric relationships for the partitioning of biomass gives the opportunity to easily shift the carbon allocation between the plant compartments under different environmental conditions. The above advancements create a modelling framework which can be further expanded to incorporate more stresses. Hence, it is believed that SEMAC can be a useful tool in the attempt to address the crop response to a changing climate.

2.3 Materials and Methods

2.3.1 GLAM model

The General Large Area Model for annual crops (GLAM) is a process based crop model which simulates the impact of climate on crop yield (*Challinor et al.*, 2004)

(Fig. 2.3). It is a relatively simple model which runs in daily time step and it is designed to operate at regional scales (*Challinor et al.*, 2005). GLAM uses a maximum daily growth rate of leaf area index which can be decreased by the water stress. The daily potential evapotranspiration is calculated by the Priestley-Taylor equation and it is partitioned into potential evaporation and potential transpiration. The actual transpiration is calculated from the potential transpiration by taking into account the soil water content. The transpiration is multiplied by the transpiration efficiency to return the daily biomass growth. The grain yield is estimated by partitioning the above-ground biomass to the grains using the harvest index. *Challinor et al.* (2004) provides a detailed description of GLAM.

In GLAM, the grain growth is dependent on canopy transpiration. However, under drought conditions, either the photosynthesis or the remobilization of pre-anthesis assimilates to the grains play a major role on grain yield (*Inoue et al.*, 2004). In order to capture this effect, the radiation use efficiency (RUE) approach i.e. the second option for simulating growth in GLAM (*Osborne et al.*, 2013) - was selected to describe the increase in biomass, only after anthesis when extremely low values of canopy transpiration were calculated. A threshold for transpiration was set below which the RUE approach was used. Severe drought effects have been previously reported to occur for wheat at anthesis in 80% of water deficit (*Mahrookashani et al.*, 2017). In accordance to that, the model threshold was set to the 0.2 value of the soil water stress factor.

2.3.2 Internal consistency in GLAM

GLAM uses a sequential method for solving the model equations at each time step. This can limit the model performance in the simulation of processes that interact in the field. Fig. 2.3 is a schematic representation of the GLAM model structure. LAI is initially estimated and the potential canopy transpiration is calculated according to the LAI value. The actual transpiration is a fraction of the potential value based on the soil water content. Under water stress, the actual transpiration is reduced due to the soil water deficit. The decreased transpiration rate reduces the production of new biomass. In such case, the growth of leaves should also be lower due to the water stress effects. However, LAI is already calculated in the model and it is used for the calculation of the other state variables. Therefore, LAI does not respond dynamically to water stress. For this reason, the soil water stress factor is computed which reduces the growth of leaves on the next time step (i.e. the next day). This is a form of inconsistency, since this time delay is not representative of the reality and limits the model skill in the simulation of the drought stress effects.

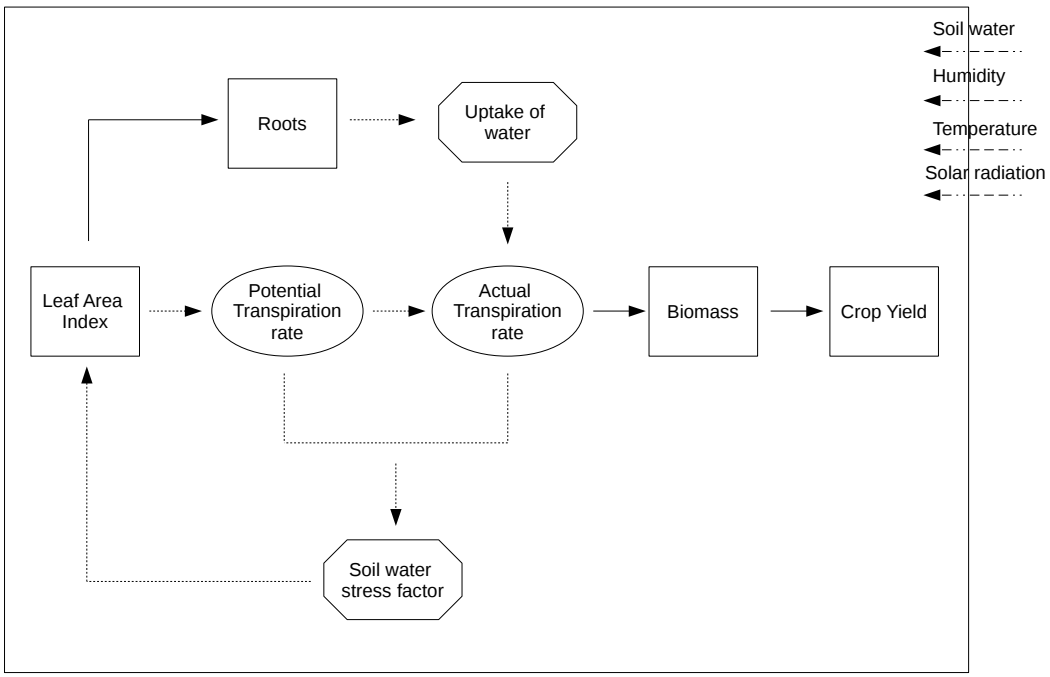

Figure 2.3: Generic scheme of GLAM model. The categorization of variables is taken from *Loomis et al.* (1979). State variables are represented by boxes, rate variables by ellipses, auxiliary variables by octagons, external variables by 2 dots - 3 dashes lines. Mass flows are represented by solid-line arrows, information flows by dashed-line arrows.

2.3.3 GLAM-Parti development

GLAM-Parti is the new version of GLAM based on the SEMAC approach (Fig. 2.4). The model modifications are described in Section 2.3.4. The alterations start with the inclusion of an allometric relationship between leaves and stems and expand with the incorporation of the new methodology. The value of LAI and the masses of leaves, stems and the total above-ground biomass are extracted simultaneously and there is no time lag between them, something that may occur in the step-by-step modelling method (e.g. the LAI value of the previous day is used for the computation of the carbon assimilation on the next day).

In GLAM-Parti, the set of model equations is initially solved to calculate the maximum plant growth at daily time step. This growth rate corresponds to the level defined only by temperature, radiation, vapour pressure deficit (VPD) and the plant properties (e.g. transpiration efficiency). Next, the available soil water is estimated. Based on the level of the water in the soil, the actual transpiration and the water stress factor are calculated. The actual transpiration is used to compute the growth of the above-ground biomass. The water stress factor is used to alter the SLA and the allocation of dry matter between leaves and stems. These modifications are incorporated into the set of

model equations which is solved again to return the values of all growth variables and the attainable production level. The yield gap parameter (YGP) is used to estimate the actual production level for all growth-reducing factors that the model implicitly takes into account. In this study, water stress is the only yield limiting factor, thus no growth reducing factors are considered.

The incorporation of the SEMAC methodology into GLAM simplifies the modelling of canopy LAI and leads to reduced parameterization requirements. The maximum LAI expansion rate $(dL/dt)_{max}$ is removed, which is a parameter used for the calculation of LAI. The model has been previously seen to be particularly sensitive to this parameter value (*Ramirez-Villegas et al.*, 2017) and its removal decreases the model error significantly (i.e. in the results, GLAM-Parti improves upon GLAM in all LAI simulations).

In this study, SEMAC stops at anthesis since at the post-anthesis period the model runs with a combination of the transpiration and the radiation use efficiency methods. This step is currently not included in GLAM-Parti, however the model is under ongoing development. At plant maturity, all leaf area is simulated to be senescent, therefore at the end of the grain-filling period if there was still green leaf area, the LAI is set to zero.

2.3.4 GLAM modifications

2.3.4.1 Leaf dynamics

In crop modelling studies, SLA is used for the simulation of the leaf dynamics. Generally, it is set either as an input parameter (*Yin and Struik*, 2010) or it is defined as a function of plant age, growth stage or the environmental conditions (*Hoogenboom et al.*, 1992; *Marcelis et al.*, 1998; *Asseng et al.*, 2003; *Leutscher and Vogelezang*, 1990). In GLAM, biomass and leaf area are simulated separately and SLA is permitted to evolve, subject to constraints based on an observed maximum value. This approach is inconsistent with SEMAC, since it does not result in full partitioning of biomass. In GLAM-Parti we make use of a significant observed relationship between SLA and temperature in various plant species (*Loveys et al.*, 2002; *Rosbakh et al.*, 2015; *Atkin et al.*, 2005). For wheat too, SLA has been previously seen to be sensitive to temperature variations (*Hotsonyame and Hunt*, 1998).

For the parameterization of SLA, data analysis was conducted on the Hot Serial Cereal experiment (*Martre et al.*, 2018). Wheat was grown in different periods of the year and the impact of temperature on growth and development was examined. Here, we tested the impact of high temperature on the evolution of the canopy SLA over time. We accumulated all daily maximum temperatures for the period from leaf emergence to the day of leaf measurement and compared them to the observed SLA as follows: SLA was calculated as the reciprocal of the measured specific leaf weight (SLW) and the data points with a coefficient of variation greater than 0.3 (i.e. 30%)

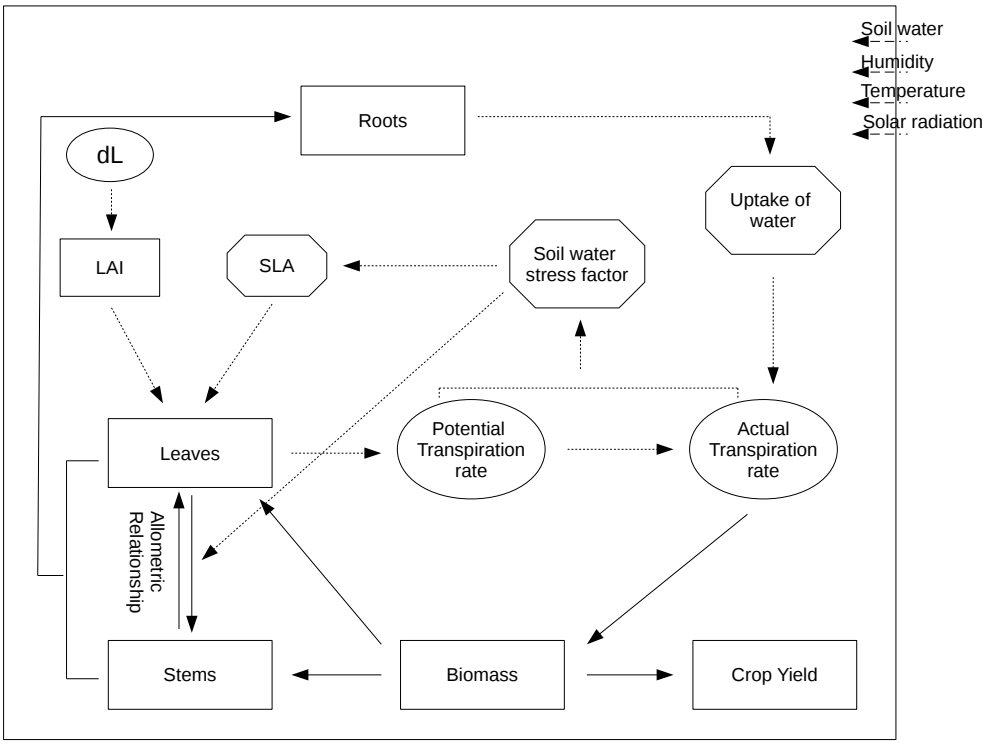

Figure 2.4: GLAM-Parti model structure. The system of equations is solved numerically by iteration with the Newton-Raphon approach. The unknown variable is dL (leaf area change). The iteration process stops when the system converges. The categorization of variables is taken from *Loomis et al.* (1979). State variables are represented by boxes, rate variables by ellipses, auxiliary variables by octagons, external variables by 2 dots - 3 dashes lines. Mass flows are represented by solid-line arrows, information flows by dashed-line arrows.

were excluded (*Taylor et al.*, 1999) (there was only one such point with value 0.49). A significant relationship was observed between the SLA and the accumulated maximum temperature index (T_{mac}) (Fig. 2.5). A quadratic model was selected to best fit the relationship:

$$SLA = 501 - 0.296 \cdot Tmac + 6.17 \cdot 10^{-5} \cdot Tmac^2 \tag{2.1}$$

where,

$$T_{mac} = \sum_{i=IEM}^{n} T_{max_i} \tag{2.2}$$

T_{max} is the daily maximum temperature, IEM is the day of crop emergence and n is the number of days after crop emergence. Eq. 2.1 describes canopy SLA as a function of the maximum temperature events accumulated over the crop growing season.

2.3.4.2 Partitioning of biomass between leaves and stems

In GLAM, LAI is the first state variable to be updated in the model based on a prescribed maximum LAI growth, which can be reduced only by limited soil water.

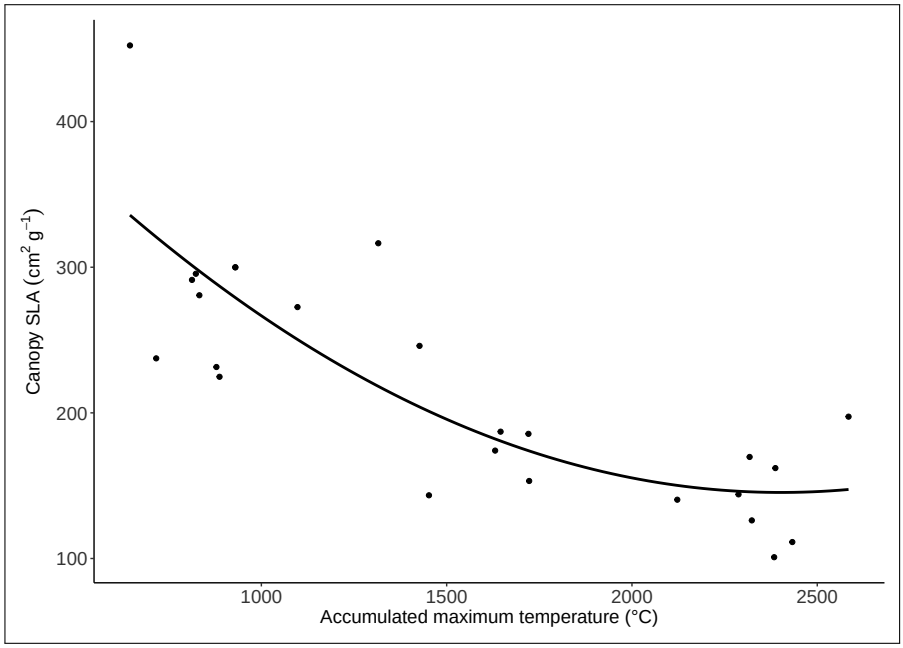

Figure 2.5: Quadratic regression between canopy SLA and the accumulated maximum temperature index. Continuous line is the regression: $y = 501 - 0.296x + 6.17 \cdot 10^{-5}x^2$ ($R^2 = 0.68,\ p < 0.01$).

For the incorporation of SEMAC, the function of LAI growth was removed. Instead, an allometric relationship was introduced which describes the partitioning of biomass between leaves and stems. According to the allometric approach the mass of stems (M_S) can be described in relation to the mass of leaves (M_L) under the generic formula (*Enquist et al.*, 1998; *Poorter et al.*, 2012):

$$M_S = h \cdot M_L^g \tag{2.3}$$

where g, h are empirically determined parameters and their values for wheat are taken from *Ratjen et al.* (2016) (i.e. the parameter h of this study is equal to the e^h of *Ratjen et al.* (2016)). The total mass of leaves (M_L) is divided into green leaves (M_{GL}) and yellow leaves (M_{YL}):

$$\begin{aligned} M_L &= M_{GL} + M_{YL} \\ &= \frac{LAI}{SLA} + M_{YL} \end{aligned} \tag{2.4}$$

The above-ground biomass (W) is divided into stems, leaves and grains. For the period before the initiation of grain development, W can be described by Eq. 2.3 and 2.4 as:

$$\begin{aligned} W &= M_L + M_S \\ &= \frac{LAI}{SLA} + M_{YL} + h \cdot (\frac{LAI}{SLA} + M_{YL})^g \end{aligned} \tag{2.5}$$

2.3.4.3 Incorporation of SEMAC into GLAM

Eq. 2.3 - 2.5 are newly imported equations in GLAM. These are combined with the existing functions to form GLAM-Parti as follows:
In GLAM, the potential evapotranspiration (E^{T}_{pot}) is calculated by the Priestley-Taylor equation as:

$$E^{T}_{pot} = \frac{\alpha}{\lambda} \cdot \frac{\Delta(R_N - G)}{\Delta + \gamma} \tag{2.6}$$

and it is partitioned to potential evaporation and transpiration, out of which the potential transpiration (T_T) is calculated as:

$$T_T = E^{T}_{pot}(1 - e^{-kLAI}) \tag{2.7}$$

The growth of the above-ground biomass (dW/dt) is defined as:

$$\frac{dW}{dt} = T_T \cdot TE \tag{2.8}$$

where TE is the transpiration efficiency and it is calculated as:

$$TE = min(\frac{E_T}{V}, E_{TN,max}) \tag{2.8a}$$

E_T is the normalised transpiration efficiency in Pa, V is the vapour pressure deficit, and $E_{TN,max}$ is the maximum transpiration efficiency in g kg^{-1}.
LAI can be expanded as:

$$LAI_n = LAI_{n-1} + dL \tag{2.9}$$

where LAI_n is the value of LAI at any given n day, LAI_{n-1} is the LAI of the previous day and dL is the leaf area change between the two consecutive days.
Finally, the above-ground biomass of the n day (W_n) is equal to the biomass of the previous day (W_{n-1}) plus the growth in biomass between the two days (dW/dt), which makes:

$$W_n - \frac{dW}{dt} - W_{n-1} = 0 \tag{2.10}$$

Eq. 2.5 - 2.10 form a system of 6 equations with 6 unknown variables which can be solved simultaneously to return the values of each unknown variable (i.e. dL, LAI_n, E^{T}_{pot}, T_T, dW/dt, W_n). For the solution of the system, Eq. 2.5 - 2.9 are substituted

into Eq. 2.10 which gives:

$$\underbrace{\frac{LAI_{n-1}+dL}{SLA}+M_{YL}+h\cdot(\frac{LAI_{n-1}+dL}{SLA}+M_{YL})^{g}}_{\mathrm{W_n}}- \underbrace{\frac{TE\cdot\alpha\cdot\Delta\cdot R_N}{\lambda\cdot(\Delta+\gamma)}(1-C_G\cdot e^{-k(LAI_{n-1}+dL)})(1-e^{-k(LAI_{n-1}+dL)})}_{\mathrm{dW/dt}}-W_{n-1}=0 \tag{2.11}$$

Eq. 2.11 forms the core of the SEMAC methodology (Fig. 2.6) and it is a function of leaf area change (dL). It can be solved numerically by iteration with the use of the Newton-Raphson method. The iteration process ends when the difference in the value between two consecutive loops is < 0.01. The extracted value of dL is used to update the variables in Eq. 2.3 - 2.9. Detailed description of the derivation of the dW/dt term in Eq. 2.11 is provided in the Appendix A. Whenever a negative value of dL is calculated, M_{YL} is updated as:

$$M_{YL(n)}=M_{YL(n-1)}+\frac{|dL|}{SLA} \tag{2.12}$$

where $M_{YL(n)}$ is the mass of yellow leaves on the n day, and $M_{YL(n-1)}$ is the mass of yellow leaves on the previous day (n-1). Eq. 2.3 - 2.11 form the 1st step of SEMAC in which no stress affects the crop growth and development (i.e. the potential production level).

2.3.4.4 Root modelling in GLAM-Parti

In GLAM the roots grow under a prescribed extraction front velocity and a prescribed root length density at the extraction front. The root length density by volume is calculated as a function of LAI and is used for the computation of the potentially extractable soil water (*Challinor et al.*, 2004). In GLAM-Parti, the modelling of root growth is modified. A root partitioning coefficient (R_c) is introduced which describes the increase in root biomass (dW_R) as a fraction of the total biomass increase (dW_T). The roots grow from plant emergence to anthesis and R_c is defined as:

$$R_C=\frac{dW_R}{dW_{AG}+dW_R} \tag{2.13}$$

Where dW_T is divided into above-ground (dW_{AG}) and root biomass growth (dW_R). The solution of Eq. 2.13 for dW_R gives:

$$dW_R=(\frac{R_C}{1-R_C})\cdot dW_{AG} \tag{2.14}$$

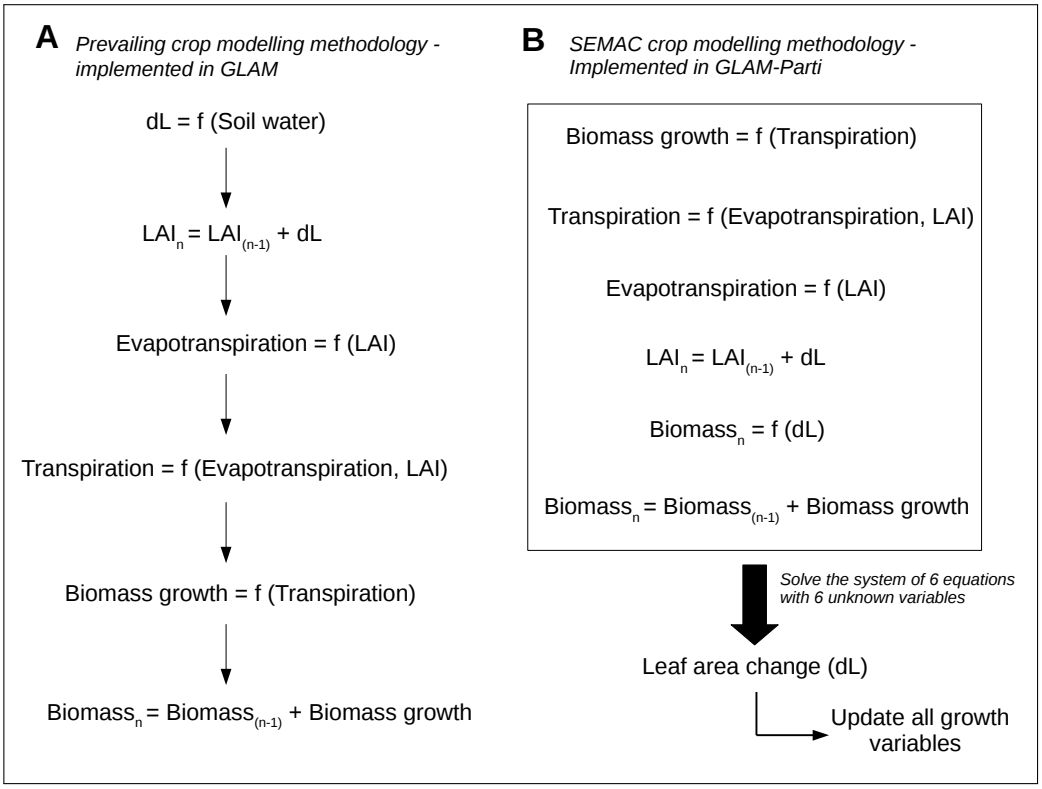

Figure 2.6: A. Well-established crop modelling methodology implemented in GLAM; B. SEMAC methodology for crop growth and development.

The computation of R_c is taken from *Baret et al.* (1992) and it is a function of the growth degree days (GDD) after sowing normalized at spiking:

$$R_C = -0.15 + 0.63 \cdot e^{-0.98 \cdot \theta^*} \tag{2.15}$$

where,

$$\theta^* = \frac{\theta - \theta_e}{\theta_s - \theta_e} \tag{2.16}$$

θ is the GDD after sowing, θ_e and θ_s are the GDD from sowing to emergence and from sowing to spiking (i.e. 150 GDD before anthesis) accordingly.

The root biomass is daily updated based on the allometric relationship of Eq. 2.14 to form the total root biomass (W_R). The W_R is divided by the specific root weight (σ) to give the total root length (R_L). The value of σ for wheat is assumed to be constant at 4.57 g km^{-1} (*King et al.*, 2003). The soil is divided into 25 layers (NSL=25), each with 10 cm thickness (DZ=10). The root length density of each soil layer ($L_{V_{SLi}}$) is estimated according to the modelling method of *King et al.* (2003):

$$L_{V_{SLi}} = (Y_{SLi} - Y_{SL(i-1)})R_L \tag{2.17}$$

where SL_i is the soil layer i and SL_{i-1} is the previous soil layer. The Y_{SLi} and $Y_{SL(i-1)}$

describe the cumulative proportion of roots from the surface to the soil layers i and i-1 accordingly. The vertical root distribution with depth (Y) is parametrized after *Gale and Grigal* (1987) as:

$$Y = 1 - \beta^d \tag{2.18}$$

where β describes the shape of the Y function and it is set to 0.953 (*King et al.*, 2003) and d is the soil depth from surface (i.e. d=i*DZ, for i=[1,NSL]). The estimated root length density per soil layer is used for the calculation of the potentially extractable soil water and the total soil water uptake (*Challinor et al.*, 2004). The value of the uptake diffusion coefficient (k_{DIF}) is taken from *Jamieson and Ewert* (1999).

2.3.5 Modelling the impact of water stress in GLAM-Parti

In GLAM the water stress factor describes the magnitude of water shortage - from full drought (value of zero), to zero water stress (value of one). For GLAM-Parti, the inverse number is used, so that the value of zero is appended to full water supply and this value increases according to the level of the water stress event. The soil water stress factor (SWFAC) is used to modify the SLA and the leaf:stem dry mass allocation. These effects are modelled below.

2.3.5.1 Water stress effects on SLA

The function of canopy SLA is given in Section 2.3.4.1. In the absence of a robust relationship between the reduction of SLA and the magnitude of the water stress event, a linear relationship is assumed. The water stress effects on SLA are incorporated into Eq. 2.2 as following:

$$T_{mac} = \sum_{i=IEM}^{n} (1 + SWFAC) \cdot T_{max_i} \tag{2.19}$$

The incorporation of Eq. 2.19 into Eq. 2.1 results in a linear decrease of the canopy SLA according to the magnitude and the total period of the drought event.

2.3.5.2 Water stress effects on leaf:stem partitioning of biomass

In water limiting environments, the stem mass (M_S) is favoured over the leaf mass (M_L) for wheat (*Ratjen et al.*, 2016). The enhancement of M_S is incorporated into GLAM-Parti as following:

$$M_{S_n} = h * (M_{L_{n-1}} + (1 + SWFAC) \cdot dM_L + M_{YL_n})^g \tag{2.20}$$

where M_{S_n} and M_{YL_n} are the mass of stems and mass of yellow leaves on the n day, $M_{L_{n-1}}$ is the mass of green leaves on the previous day and dM_L is the leaf mass change

between the two days. Eq. 2.20 can be used to describe Eq. 2.10 as:

$$M_{L_n} + M_{YL_n} + h * (M_{L_{n-1}} + (1 + SWFAC) \cdot dM_L + M_{YL_n})^g - \frac{dW}{dt} - W_{n-1} = 0 \quad (2.21)$$

and Eq. 2.21 can be described as a function of leaf area change (dL) as following:

$$\frac{LAI_{n-1} + dL}{SLA} + M_{YL_n} + h \cdot (\frac{LAI_{n-1} + (1 + SWFAC) \cdot dL}{SLA} + M_{YL_n})^g - \frac{dW}{dt} - W_{n-1} = 0 \quad (2.22)$$

Eq. 2.22 solves the system of equations for crop growth and development under water stress conditions. It is solved numerically with the Newton-Raphson method - similarly to Eq. 2.11 - to return the value of dL and calculate LAI as well as the masses of leaves, stems, and the total biomass under water stress. It consists of the second step of SEMAC, in which the water stress effects are incorporated into the model. The solution of Eq. 2.22 ensures consistency between the state variables and it outputs the attainable production level.

2.3.6 Sensitivity analysis to determine initial conditions for LAI

Eq. 2.11 does not converge for the first day after crop emergence, where the biomass of the previous day (W_{n-1}) equals zero. As a result, the solution of Eq. 2.11 does not return any real value of dL on that day. In order to solve this issue, an initial LAI value (LAI_{ini}) was prescribed into the model. LAI_{ini} consists of the initial condition of growth in GLAM-Parti and the model starts calculating the leaf area change from the second day after emergence. The baseline value of $LAI_{ini} = 0.1365$ m^2 m^{-2} was selected the model runs (*Stella et al.*, 2014). The evolution of LAI is sensitive to LAI_{ini}, since every leaf area change depends on the LAI value of the previous time step. Analysis was conducted to evaluate the model performance over a wide range of LAI_{ini} values (interval (0.0007 - 0.3 m^2 m^{-2}), *Ma et al.*, 2013). The model was calibrated for each LAI_{ini} using the methodology explained in Section 2.3.10.

2.3.7 Methods to compare sequential and simultaneous modelling methodologies

A new model version (GLAM-$Parti_{seq}$) was developed to test the contribution of the simultaneous equation modelling methodology to the model output. The new version is identical to GLAM-Parti in terms of the model equations but it uses sequential method to solve them. In order to do this Eq. 2.11 was removed from the model. Instead, we use the LAI value of the previous time step (i.e. the previous day) to solve the model equations of the next day. The other model processes are not modified. Thus, the accumulation of biomass is estimated, which is partitioned into leaves and stems according to their allometric relationship. Given the mass of leaves and the canopy

SLA, a new LAI is calculated, which is used for the solution of the model equations on the next day.

For a given set of equations there should be one set of parameters which optimizes the model output. GLAM-Parti and GLAM-Parti$_{seq}$ use the same set of equations but they differ in the model structure. As a result, one set of parameters is expected to lead to different model output in the two model versions. We made the assumption that GLAM-Parti provides higher internal consistency and that the parameters from the calibration of GLAM-Parti are the optimal for our set of model equations. If this is true, then GLAM-Parti should exhibit higher skill when the two model versions run with the parameters from its calibration. If not, then the assumption that GLAM-Parti improves the model performance due to the simultaneous modelling approach is wrong. Then we calibrated GLAM-Parti$_{seq}$, which resulted in new model output (i.e. we call it GLAM-Parti$_{seq\text{-}cal}$). If GLAM-Parti is still performing better than GLAM-Parti$_{seq\text{-}cal}$, this validates the assumption that the calibration of GLAM-Parti provides the optimal set of parameters for our set of model equations. The differences between GLAM-Parti and GLAM-Parti$_{seq}$ reveal the limitations of the sequential modelling approach. The comparison between GLAM-Parti and GLAM-Parti$_{seq\text{-}cal}$ shows the extend to which the calibration can compensate for the model limitations due to the step-wise modelling method.

2.3.8 Experimental design

GLAM, GLAM-Parti and GLAM-Parti$_{seq}$ were tested against field data for wheat under drought stress. The experiment, reported by *Jamieson et al.* (1995), was held in a mobile rainshelter at the New Zealand Institute for Crop and Food research experiment station at Lincoln in Canterbury (latitude 43°38' S, longitude 172°30' E). 'Batten' wheat was sown on 8 June 1991. The rainshelter was used to impose the plants to various levels of drought stress. Four treatments were chosen out of the total set of experiments for analysis here. Treatment 1 (RS1) is the control experiment which is well irrigated with no water stress, treatment 5 (RS5) is imposed to early drought, treatment 6 (RS6) is the late drought and treatment 11 (RS11) is the full drought experiment.

2.3.9 Statistical measures

The calibration and evaluation of all model versions was done using the root mean square error (RMSE) and model efficiency index (MEI) according to the following formulas:

$$RMSE = \sqrt{\frac{\sum_{i=1}^{n}(P_i - O_i)^2}{n}} \tag{2.23}$$

where P_i and O_i are the estimated and observed values accordingly and n equals the number of observations.

$$MEI = 1 - \frac{\sum_{i=1}^{n}(O_i - P_i)^2}{\sum_{i=1}^{n}(O_i - \bar{O})^2} \tag{2.24}$$

MEI is a measure of the model skill. It is in the range of $(-\infty, 1]$, where a value of 1 indicates ideal fit to the observations. Values below zero indicate that the mean observed value is a better predictor than the model (*Krause et al.*, 2005).

2.3.10 Model calibration

GLAM, GLAM-Parti and GLAM-Parti$_{seq}$ were calibrated against the observed data. Initially, the simulated phenology of the models was set to meet the observed anthesis and maturity dates of the fully irrigated treatment. This was done to avoid any model bias from sources different than the water stress effects. The initial soil water and the soil characteristics were set up using the observed values. For transpiration efficiency (E_T) and maximum transpiration efficiency ($E_{TN,max}$), an optimizer was developed to test all possible combinations in their total range of values (see Appendix A for parameter ranges). The optimizer selected the combination of E_T and $E_{TN,max}$ which minimized the RMSE between all observed and simulated above-ground biomass values in the control experiment (RS1). For radiation use efficiency (RUE), the optimizer selected the value which minimized the RMSE between all observed and simulated above-ground biomass in the early drought treatment (RS5). This was done because RUE was used only after anthesis in the drought stress simulations (Section 2.3.1). Similar process was followed for the maximum LAI expansion rate $(dL/dt)_{max}$ and the rate of change of harvest index (dHI/dt). The optimizer selected the values which minimized the RMSE between observed and simulated LAI and grain mass of the control treatment (RS1) accordingly. The step for the runs of the optimizer was 0.1 for E_T, $E_{TN,max}$ and RUE, 0.0025 for $(dL/dt)_{max}$ and 0.00025 for dHI/dt. The $(dL/dt)_{max}$ parameter was used in all GLAM-Parti versions only for the period after anthesis when SEMAC stops and GLAM-Parti runs under the GLAM approach. The values of all calibrated parameters are provided in the Table A.1 of the Appendix A. The extinction coefficient k for wheat was set to 0.737 (*Kanemasu et al.*, 1985) and the maximum transpiration rate (T_{Tmax}) was set to 0.75 cm day^{-1} (*Liu et al.*, 2002). All other parameter values were taken from *Challinor et al.* (2004). The yield-gap parameter (C_{YG}) was set to one because limited water supply was the only yield-reducing factor.

2.4 Results

2.4.1 Test GLAM and GLAM-Parti overall model performance

Table 2.1 shows the MEI and RMSE of GLAM and GLAM-Parti for LAI, biomass, grain yield and cumulative evapotranspiration in all treatments. Both measures were calculated based on all simulated and observed values of the variables during the whole growing season. The mean MEI ($\overline{MEI}$) is the numerical mean of the four compared variables in each treatment.

Both models demonstrated a good agreement with the observations in the control experiment where no water stress effects the wheat (Fig. 2.7). The evapotranspiration, above-ground biomass and yield are well simulated in both models (i.e. all MEI values are greater or equal 0.94) and their overall performance is satisfactory. GLAM slightly overestimates the final yield, whilst GLAM-Parti overestimates the final biomass. Nevertheless, the differences are not large. GLAM is also in closer agreement with the maximum observed LAI value, whilst both models show very similar results in the simulation of the cumulative evapotranspiration. Overall, GLAM and GLAM-Parti show good performance in the simulation of the control treatment (GLAM $\overline{MEI} = 0.88$, GLAM-Parti $\overline{MEI} = 0.92$).

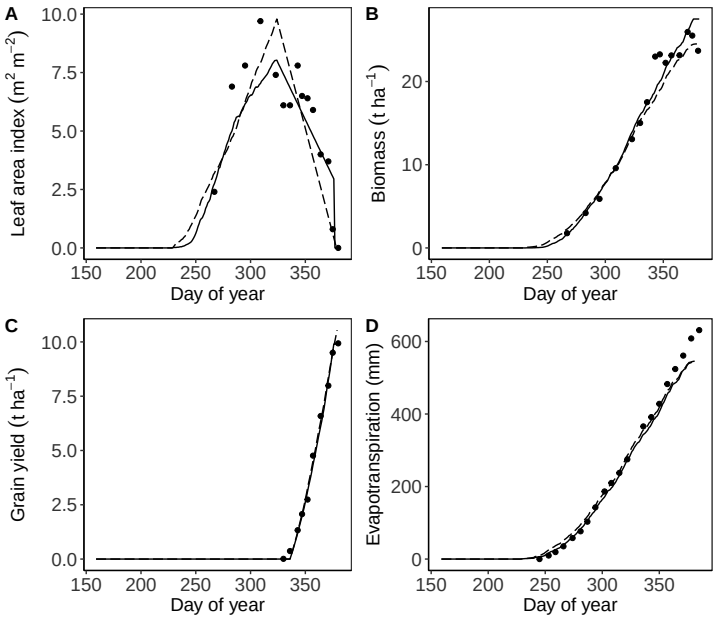

Figure 2.7: Observed values (•), GLAM (−−) and GLAM-Parti (-) output in the control experiment (RS1) for: A. leaf area index (LAI), B. above-ground biomass, C. grain yield, D. cumulative evapotranspiration.

Table 2.1: Model efficiency index (MEI) and root mean square error (RMSE) of GLAM and GLAM-Parti for LAI (m^2 m^{-2}), Biomass (t ha^{-1}), Grain yield (t ha^{-1}) and Evapotranspiration (mm) in the four water treatments. RS1 is the control experiment, RS5 is early drought, RS6 is late drought and RS11 is the full drought experiment. $\overline{MEI}$ is the numerical mean of the four variables in each water treatment.

Treatment	Model	LAI	Biomass	Grain yield	Evapotranspiration	
		MEI / RMSE	MEI / RMSE	MEI / RMSE	MEI / RMSE	$\overline{MEI}$
RS1	GLAM	0.59 / 1.69	0.94 / 1.97	0.99 / 0.26	0.99 / 22.31	0.88
RS5	GLAM	0.61 / 1.30	0.44 / 3.39	0.84 / 0.74	0.89 / 25.34	0.70
RS6	GLAM	0.40 / 1.78	0.71 / 2.89	0.94 / 0.49	0.84 / 36.03	0.72
RS11	GLAM	0.39 / 1.50	0.56 / 2.86	0.85 / 0.55	0.84 / 21.95	0.66
RS1	GLAM-Parti	0.74 / 1.34	0.95 / 1.81	1.00 / 0.23	0.99 / 23.19	0.92
RS5	GLAM-Parti	0.95 / 0.45	0.98 / 0.69	0.97 / 0.32	0.91 / 23.15	0.95
RS6	GLAM-Parti	0.80 / 1.00	0.97 / 0.99	0.98 / 0.29	0.82 / 38.76	0.89
RS11	GLAM-Parti	0.93 / 0.51	0.99 / 0.47	0.96 / 0.29	0.86 / 20.36	0.94

On the other hand, the performance of the two models varies considerably in the water stress treatments. In the early drought experiment (RS5), GLAM-Parti shows very good fit to the observations. In Fig. 2.8, both the leaf area development and the onset of leaf senescence are accurately estimated, whilst the peak LAI value is slightly underestimated. The simulated biomass and yield are also in close agreement with the observations (i.e. RMSE for biomass equals 0.69 and RMSE for yield equals 0.32), however the final yield is underestimated. On the contrary, GLAM shows lower skill in the simulation of RS5. The RMSE for LAI is higher in GLAM (1.30) than GLAM-Parti (0.45) and the biomass is underestimated during almost the whole growing season. As a result, the grain growth and final yield are underestimated (Fig. 2.8). Regarding the evapotranspiration, both models show similar results. Initially, they both overestimate the cumulative evapotranspiration and underestimate it later in the season. In summary, GLAM-Parti improves upon GLAM in the simulation of the early drought treatment (GLAM $\overline{MEI} = 0.70$, GLAM-Parti $\overline{MEI} = 0.95$).

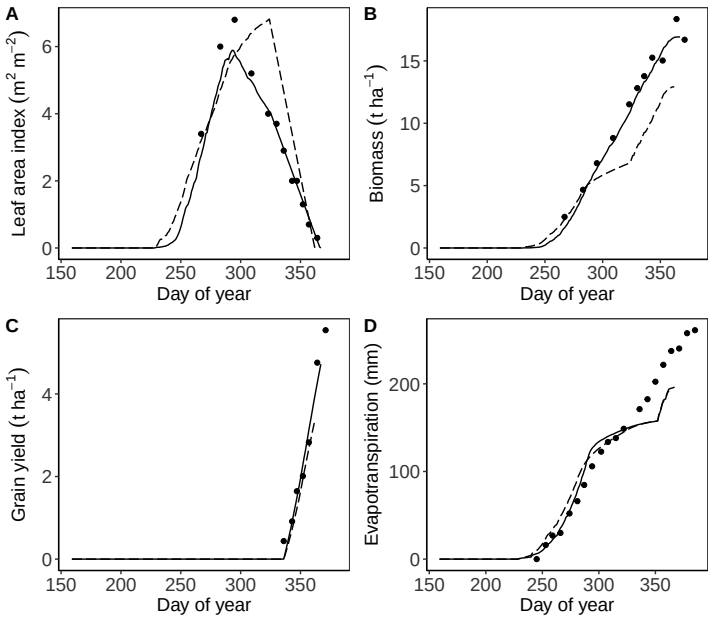

Figure 2.8: Observed values (·), GLAM (−−) and GLAM-Parti (-) output in the early drought treatment (RS5) for: A. leaf area index (LAI), B. above-ground biomass, C. grain yield, D. cumulative evapotranspiration.

In the late drought experiment (RS6), GLAM-Parti does not show an optimal agreement with the observations regarding the LAI development (RMSE = 1.00). In Fig. 2.9, the peak LAI value is slightly underestimated and the onset of LAI decline is delayed in comparison with the observations. This is due to the initiation of the water stress effects in the model later than the reality. In addition, the LAI decline rate is underestimated after anthesis. As a result, the model simulates an increased number of grain filling days, which leads to a significant overestimation of the final grain yield. Nevertheless, the above-ground biomass is well estimated (i.e. RMSE = 0.99). On

the other hand, GLAM shows lower performance in the simulation of LAI in the RS6 treatment (RMSE = 1.78). The above-ground biomass is underestimated and this leads to an underestimation of the final yield. Moreover, both models show similar results in the simulation of evapotranspiration. They are in good agreement with the observations apart from the last period of the crop cycle when it is underestimated. Overall, GLAM-Parti improves over GLAM in the simulation of the RS6 treatment (GLAM $\overline{MEI}$=0.89, GLAM-Parti $\overline{MEI}$=0.72).

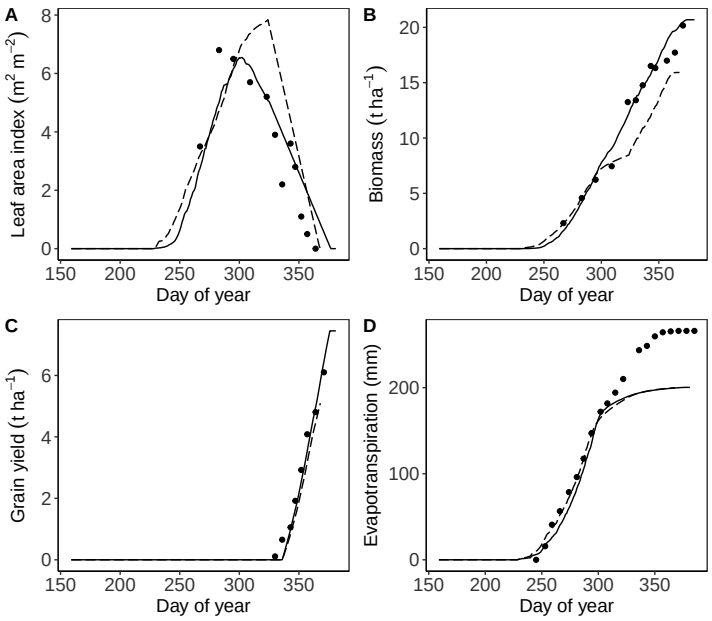

Figure 2.9: Observed values (·), GLAM (−−) and GLAM-Parti (-) output in the late drought experiment (RS6) for: A. leaf area index (LAI), B. above-ground biomass, C. grain yield, D. cumulative evapotranspiration.

In the full drought experiment (RS11), the leaf growth and senescence rate are accurately simulated in GLAM-Parti (Fig. 2.10) and the LAI is well estimated (RMSE = 0.51). Similarly, the model shows a very good fit to the observed biomass (RMSE = 0.47), whilst the final yield is slightly underestimated (RMSE = 0.29). On the contrary, GLAM shows a lower performance in the simulation of leaf growth and senescence and the estimation of LAI (RMSE = 1.50). The above-ground biomass is underestimated during almost the whole crop season, as well as the grain yield. The cumulative evapotranspiration shows similar pattern in both models, by being overestimated during the most part of the growing season and underestimated in the final part. In summary, GLAM-Parti advantages over GLAM in the simulation of the full drought treatment (GLAM $\overline{MEI}$=0.66, GLAM-Parti $\overline{MEI}$=0.94).

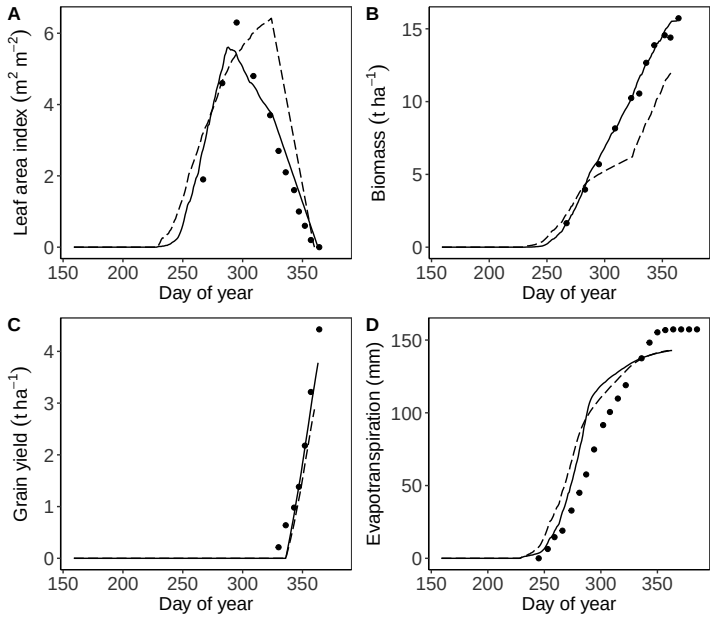

Figure 2.10: Observed values (·), GLAM (−−) and GLAM-Parti (-) output in the full drought experiment (RS11) for: A. leaf area index (LAI), B. above-ground biomass, C. grain yield, D. cumulative evapotranspiration.

2.4.2 Results of sensitivity analysis

Fig. 2.11 shows the RMSE for LAI, biomass, grain yield and evapotranspiration in the total range of LAI_{ini} in GLAM-Parti. For all compared variables, the lowest RMSE was achieved in the [0.1365-0.3] range. For the LAI_{ini} values in the low range ([0.0007-0.01]), the model showed a consistently higher RMSE for all variables, especially for LAI and biomass. The total RMSE was at least 27.5 % higher for LAI, 17.9 % higher for biomass, 5.6% higher for grain yield and 1.7% higher for evapotranspiration in the low LAI_{ini} range. This further supports the use of a LAI_{ini} value in the [0.1365-0.3] range for the model runs. Furthermore, Fig. 2.11 shows that the model calibration does not compensate for the variability in LAI_{ini} at the low range ([0.0007-0.01]). Hence, in GLAM-Parti, attention should be given to the parameterization of LAI_{ini}, since the model can be sensitive to its value.

2.4.3 Comparison of simultaneous and sequential modelling approaches

GLAM, GLAM-Parti, GLAM-Parti$_{seq}$ and GLAM-Parti$_{seq\text{-}cal}$ were compared against the observations for LAI, biomass, grain yield and evapotranspiration in the four water treatments. The RMSE was used to measure the model skill and it was calculated based on all observed and simulated values of each variable during the growing season. Fig 2.12 shows that GLAM exhibits higher total RMSE in all treatments than any GLAM-Parti version by at least 46.9 % for LAI, 92.9 % for biomass, 39.9 % for grain yield and 11.7 % for evapotranspiration (Fig. 2.12). This reveals that the model modifications

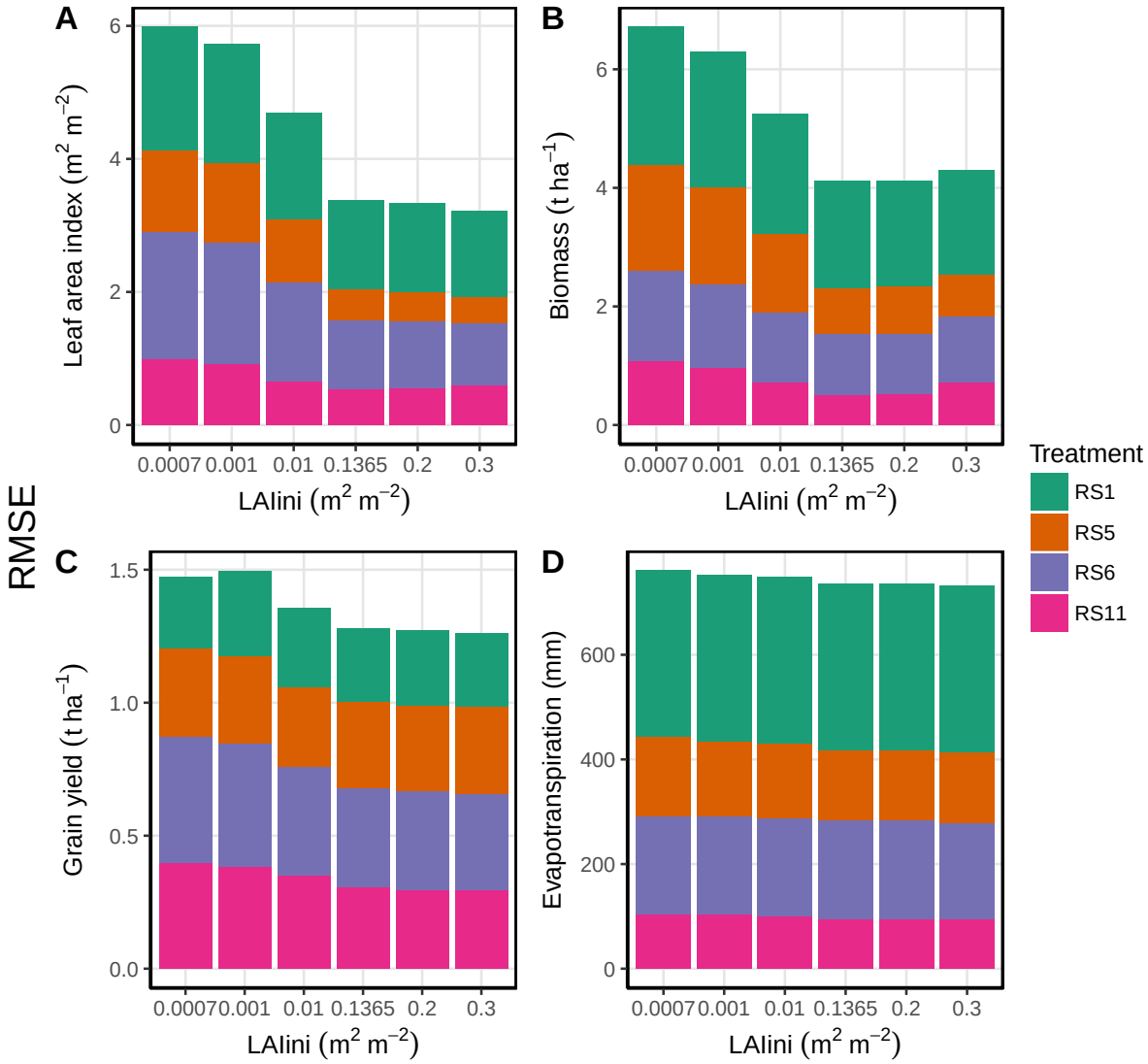

Figure 2.11: Barplots of the root mean square error (RMSE) between modelled (GLAM-Parti) and observed state variables: A. leaf area index (LAI), B. above-ground biomass, C. grain yield, D. cumulative evapotranspiration in the different water treatments: Control treatment (RS1), early drought treatment (RS5), late drought treatment (RS6), full drought treatment (RS11).

lead to significant improvement in the overall performance regardless of the modelling methodology implemented (i.e. sequential or simultaneous). Next, the impact of the model structure was tested by comparing GLAM-Parti with GLAM-Parti$_{seq}$. The total RMSE of GLAM-Parti$_{seq}$ was higher than GLAM-Parti as following: 30.4% for LAI, 49.1% for biomass, 29.3% for yield and 7.2% for evapotranspiration. Similarly, the total RMSE of GLAM-Parti$_{seq\text{-}cal}$ was higher than GLAM-Parti by 25.2% for LAI, 28.6% for biomass, 7.9% for yield and 4.9% for evapotranspiration. The above results highlight the need of solving the model equations simultaneously to overcome the structural limitations of the sequential modelling approach. In all comparisons of this study, GLAM-Parti improves upon any model version. The calibration can only partially but

not fully compensate for the inconsistencies of the sequential method. Therefore, our results indicate that the incorporation of SEMAC increases the model skill both due to the model modifications and the simultaneous modelling methodology.

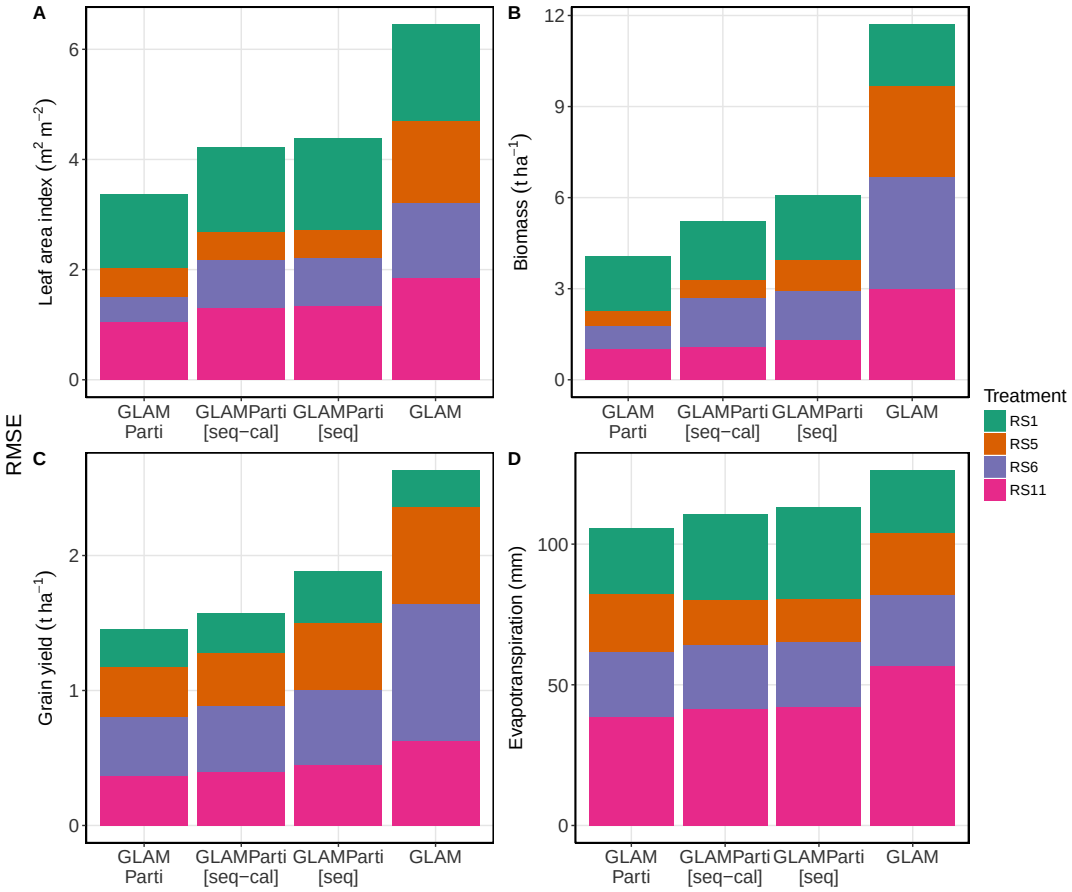

Figure 2.12: Barplots of the root mean square error (RMSE) between modelled and observed state variables: A. leaf area index (LAI), B. above-ground biomass, C. grain yield, D. cumulative evapotranspiration in the different water treatments: Control treatment (RS1), early drought treatment (RS5), late drought treatment (RS6), full drought treatment (RS11). The four models under comparison are: GLAM, GLAM-Parti, GLAM-Parti$_{\text{seq}}$ and GLAM-Parti$_{\text{seq-cal}}$.

2.5 Discussion

The incorporation of SEMAC into GLAM leads to a significant model improvement in the four rain-shelter experiments. The major differences between the two model versions rely on the simulation of the leaf dynamics, the partitioning of dry matter to the plant compartments and the model structure. The structure of GLAM requires the use of the water stress factor on the reduction of LAI growth under drought. On the contrary, GLAM-PARTI removes the stress effects from LAI. This is crucial for the model ability to simulate the observed leaf dynamics and the overall plant growth. In the experiments, under water stress there is premature leaf senescence which leads

to an earlier LAI decline. This effect cannot be captured in GLAM with the use of the water stress factor acting on LAI. The SWFAC takes only positive values (from zero to one), and when applied to the leaf area change, it leads to an increased trend of LAI growth (even though at a reduced rate) instead of the observed decline. This opposite leaf area trend gives a significant error in GLAM and it contributes to the limited model skill in capturing the water stress effects.

On the other hand, the SEMAC methodology is seen to be successful in the prediction of the leaf dynamics. The canopy SLA varies during the season and this affects both the already formed leaf tissue and the newly formed leaf area (i.e. in Eq. 2.11 the SLA acts both on the already existing LAI and the newly formed leaf area (dL)). Thus, the SLA of the previously formed leaf tissue is not conserved (*Ratjen and Kage*, 2013). The water stress factor is removed from LAI and the model error is reduced. In GLAM-Parti, the LAI value is extracted by the system of equations after incorporating the water stress effects. This technique explicitly takes into account the drought-induced changes on leaf growth and development and enables the prediction of the acceleration of leaf senescence without further parameterization. Fig. 2.13 shows the simulated LAI of all treatments until the day of anthesis, when SEMAC stops. It can be seen that the LAI curve of all drought treatments declines earlier than the control. The maximum LAI value is lower in all water stress treatments, and the LAI profile is altered, with early senescence affecting the wheat. The improved simulation of leaf senescence is due to the SEMAC methodology which introduces modifications to the leaf dynamics and the partitioning of dry matter and it extracts the leaf area change from the system of equations. Thus, the leaf area change is not restricted only to positive values during the pre - senescence stage (i.e. as in GLAM with the use of the SWFAC on LAI), but it can also be negative during any part of the crop cycle depending on the existence and the magnitude of the stress event. As a result, GLAM-Parti successfully captures the premature leaf senescence without the need of downscaling into leaf level processes. This is an important trait of SEMAC and it can be used as a significant tool in the attempt to model the plant performance in various stress environments. It is also a key aspect for the improved simulation of the drought effects in this study. The same modifications could not be implemented in the original GLAM model where LAI and biomass are not jointly determined. Hence, the inclusion of SEMAC improves the estimation of the water stress effects on wheat.

SEMAC provides a robust model structure which leads to a more realistic representation of crop growth and development as well as an improved simulation of the water stress effects. Moreover, the methodology follows the general remark that an improvement in the simulation of the leaf dynamics is essential for the further development of crop models (*Ewert*, 2004). This is especially true under stress conditions where modelling of leaf development becomes more complex and it can lead to systematic errors. For instance, it has already been seen that in modelling of heat stress, the omission

of the acceleration of leaf senescence for wheat increases the model error significantly (*Maiorano et al.*, 2017). Here, the capture of premature leaf senescence under drought in GLAM-Parti significantly improves the model performance.

The contribution of the simultaneous solution of the model equations to the model performance was separated from the model modifications. For this reason, GLAM-Parti was re-designed to solve the model equations sequentially (GLAM-Parti$_{seq}$). The comparison of GLAM-Parti and GLAM-Parti$_{seq}$ highlights the limitations of the sequential modelling approach. GLAM-Parti$_{seq}$ shows higher RMSE than GLAM-Parti in all compared variables. This reveals that the inconsistencies introduced by the sequential solution of equations affect the model skill. GLAM-Parti$_{seq\text{-}cal}$ improves the model performance but it does not fully compensate for the inconsistencies of the sequential approach. As a result, GLAM-Parti$_{seq\text{-}cal}$ has higher RMSE than GLAM-Parti for all compared variables. Thus, the simultaneous equation modelling leads to significant model improvement due to the robustness of the model structure.

SEMAC can be implemented in other transpiration or radiation use efficiency models with a similar methodology to the one presented here. Initially, allometric relationships should be introduced to partition the biomass (W_n) to the different plant compartments. This gives the opportunity to express W_n as function of LAI. The accumulation of new biomass (dW/dt) can also be expressed as function of LAI. For transpiration driven models, this can be done using an approach similar to the one presented here. In radiation use efficiency models, dW/dt can be expressed as function of LAI as shown in Fig. 2.2. The expression of W_n and dW/dt as function of LAI develops an equation similar to Eq. 2.11 which is solved to return the LAI value. This is done twice, initially for optimal environmental conditions, where the impact of stresses is ignored and then again after incorporating the stress effects. LAI is then used to calculate all variables in the system of equations. Regarding the stress effects, these can be simulated by reducing the accumulation of new biomass, altering the carbon allocation between the plant parts and adjusting the canopy SLA. Various models use different techniques to simulate these modifications. The model performance will depend on the efficiency to capture the above-mentioned effects at the canopy level. More effort may be needed to implement SEMAC in more detailed crop models (i.e. photosynthesis based models), where the model complexity may increase the difficulty of solving the system of equations simultaneously. Currently, there is no clear path on how to incorporate SEMAC in these models. Thus, the approach is mainly aimed to radiation or transpiration based models of medium complexity like GLAM. However, the possibility of implementing SEMAC in more complex models is not excluded, but simplifications in the model structure may be needed.

Finally, in the late drought treatment GLAM-Parti overestimates the final yield. This is due to the increased number of grain filling days in the model simulation. Currently SEMAC stops at anthesis and during that period GLAM-Parti runs under

the GLAM approach. Thus, SEMAC needs to be expanded for the period after anthesis. In addition, the modelling of yellow leaf mass should be improved, since Eq. 2.12 is currently not included into the system of equations.

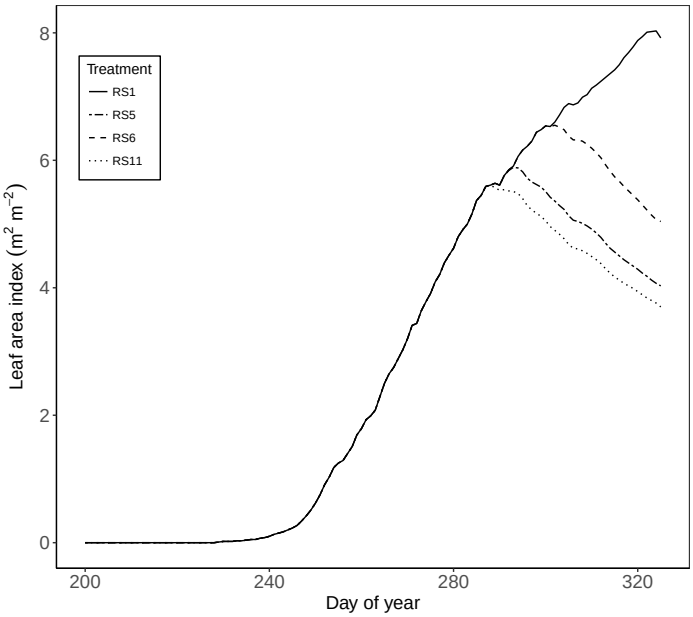

Figure 2.13: Simulated LAI of all treatments until day of anthesis in GLAM-Parti. Control treatment (RS1) (continuous line), early drought (RS5) (twodash line), late drought (RS6) (dashed line), full drought (RS11) (dotted line).

2.6 Conclusion

The application of SEMAC to crop modelling results in a new model where all equations for crop growth and development are combined and solved simultaneously. It is adopted here into the GLAM crop model and a new model version is formed (GLAM-Parti). The new model is primarily designed to deal with stress conditions, where various processes are modified and modelling the plant performance becomes more difficult.

The incorporation of SEMAC into GLAM simplifies the model algorithms and improves upon the simulation of several plant processes (e.g. LAI development, acceleration of leaf senescence under water stress conditions, leaf:stem partitioning of biomass). These alterations lead to an improved model performance and a more realistic model output. We demonstrated this by testing the two model versions against different levels of water stress. GLAM-Parti showed a clear improvement over GLAM in all drought simulations. In addition, GLAM-Parti retains its confidence at all levels of water stress in the treatments (i.e. from early to full drought treatment).

In general, we believe that a robust model structure is essential for the realistic simulation of crop performance under stress conditions. The success of SEMAC relies on the improved model structure, the better representation of the leaf dynamics and the

improved internal model consistency. SEMAC can be further extended to incorporate more stresses. Application of SEMAC to other crop models would follow a similar methodology to that presented here. It would be very interesting to see if similar improvements in skill result. Finally, it is believed that SEMAC can be a useful tool for the simulation of the crop performance under climate variability and change where multiple stresses may act on crops simultaneously.

Software and data availability

The GLAM model was developed in FORTRAN by Andy Challinor (a.j.challinor@leeds.ac.uk) and it was firstly released in 2004. The software requires a FORTRAN compiler under any operating system. The GLAM-Parti model presented in this paper was developed by Ioannis Droutsas (eegdr@leeds.ac.uk) and it is a new version of GLAM based on the SEMAC approach. GLAM is freely available following registration, please visit: https://environment.leeds.ac.uk/climate-change-impacts/doc/general-large-area-model-annual-crops. The GLAM-Parti version is currently being developed and prepared for general release. The experimental rain shelter data used in this paper has already been published by *Jamieson et al.* (1995). The dataset is available at: https://bitbucket.org/masemenov/lincoln/src/master/

Acknowledgements

I.D. gratefully acknowledges the Oatley PhD Scholarship for the financial support. AJC gratefully acknowledges the support of the Collaborative Research Program from CGIAR and Future Earth on Climate Change, Agriculture and Food Security (CCAFS), International Centre for Tropical Agriculture (CIAT), A.A. 6713, Cali, Colombia. Rothamsted Research receives grant-aided support from the Biotechnology and Biological Sciences Research Council (BBSRC) Designing Future Wheat programme [BB/P016855/1]. We thank the two anonymous reviewers whose comments have significantly improved this manuscript.

References

Affholder, F., P. Tittonell, M. Corbeels, S. Roux, N. Motisi, P. Tixier, and J. Wery (2012), Ad hoc modeling in agronomy: what have we learned in the last 15 years?, *Agronomy Journal*, *104*(3), 735–748. 2.1

Asseng, S., N. C. Turner, T. Botwright, and A. G. Condon (2003), Evaluating the impact of a trait for increased specific leaf area on wheat yields using a crop simulation model, *Agronomy Journal*, *95*(1), 10–19. 2.3.4.1

Asseng, S., P. Jamieson, B. Kimball, P. Pinter, K. Sayre, J. Bowden, and S. Howden (2004), Simulated wheat growth affected by rising temperature, increased water deficit and elevated atmospheric co2, *Field Crops Research*, *85*(2-3), 85–102. 2.2.3

Asseng, S., F. Ewert, C. Rosenzweig, J. Jones, J. Hatfield, A. Ruane, K. J. Boote, P. J. Thorburn, R. P. Rötter, D. Cammarano, et al. (2013), Uncertainty in simulating wheat yields under climate change, *Nature Climate Change*, *3*(9), 827. 2.1

Asseng, S., F. Ewert, P. Martre, R. P. Rötter, D. Lobell, D. Cammarano, B. Kimball, M. Ottman, G. Wall, J. W. White, et al. (2015), Rising temperatures reduce global wheat production, *Nature Climate Change*, *5*(2), 143. 2.1

Atkin, O. K., B. Loveys, L. J. Atkinson, and T. Pons (2005), Phenotypic plasticity and growth temperature: understanding interspecific variability, *Journal of Experimental Botany*, *57*(2), 267–281. 2.3.4.1

Baldocchi, D. (1994), An analytical solution for coupled leaf photosynthesis and stomatal conductance models, *Tree Physiology*, *14*(7-8-9), 1069–1079. 2.2.1

Baret, F., A. Olioso, and J. Luciani (1992), Root biomass fraction as a function of growth degree days in wheat, *Plant and soil*, *140*(1), 137–144. 2.3.4.4

Brisson, N., and M.-L. Casals (2005), Leaf dynamics and crop water status throughout the growing cycle of durum wheat crops grown in two contrasted water budget conditions, *Agronomy for sustainable development*, *25*(1), 151–158. 2.2.3

Challinor, A., T. Wheeler, P. Craufurd, J. Slingo, and D. Grimes (2004), Design and optimisation of a large-area process-based model for annual crops, *Agricultural and forest meteorology*, *124*(1-2), 99–120. 2.3.1, 2.3.4.4, 2.3.4.4, 2.3.10

Challinor, A., J. Slingo, T. Wheeler, and F. Doblas-Reyes (2005), Probabilistic simulations of crop yield over western india using the demeter seasonal hindcast ensembles, *Tellus A*, *57*(3), 498–512. 2.3.1

Challinor, A. J., F. Ewert, S. Arnold, E. Simelton, and E. Fraser (2009), Crops and climate change: progress, trends, and challenges in simulating impacts and informing adaptation, *Journal of experimental botany*, *60*(10), 2775–2789. 2.1

Challinor, A. J., M. S. Smith, and P. Thornton (2013), Use of agro-climate ensembles for quantifying uncertainty and informing adaptation, *Agricultural and Forest Meteorology*, *170*, 2–7. 2.1

Challinor, A. J., J. Watson, D. Lobell, S. Howden, D. Smith, and N. Chhetri (2014), A meta-analysis of crop yield under climate change and adaptation, *Nature Climate Change*, *4*(4), 287. 2.1

Challinor, A. J., C. Müller, S. Asseng, C. Deva, K. J. Nicklin, D. Wallach, E. Vanuytrecht, S. Whitfield, J. Ramirez-Villegas, and A.-K. Koehler (2018), Improving the use of crop models for risk assessment and climate change adaptation, *Agricultural systems*, *159*, 296–306. 2.1

Chenu, K., J. R. Porter, P. Martre, B. Basso, S. C. Chapman, F. Ewert, M. Bindi, and S. Asseng (2017), Contribution of crop models to adaptation in wheat, *Trends in plant science*, *22*(6), 472–490. 2.1

Chou, J. C., and M. Kamel (1988), Quaternions approach to solve the kinematic equation of rotation, a/sub a/a/sub x/= a/sub x/a/sub b/, of a sensor-mounted robotic manipulator, in *Robotics and Automation, 1988. Proceedings., 1988 IEEE International Conference on*, pp. 656–662, IEEE. 2.1

Cramer, G. R., K. Urano, S. Delrot, M. Pezzotti, and K. Shinozaki (2011), Effects of abiotic stress on plants: a systems biology perspective, *BMC plant biology*, *11*(1), 163. 2.2.2

Enquist, B. J., J. H. Brown, and G. B. West (1998), Allometric scaling of plant energetics and population density, *Nature*, *395*(6698), 163. 2.3.4.2

Ewert, F. (2004), Modelling plant responses to elevated co2: how important is leaf area index?, *Annals of botany*, *93*(6), 619–627. 2.5

Ewert, F., R. P. Rötter, M. Bindi, H. Webber, M. Trnka, K. C. Kersebaum, J. E. Olesen, M. K. van Ittersum, S. Janssen, M. Rivington, et al. (2015), Crop modelling for integrated assessment of risk to food production from climate change, *Environmental Modelling & Software*, *72*, 287–303. 2.2.3

Fernández, R. J., and J. F. Reynolds (2000), Potential growth and drought tolerance of eight desert grasses: lack of a trade-off?, *Oecologia*, *123*(1), 90–98. 2.2.3

Gale, M., and D. Grigal (1987), Vertical root distributions of northern tree species in relation to successional status, *Canadian Journal of Forest Research*, *17*(8), 829–834. 2.3.4.4

Goudriaan, J., and H. Van Laar (1994), *Modelling Potential Crop Growth Processes: Textbook with Exercises*, vol. 2, Springer Science & Business Media. 2.2.1

Gray, S. B., and S. M. Brady (2016), Plant developmental responses to climate change, *Developmental biology*, *419*(1), 64–77. 2.2.4

Hoogenboom, G., J. Jones, and K. Boote (1992), Modeling growth, development, and yield of grain legumes using soygro, pnutgro, and beangro: a review, *Transactions of the ASAE*, *35*(6), 2043–2056. 2.3.4.1

Hotsonyame, G., and L. Hunt (1998), Seeding date, photoperiod and nitrogen effects on specific leaf area of field-grown wheat, *Canadian journal of plant science*, *78*(1), 51–61. 2.3.4.1

Howden, S. M., J.-F. Soussana, F. N. Tubiello, N. Chhetri, M. Dunlop, and H. Meinke (2007), Adapting agriculture to climate change, *Proceedings of the national academy of sciences*, *104*(50), 19,691–19,696. 2.1

Inoue, T., S. Inanaga, Y. Sugimoto, and K. El Siddig (2004), Contribution of preanthesis assimilates and current photosynthesis to grain yield, and their relationships to drought resistance in wheat cultivars grown under different soil moisture, *Photosynthetica*, *42*(1), 99–104. 2.3.1

Jamieson, P., and F. Ewert (1999), The role of roots in controlling soil water extraction during drought: an analysis by simulation, *Field Crops Research*, *60*(3), 267–280. 2.3.4.4

Jamieson, P., R. Martin, and G. Francis (1995), Drought influences on grain yield of barley, wheat, and maize, *New Zealand journal of crop and horticultural science*, *23*(1), 55–66. 2.3.8, 2.6

Jamieson, P., J. Porter, J. Goudriaan, J. v. Ritchie, H. Van Keulen, and W. Stol (1998), A comparison of the models afrcwheat2, ceres-wheat, sirius, sucros2 and swheat with measurements from wheat grown under drought, *Field Crops Research*, *55*(1-2), 23–44. 2.2.3

Jones, G. D., B. Droz, P. Greve, P. Gottschalk, D. Poffet, S. P. McGrath, S. I. Seneviratne, P. Smith, and L. H. Winkel (2017), Selenium deficiency risk predicted to increase under future climate change, *Proceedings of the National Academy of Sciences*, p. 201611576. 2.1

Kanemasu, E., G. Asrar, and M. Fuchs (1985), Application of remotely sensed data in wheat growth modelling, in *Wheat Growth and Modelling*, pp. 357–369, Springer. 2.3.10

King, J., A. Gay, R. SYLVESTER-BRADLEY, I. Bingham, J. Foulkes, P. Gregory, and D. Robinson (2003), Modelling cereal root systems for water and nitrogen capture: towards an economic optimum, *Annals of Botany*, *91*(3), 383–390. 2.3.4.4, 2.3.4.4

Krause, P., D. Boyle, and F. Bäse (2005), Comparison of different efficiency criteria for hydrological model assessment, *Advances in geosciences*, *5*, 89–97. 2.3.9

Lefcheck, J. S. (2016), piecewisesem: Piecewise structural equation modelling in r for ecology, evolution, and systematics, *Methods in Ecology and Evolution*, *7*(5), 573–579. 2.1

Leutscher, K., and J. Vogelezang (1990), A crop growth simulation model for operational management support in pot plant production, *Agricultural systems*, *33*(2), 101–114. 2.3.4.1

Liu, C., X. Zhang, and Y. Zhang (2002), Determination of daily evaporation and evapotranspiration of winter wheat and maize by large-scale weighing lysimeter and micro-lysimeter, *Agricultural and Forest Meteorology*, *111*(2), 109–120. 2.3.10

Loomis, R. S., R. Rabbinge, and E. Ng (1979), Explanatory models in crop physiology, *Annual Review of Plant Physiology*, *30*(1), 339–367. (document), 2.3, 2.4

Loveys, B., I. Scheurwater, T. Pons, A. Fitter, and O. Atkin (2002), Growth temperature influences the underlying components of relative growth rate: an investigation using inherently fast-and slow-growing plant species, *Plant, Cell & Environment*, *25*(8), 975–988. 2.3.4.1

Ma, G., J. Huang, W. Wu, J. Fan, J. Zou, and S. Wu (2013), Assimilation of modis-lai into the wofost model for forecasting regional winter wheat yield, *Mathematical and Computer Modelling*, *58*(3-4), 634–643. 2.3.6

Mahrookashani, A., S. Siebert, H. Hüging, and F. Ewert (2017), Independent and combined effects of high temperature and drought stress around anthesis on wheat, *Journal of Agronomy and Crop Science*, *203*(6), 453–463. 2.3.1

Maiorano, A., P. Martre, S. Asseng, F. Ewert, C. Müller, R. P. Rötter, A. C. Ruane, M. A. Semenov, D. Wallach, E. Wang, et al. (2017), Crop model improvement reduces the uncertainty of the response to temperature of multi-model ensembles, *Field crops research*, *202*, 5–20. 2.5

Marcelis, L., and E. Heuvelink (2007), Concepts of modelling carbon allocation among plant organs, *Frontis*, pp. 103–111. 2.2.1

Marcelis, L., E. Heuvelink, and J. Goudriaan (1998), Modelling biomass production and yield of horticultural crops: a review, *Scientia Horticulturae*, *74*(1-2), 83–111. 2.1, 2.3.4.1

Martre, P., B. A. Kimball, M. J. Ottman, G. W. Wall, J. W. White, S. Asseng, F. Ewert, D. Cammarano, A. Maiorano, P. K. Aggarwal, et al. (2018), The hot serial cereal experiment for modeling wheat response to temperature: field experiments and agmip-wheat multi-model simulations, *Open Data Journal for Agricultural Research*, *4*, 28–34. 2.3.4.1

Mittler, R. (2006), Abiotic stress, the field environment and stress combination, *Trends in plant science*, *11*(1), 15–19. 2.2.4

Myers, S. S., A. Zanobetti, I. Kloog, P. Huybers, A. D. Leakey, A. J. Bloom, E. Carlisle, L. H. Dietterich, G. Fitzgerald, T. Hasegawa, et al. (2014), Increasing co 2 threatens human nutrition, *Nature*, *510*(7503), 139. 2.1

Oldroyd, J. (1950), On the formulation of rheological equations of state, *Proc. R. Soc. Lond. A*, *200*(1063), 523–541. 2.1

Osborne, T., G. Rose, and T. Wheeler (2013), Variation in the global-scale impacts of climate change on crop productivity due to climate model uncertainty and adaptation, *Agricultural and Forest Meteorology*, *170*, 183–194. 2.3.1

Passioura, J. B. (1996), Simulation models: science, snake oil, education, or engineering?, *Agronomy Journal*, *88*(5), 690–694. 2.1

Poorter, H., K. J. Niklas, P. B. Reich, J. Oleksyn, P. Poot, and L. Mommer (2012), Biomass allocation to leaves, stems and roots: meta-analyses of interspecific variation and environmental control, *New Phytologist*, *193*(1), 30–50. 2.2.2, 2.3.4.2

Porter, J. R., L. Xie, A. J. Challinor, K. Cochrane, S. M. Howden, M. M. Iqbal, D. B. Lobell, M. I. Travasso, N. C. Netra Chhetri, K. Garrett, et al. (2014), Food security and food production systems. 2.1

Raes, D., P. Steduto, T. C. Hsiao, and E. Fereres (2009), Aquacropthe fao crop model to simulate yield response to water: Ii. main algorithms and software description, *Agronomy Journal*, *101*(3), 438–447. 2.2.3

Ramirez-Villegas, J., A.-K. Koehler, and A. J. Challinor (2017), Assessing uncertainty and complexity in regional-scale crop model simulations, *European Journal of Agronomy*, *88*, 84–95. 2.3.3

Ratjen, A., D. Neukam, and H. Kage (2016), A simple drought-sensitive model for leaf: Stem partitioning of wheat, *Journal of agronomy and crop science*, *202*(4), 300–308. 2.2.3, 2.3.4.2, 2.3.5.2

Ratjen, A. M., and H. Kage (2013), Is mutual shading a decisive factor for differences in overall canopy specific leaf area of winter wheat crops?, *Field Crops Research*, *149*, 338–346. 2.5

Rivington, M., and J. Koo (2010), Report on the meta-analysis of crop modelling for climate change and food security survey. 2.1

Rosbakh, S., C. Römermann, and P. Poschlod (2015), Specific leaf area correlates with temperature: new evidence of trait variation at the population, species and community levels, *Alpine botany*, *125*(2), 79–86. 2.3.4.1

Sieling, K., U. Böttcher, and H. Kage (2016), Dry matter partitioning and canopy traits in wheat and barley under varying n supply, *European journal of agronomy*, *74*, 1–8. 2.2.2

Sinclair, T. R., and N. Seligman (2000), Criteria for publishing papers on crop modeling, *Field Crops Research*, *68*(3), 165–172. 2.1

Stella, T., N. Frasso, G. Negrini, S. Bregaglio, G. Cappelli, M. Acutis, and R. Confalonieri (2014), Model simplification and development via reuse, sensitivity analysis and composition: a case study in crop modelling, *Environmental modelling & software*, *59*, 44–58. 2.1, 2.3.6

Tao, F., R. P. Rötter, T. Palosuo, C. Gregorio Hernández Díaz-Ambrona, M. I. Mínguez, M. A. Semenov, K. C. Kersebaum, C. Nendel, X. Specka, H. Hoffmann, et al. (2018), Contribution of crop model structure, parameters and climate projections to uncertainty in climate change impact assessments, *Global change biology*, *24*(3), 1291–1307. 2.1

Taylor, S., M. Payton, and W. Raun (1999), Relationship between mean yield, coefficient of variation, mean square error, and plot size in wheat field experiments, *Communications in Soil Science and Plant Analysis*, *30*(9-10), 1439–1447. 2.3.4.1

Van Ittersum, M., and R. Rabbinge (1997), Concepts in production ecology for analysis and quantification of agricultural input-output combinations, *Field crops research*, *52*(3), 197–208. (document), 2.1

van Ittersum, M. K., P. A. Leffelaar, H. Van Keulen, M. J. Kropff, L. Bastiaans, and J. Goudriaan (2003), On approaches and applications of the wageningen crop models, *European journal of agronomy*, *18*(3-4), 201–234. (document), 2.2.1, 2.1

Weiner, J. (2004), Allocation, plasticity and allometry in plants, *Perspectives in Plant Ecology, Evolution and Systematics*, *6*(4), 207–215. 2.2.2

Yin, X., and P. Struik (2009), C3 and c4 photosynthesis models: an overview from the perspective of crop modelling, *NJAS-Wageningen Journal of Life Sciences*, *57*(1), 27–38. 2.2.1

Yin, X., and P. C. Struik (2010), Modelling the crop: from system dynamics to systems biology, *Journal of Experimental Botany*, *61*(8), 2171–2183. 2.3.4.1

Zeng, D., and J. Cai (2005), Simultaneous modelling of survival and longitudinal data with an application to repeated quality of life measures, *Lifetime Data Analysis*, *11*, 151–174. 2.1

Zhang, B., W. Liu, S. X. Chang, and A. O. Anyia (2010), Water-deficit and high temperature affected water use efficiency and arabinoxylan concentration in spring wheat, *Journal of cereal science*, *52*(2), 263–269. 2.2.3

Zhang, S., and F. Tao (2013), Modeling the response of rice phenology to climate change and variability in different climatic zones: comparisons of five models, *European journal of agronomy*, *45*, 165–176. 2.1

Zhao, C., B. Liu, S. Piao, X. Wang, D. B. Lobell, Y. Huang, M. Huang, Y. Yao, S. Bassu, P. Ciais, et al. (2017), Temperature increase reduces global yields of major crops in four independent estimates, *Proceedings of the National Academy of Sciences*, *114*(35), 9326–9331. 2.1

Chapter 3

A new model of ozone stress in wheat including grain yield loss and plant acclimation to the pollutant

I. Droutsas[1,2], A. J. Challinor[1,2], S. R. Arnold[1], T. N. Mikkelsen[1] and E. M. . Hansen[1]

[1] *Institute for Climate and Atmospheric Science, School of Earth and Environment, University of Leeds, LS2 9JT Leeds, UK*

[2] *Priestley International Centre for Climate, University of Leeds, LS2 9JT, Leeds, UK*

[3] *Department of Environmental Engineering, Technical University of Denmark, DK-2800 Lyngby, Denmark*

[4] *Department of People and Technology, Roskilde University, Universitetsvej 1, DK-4000 Roskilde, Denmark*

Abstract

Surface ozone (O_3) is an important air pollutant globally and enhanced concentrations lead to crop yield penalties in many parts of the world. Crop models simulate production and yield and they are often used for various applications. However, most of the existing models neglect the effect of O_3 and only limited parameterization schemes exist. In addition, the existing O_3 modelling approaches do not take into account the plant acclimation to the pollutant as a mechanism of survival and maintenance of performance. Here, we introduce a simple modelling method to simulate the O_3 damage to wheat with consideration of the plant acclimation process. The O_3 parameterization scheme was incorporated into the GLAM-Parti crop model, resulting in a new model

version GLAM-ROC (i.e. GLAM - Relative Ozone Concentrations). The new model simulates the effect of O_3 on crop growth and development and was evaluated against data from control-environment chambers with high O_3 concentration levels and variable duration of exposure to the pollutant. GLAM-ROC successfully reproduced the observed plant response to O_3 as well as the final biomass and yield. The incorporation of plant acclimation allowed the prediction of crop yield loss at variable duration of O_3 exposure. The statistical response formula neglected the acclimation process and overestimated the relative O_3 damage to yield by 56.5%, when fumigation increased from 32 to 106 days. We conclude that the plant acclimation to chronic O_3 environment is significant and should be taken into account for the effect of O_3 on wheat performance and yield.

3.1 Introduction

Ground-level ozone (O_3) is a highly phytotoxic air pollutant at global scale (*Ashmore*, 2005; *Ainsworth*, 2017). Current O_3 levels induce crop yield damage and lead to decreased food supply and economic loss (*Emberson et al.*, 2009; *McGrath et al.*, 2015). *Avnery et al.* (2011) estimated that global yields of soybean and wheat were reduced by up to 14 and 15% respectively for the year 2000 due to O_3 pollution. *Mills et al.* (2018) estimated that in highly polluted regions of N India and NW China the O_3 damage to wheat yield exceeded 15% on average for the years 2010 - 2012. O_3 concentrations are projected to remain enhanced in many regions in the future, potentially posing serious threat to agriculture (*Sicard et al.*, 2017).

The main mechanisms through which O_3 affects crops are by inhibiting photosynthesis, accelerating the plant senescence rate and causing leaf chlorosis or necrosis under under acute exposure (*Heath*, 1994; *Farage and Long*, 1999; *Fiscus et al.*, 2005). These effects result in decreased photosynthate allocation to the grain, reduced productivity and lower yield (*Wilkinson et al.*, 2012). The range of effects depends upon the concentration level of the pollutant, the time and duration of exposure (*Heath et al.*, 2009), the plant sensitivity (*Van Goethem et al.*, 2013) and the stage of plant development (*Tiedemann and Pfähler*, 1994; *Mulholland et al.*, 1998).

The effect of O_3 on crop yield has been extensively studied and various modelling approaches have been suggested. Initially, different metrics were developed to link the plant O_3 exposure to the reduction in grain yield. These metrics accumulate the O_3 concentration during the crop-growing season (e.g. AOT40, M7, SUM06, W126) and relate the effect to yield according to a statistical response function (e.g. *Fuhrer et al.*, 1997; *Mauzerall and Wang*, 2001). However, various interactions between the crops and their surrounding environment modify the magnitude of this relationship (*Musselman et al.*, 2006). This is a major limitation of exposure-based approaches and so O_3 effects were later introduced into more complex models of plant growth and development.

The family of more complex models tend to use stomatal flux parameterizations (e.g. *Emberson et al.*, 2000; *Pleijel et al.*, 2007) such as those found in crop models (e.g. *Ewert and Porter*, 2000; *Schauberger et al.*, 2019). These models can improve upon the exposure-based estimation of O_3 damage to crop productivity and yield by simulating the stomatal limitations which regulate O_3 uptake by the plants (*Challinor et al.*, 2009; *Pleijel et al.*, 2004). Nevertheless, the modelling of stomatal conductance is difficult and it is not clear which of the many models of different complexity (*Damour et al.*, 2010) is closest to reality. Modelled responses to CO_2 concentration, temperature, air humidity, light and soil water content differ (*Buckley and Mott*, 2013), resulting in different errors in the calculation of O_3 uptake and damage.

Plants can adjust their physiological and metabolic processes to enhance their stress tolerance over time (*Bruce et al.*, 2007). Under long-term O_3 exposure, the plant anti-oxidative enzyme activity increases (*Gillespie et al.*, 2011, 2012), working as a mechanism of defence in favour of closing stomata to avoid take-up of O_3 (*Feng et al.*, 2016). This acclimation mechanism allows stomata to remain partially open and support gas exchange for photosynthesis, thus avoiding high reductions in biomass accumulation (*Chen et al.*, 2011). The acclimation process in stress environments improves the plant response to the stressor (*Kollist et al.*, 2018) and leads to optimisation of productivity and yield. *Held et al.* (1991) exposed radish plants to high O_3 either six days after germination or three days later and found that the plants which were exposed to the pollutant for the longer period exhibited higher dry mass than the plants exposed to O_3 later, implying an acclimation mechanism. Trees can also compensate for the negative O_3 effects by activating acclimation mechanisms. *Mikkelsen and Ro-Poulsen* (1994) reported higher photosynthesis levels of Norway spruce in the morning before 8-h daily O_3 fumigation, as well as five days post-O_3 fumigation in comparison with non-fumigated trees. Crop models do not usually parameterize for plant acclimation to chronic O_3 stress. One barrier to the development of acclimation parameterizations in crop models is that the models are not evaluated under variable duration of exposure to O_3.

The purpose of this study is to incorporate the effect of O_3 into a crop model by accounting for the concentration level of the pollutant, the stage of plant development and the duration of plant exposure. The wheat crop was selected as case study since it is particularly sensitive to O_3 (*Barnes et al.*, 1990; *Farage et al.*, 1991; *Burney and Ramanathan*, 2014), an important staple crop at global level (*FAO et al.*, 2017) and there is excellent data availability. The GLAM-Parti crop model was used to incorporate the effect of O_3 on wheat, resulting in a new model version called GLAM-ROC (i.e. GLAM-Relative Ozone Concentrations). Prior to the incorporation of the O_3 effect, the allometric relationships for partitioning plant biomass in GLAM-Parti were extended to the full crop cycle, since the model was previously developed with the GLAM approach for post-anthesis crop growth and development.

3.2 Materials and methods

3.2.1 Wheat varieties and growing conditions

Two modern spring wheat varieties were considered in this study, Lennox (Saaten-Union) used in southern France and KWS Bittern (DanishAgro) used in Denmark. Lennox was used for the development of the O_3 algorithm in the model and KWS Bittern for the model evaluation. The plants were grown in 24 m^2 chambers in the RERAF (Risø Environmental Risk Assessment Facility) climate phytotron at the Technical University of Denmark, Campus Risø, Roskilde. The plants were sown in 11 L pots filled with 4 kg of sphagnum (Pindstrup Substrate No. 4, Pindstrup Mosebrug A/S, Ryomgaard, Denmark) and reduced to eight plants after germination, corresponding to $\sim$ 165 plants m^{-2}. Light intensity in the chambers was approximately 400 mol photons m^{-2} s^{-1} PAR (photosynthetically active radiation) at canopy height and was provided for 16 h d^{-1}. The growing conditions in the chambers are shown in Table 3.1. The plants were watered three times a week to ensure full water supply. No additional nutrients were added to the pots since the sphagnum was nutrient enriched. Both varieties were represented by five replicates in each treatment. Detailed description of the experimental set-up is given in *Hansen et al.* (2019), *Frenck et al.* (2011) and *Ingvordsen et al.* (2015).

Table 3.1: Mean and standard deviation of growing conditions in RERAF chambers for wheat culitvars Lennox and KWS Bittern.

Treatment	Temperature, day/night (C)	Humidity, day/night (%)	$[O_3]$ (ppb)	$[CO_2]$ (ppm)
Control	19.4± 2.5 / 13.8± 4.1	53.7± 5.3 / 65.8± 8.3	6.4 ± 2.1	534 ± 109
Episodic	19.4± 2.5 / 14.0± 4.1	54.2± 5.2 / 65.5± 8.0	84.5 ± 28.1	539 ± 109
Chronic	19.4± 2.5 / 13.9± 4.1	53.7± 5.4 / 65.5± 8.3	78.8 ± 32.4	537 ± 111

3.2.2 Ozone treatments

O_3 was generated by UV Pro 550 A ozone generators (Crystal Air Products and Services, Langley, BC, Canada). The experiments included 3 levels of fumigation: i) no O_3 enrichment (Control); ii) episodic O_3 exposure (Episodic) ; and iii) full-time O_3 exposure (Chronic) (Fig. 3.1 and Table 3.1). In the Control treatment, O_3 concentration in the climate chambers was 6.4 ± 2.1 ppb during the whole crop cycle. In the Chronic treatment, the plants were exposed to 78.8 ± 32.4 ppb O_3 concentration during the daylight hours from sowing (Zadoks Stage 01 - ZS 01) to harvest maturity (ZS 99). In the Episodic treatment, O_3 concentration was 84.5 ± 28.1 ppb during the daylight hours and the duration of plant exposure was from the first node stage (ZS 31) until anthesis was complete (ZS 69). During the night, in both the Chronic and Episodic treatment, O_3 concentration was reduced to the Control level.

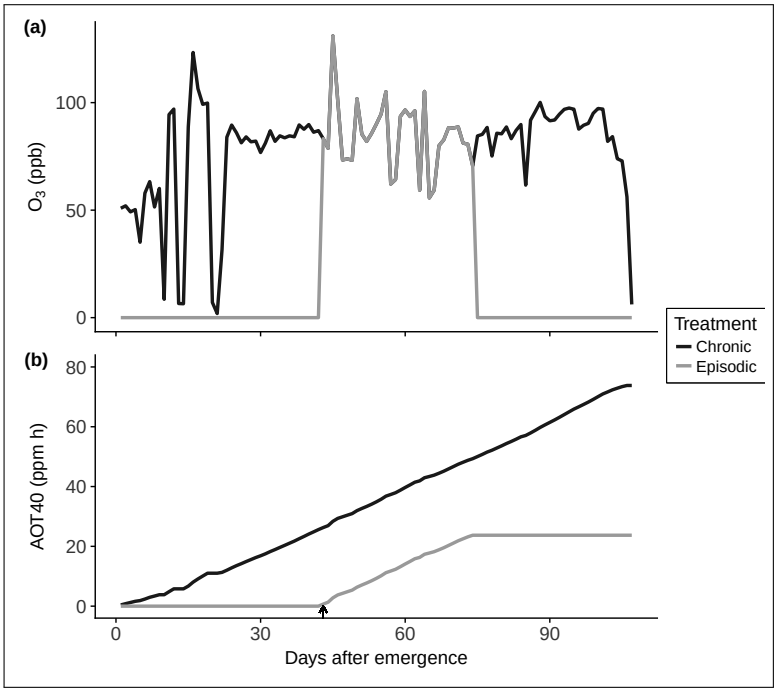

Figure 3.1: (a) Daily mean O_3 concentration (ppb) and (b) cumulative O_3 exposure above 40 ppb (AOT40) calculated from hourly [O_3] in Chronic and Episodic treatment. Arrow indicates day when plants reached ZS 31 (Zadoks stage 31).

3.2.3 Plant measurements and calculation of evapotranspiration and water use efficiency

At the end of the experiment, the plants were harvested and dried for 48 h at 80 °C. The above-ground biomass and grain yield were measured in g pot^{-1} and were converted to g m^{-2} using the pot dimensions. This allowed direct comparison between the observations and the model output. The plant water consumption (g pot^{-1}) was calculated as the difference in pot weight between two consecutive measurements. Assuming that the increase in plant weight between two measurements was negligible, we calculated canopy evapotranspiration (ET) (mm) as following:

$$ET = ((Wp_n - Wp_{n+1})/\rho \cdot pot) \cdot 1000mm/m \tag{3.1}$$

where Wp_n and Wp_{n+1} are the pot weight directly after the n irrigation (kg) and directly before the n+1 irrigation (kg) respectively, pot is the number of pots per m^2 and ρ is water density (997 kg m^3). Harvest index (HI) was calculated as the ratio of grain yield to above-ground biomass.

The biomass, grain yield, ET, HI and water use efficiency (WUE) of Lennox and KWS Bittern wheat in the experiments were calculated as the mean of the 5 replicates. The replicate 2 of Lennox in the Control and the replicate 5 of KWS Bittern in the Chronic treatment were disregarded due to errors in the measurements of pot weight.

Also WUE (g m^{-2} mm^{-1}) was defined as the ratio of the above-ground biomass (g m^{-2}) to total ET (mm) at harvest.

3.2.4 Ozone metrics

The AOT40 index (Accumulated ozone exposure above a threshold of 40 ppbv) was calculated as follows:

$$AOT40 = \sum_{i=1}^{n} DOE40_i \tag{3.2}$$

where n is the number of days in the growing season, i is the day index and DOE40 is the daily O_3 exposure (ppm h) defined as:

$$DOE40 = \sum_{j=1}^{m} max([O_3]_j - 40ppb, 0) \cdot 0.001\, ppmh\, ppbh^{-1} \tag{3.3}$$

where $[O_3]$ is the one hour mean O_3 concentration (ppb), m is the number of daylight hours per day and j is the hour index.

3.2.5 GLAM-Parti model

The GLAM-Parti crop model was developed based on the General Large Area Model for annual crops (GLAM) which is a relatively simple model designed to operate at regional scale (*Challinor et al.*, 2004). The model was selected for the incorporation of the effect of O_3 on wheat, since it was developed with the SEMAC approach (Simultaneous Equation Modelling for Annual Crops), a novel crop modelling methodology which provides with a consistent representation of abiotic stresses and ensures internal consistency in the simulation of crop growth and development under environmental stress conditions (*Droutsas et al.*, 2019). GLAM-Parti uses transpiration efficiency to simulate crop growth and allometric relationships for partitioning the biomass to the plant compartments. The daily potential evapotranspiration is calculated by the Priestley-Taylor approach and is partitioned into potential evaporation and potential transpiration. The actual transpiration is computed from the potential transpiration rate by taking into account the soil water content. The transpiration is multiplied by the transpiration efficiency to return the daily biomass growth.

Two major modifications were implemented into GLAM-Parti for this study. Firstly, the canopy SLA was expressed as function of LAI (see B.0.1). In addition, the plant biomass partitioning scheme with allometric relationships was extended to the post-anthesis period (see B.0.2). This method replaced the previously used GLAM approach for simulating crop growth and development after anthesis in GLAM-Parti.

3.2.6 GLAM-ROC development

GLAM-ROC is the version of GLAM-Parti which incorporates the effect of O_3 on crop growth and development. The O_3 damage to wheat was introduced into the model by reducing the canopy ET as well as transpiration efficiency (TE) in daily time step. The effect of O_3 on ET was related to the AOT40 index and the reduction in TE was expressed as function of $[O_3]$. An acclimation factor was introduced to simulate the plant adjustment to stress conditions with increased O_3 exposure. Harvest Index was also reduced to account for decreased allocation of assimilates to the grains under exposure to enhanced O_3 during the grain-filling period.

3.2.6.1 Modelling ozone effects on evapotranspiration

Plant exposure to O_3 decreases leaf transpiration due to stomatal closure (*Temple*, 1986; *Bernacchi et al.*, 2011), which may have widespread implications for atmospheric moisture and climate (*Arnold et al.*, 2018; *Lombardozzi et al.*, 2012). Data analysis was conducted to examine the effect of O_3 on cumulative evapotranspiration (CET) during the exposure to the pollutant. CET was calculated as:

$$CET = \sum_{i=1}^{n} ET_i \tag{3.4}$$

where ET is canopy evapotranspiration, i is the day index and n is the number of days after planting. Data from the variety Lennox was used to compare the differences in CET between the Control, Chronic and Episodic treatment.

CET exhibited a significant response to O_3 in both the Episodic and Chronic treatment, which showed 6.2% and 13.4% lower end-of-season CET respectively in comparison with the Control (Fig. 3.2). Nevertheless, the O_3 impact varied in magnitude with time and the plant sensitivity to O_3 was investigated according to the growth stage. The crop cycle was separated into three stages, from seed germination (ZS 01) to the first node stage (ZS 31) (Stage 1), the first node stage to the end of anthesis (ZS 69) (Stage 2) and from the end of anthesis to harvest maturity (ZS 99) (Stage 3). We used the Pearson test to examine the differences in CET between the Control and Chronic as well as Control and Episodic treatment (Table 3.2). During Stage 1, there was a weak, non-significant correlation between the two variables (p-value >0.05). At that stage, only the plants in the Chronic treatment were fumigated with O_3. This shows that the effect of O_3 before ZS 31 was not significant. On the other hand, during Stages 2 and 3 there was a significant positive correlation in the difference in CET between Control and Chronic and Control and Episodic treatment (i.e. p-value < 0.001 in both stages). This implies that the O_3 impact was significant during Stages 2 and 3. Thus, the negative effects of O_3 on wheat were considered to initiate at the onset of stem elongation (ZS 31) until crop maturity.

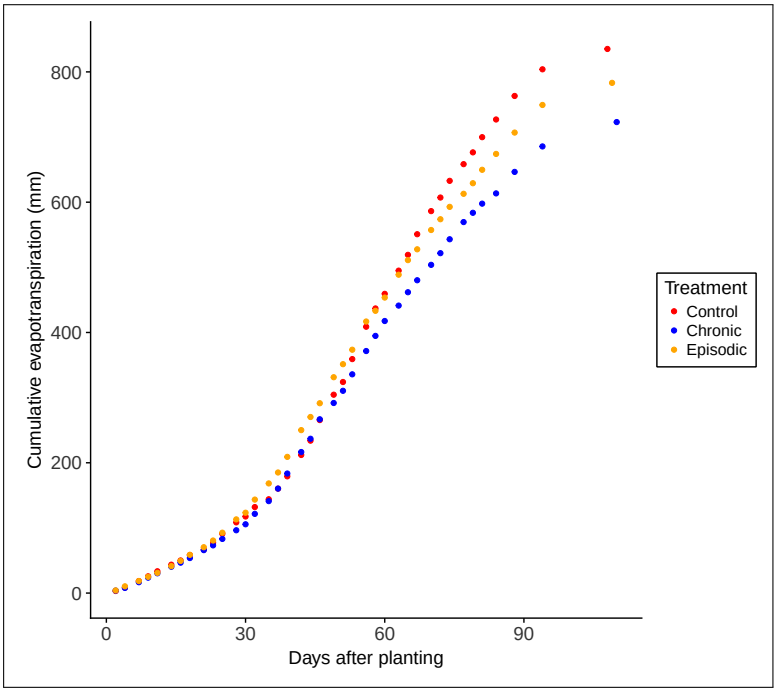

Figure 3.2: Cumulative evapotranspiration (CET) (mm) of wheat variety Lennox from planting to harvest for Control, Chronic and Episodic O_3 treatment.

Table 3.2: Correlation coefficients for difference in cumulative evapotranspiration (CET) between Control and Chronic as well as Control and Episodic O_3 treatment. Stage 1 is from seed germination (ZS 01) to first node (ZS 31), Stage 2 is from first node to end of anthesis (ZS 69) and Stage 3 is from end of anthesis to harvest maturity (ZS 99).

	corr	p-value	Test
Stage 1	0.28	0.28	Pearson
Stage 2	0.98	<0.001	Pearson
Stage 3	0.97	<0.001	Pearson

Next, we calculated the percentage change in CET (pCET) between the control and O_3-fumigated plants as follows:

$$pCET_{oz} = (CET_{cc} - CET_{oz})/CET_{oz} \tag{3.5}$$

$$pCET_{ep.oz} = (CET_{cc} - CET_{ep.oz})/CET_{ep.oz} \tag{3.6}$$

where $pCET_{oz}$ is the percentage change in CET between the Control and Chronic treatment and $pCET_{ep.oz}$ is the percentage change in CET between the Control and Episodic treatment. Since only the differences after Stage 1 were considered, we normalized $pCET_{oz}$ and $pCET_{ep.oz}$ by subtracting their value at the end of Stage 1. We also calculated the AOT40 index for the same time period (i.e. for Stages 2 and 3).

Fig. 3.3 (a) shows that the plants in the Episodic treatment were significantly more

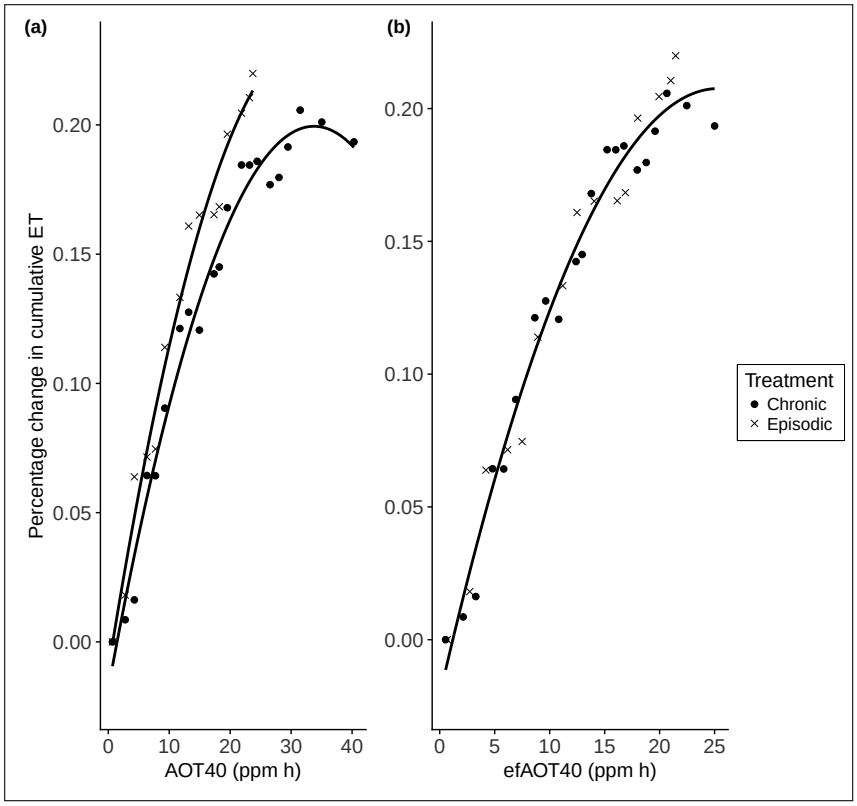

Figure 3.3: (a) Percentage change in cumulative evapotranspiration (pCET) of wheat variety Lennox between Control and Chronic treatment as well as Control and Episodic O_3 treatment plotted against AOT40; (b) pCET expressed as function of effective AOT40 (efAOT40) and continuous black line is the regression: y= -0.021 + 0.018 x - 0.000356 x^2 (R^2=0.98, p<0.01). All pCET values were calculated for Stages 2, 3 after normalization at the end of Stage 1. AOT40 and efAOT40 were calculated for the same stages.

affected by the O_3 exposure than the plants in the Chronic treatment and exhibited higher values of pCET. In other words, the plants which started in the low O_3 environment and were transferred to high O_3 at ZS 31 were more sensitive to the pollutant than the plants which grew at high [O_3] from emergence. Thus, the early fumigation with O_3 in the Chronic treatment decreased the plant sensitivity later in the season. This is in accordance with previous studies which report that the priming of plants can lead to improved performance at a subsequent abiotic stress event (*Tanou et al.*, 2012; *Wang et al.*, 2014; *Li et al.*, 2014). The plants in the Episodic treatment were not fumigated with O_3 at Stage 1 and exhibited higher sensitivity to the pollutant during Stage 2.

3.2.6.2 Acclimation factor

The duration of plant exposure to O_3 affected the relationship between pCET and AOT40 (Fig. 3.3 (a)). We introduced the effective AOT40 index (efAOT40) which accounts for the variability in the effect of O_3 on wheat over time. The efAOT40 index

represents the part of daily O_3 exposure which is limiting for the plant growth and is defined as:

$$efAOT40 = \sum_{i=1}^{n}(1 - f_{acl_i})DOE40_i \tag{3.7}$$

where n is the number of days in the growing season, i is the day index and f_{acl} is an acclimation factor that accounts for the plant adjustment to O_3 over time. f_{acl} is a function of the number of days that DOE40 is above zero (ND_{oz}), it is in the [0,1] range and is updated in daily time step as follows:

$$f_{acl} = a_1 * f(ND_{oz}) \tag{3.8}$$

where a_1 is an empirical constant and ND_{oz} starts at zero at planting and is updated in daily time step as follows:

$$ND_{oz(i)} = \begin{cases} ND_{oz(i-1)} + 1 & DOE40_i > 0 \\ ND_{oz(i-1)} & DOE40_i = 0 \end{cases} \tag{3.9}$$

where i is the day after planting and i-1 is the previous day.

Due to incomplete understanding of the plant acclimation process to chronic O_3 stress, different equations were tested for the parameterization of f_{acl}. We evaluated the fit of a linear, quadratic and square root function in the expression of f_{acl} against ND_{oz} (Table 3.3). The parameter a_1 was calibrated to minimize RMSE for pCET between the Chronic and Episodic treatment when expressed against efAOT40. RMSE was calculated as follows:

$$RMSE = \sqrt{\frac{\sum_{i=1}^{n}(pCET_{oz_i} - pCET_{ep.oz_i})^2}{n}} \tag{3.10}$$

where i is the day index and n is the number of observations.

For the derivation of Eq. 3.8, the linear shape was selected since it provided the lowest RMSE between all functions tested (Table 3.3). The relationship between pCET and efAOT40 was described by a second degree polynomial model (Fig. 3.3 (b)), which was used in GLAM-ROC to estimate the O_3-induced reduction on potential ET (i.e. the canopy ET rate under optimal growth conditions). Detailed information about the incorporation of the above-mentioned formula into the model is given in the B.0.3.

Table 3.3: Evaluation of different line shapes in the expression of acclimation factor (f_{acl}) as function of the number of days of O_3 exposure (ND_{oz}). The empirical parameter a_1 was calibrated to minimize RMSE between $pCET_{oz}$ and $pCET_{ep.oz}$ when expressed against efAOT40.

Line shape	Function	Calibrated value of a_1	RMSE
Linear	a_1 ND_{oz}	0.006	0.0124
Quadratic	a_1 ND_{oz}^2	0.0001	0.0182
Root	a_1 $\sqrt{ND_{oz}}$	0.05	0.0136

3.2.6.3 Ozone effects on transpiration efficiency and partitioning to grains

Exposure to O_3 induces up-regulation of the plant antioxidant metabolism which is energy demanding and the plants suppress their growth to use their resources for reducing the stress damage (*Betzelberger et al.*, 2010; *Fatima et al.*, 2019). As a result TE decreases, since the plant growth reduction exceeds the reduction in ET (*VanLoocke et al.*, 2012). HI also decreases due to reduced allocation of assimilates to the grains (*Pleijel et al.*, 2014).

In GLAM-ROC, we applied O_3-induced modifications on both TE and the rate of increase of HI (dHI/dt). TE is defined as:

$$TE = min(\frac{E_T}{VPD}, E_{TN,max}) \tag{3.11}$$

where E_T is normalised transpiration efficiency in Pa, VPD is vapour pressure deficit (kPa), and $E_{TN,max}$ is the maximum transpiration efficiency in g kg^{-1}. In this study, temperature and humidity were controlled (see Table 3.1) and VPD did not fluctuate significantly for most of the days in the growing season, thus for simplicity TE was set equal to $E_{TN,max}$. The effect of O_3 on TE was related to the effective $[O_3]$ index (ef$[O_3]$). This index is calculated similarly to efAOT40 to simulate the plant adjustment to chronic O_3 stress which leads to optimization of biomass productivity over time. ef$[O_3]$ is a fraction of daily $[O_3]$ defined as follows:

$$ef[O_3] = (1 - f_{acl}) \cdot [O_3] \tag{3.12}$$

where $[O_3]$ is the daily mean O_3 concentration during the daylight hours and f_{acl} is calculated in Eq. 3.8. For dHI/dt, no acclimation mechanism was assumed to impact on the allocation of assimilates to the grains, thus the effect was related to $[O_3]$.

The effects of O_3 on both TE and dHI/dt were initiated above 10 ppb which is the O_3 level of the pre-industrial period (*Marenco et al.*, 1994). This threshold was set since GLAM-ROC is designed to simulate the effect of O_3 pollution on wheat in comparison with the pre-industrial period. TE and dHI/dt decreased linearly above the 10 ppb $[O_3]$ threshold as follows (Fig. 3.4): ef$[O_3]$ is a fraction of daily $[O_3]$ defined as follows:

$$\frac{TE_{oz}}{TE_c} = \begin{cases} 1 & [O_3] < 10ppb \\ c_1 \cdot ef[O_3] + d_1 & [O_3] \geq 10ppb \end{cases} \tag{3.13}$$

$$\frac{(dHI/dt)_{oz}}{(dHI/dt)_c} = \begin{cases} 1 & ef[O_3] < 10ppb \\ c_2 \cdot ef[O_3] + d_2 & ef[O_3] \geq 10ppb \end{cases} \tag{3.14}$$

where TE_c, TE_{oz}, $(dHI/dt)_c$ and $(dHI/dt)_{oz}$ are the control and O_3-limited TE and

dHI/dt respectively.

Feng et al. (2008) summarizes various experiments with wheat plants fumigated with different O_3 levels. The study finds that the aboveground biomass is decreased by an average of 18% at [O_3] of 72 ppb in comparison with carbon-filtered treatments. Similarly, HI reduces by 9% at the same [O_3] level. Following the above findings, the slope and intercept of Eq. 3.13, 3.14 were calculated accordingly and their values are given in Table B.1.

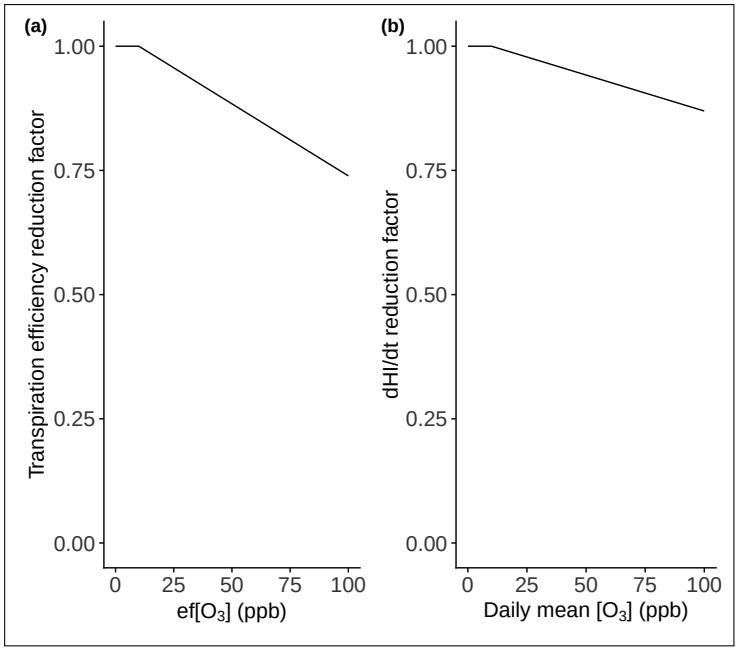

Figure 3.4: O_3-induced reduction (a) in transpiration efficiency (TE) relative to control expressed against effective daily mean [O_3] (ef[O_3]), (b) in the rate of increase of HI (dHI/dt) relative to control expressed as function of daily mean [O_3].

3.2.7 Model calibration and evaluation measures

The GLAM-ROC model was calibrated against the observed data for KWS Bittern wheat in the Control treatment. The metric used for the model calibration was the absolute error (AE) according to the following formula:

$$AE = |O - S| \tag{3.15}$$

where O and S are the observed and simulated values of the compared variables. The model performance was evaluated with the absolute percent error between the observed and simulated value of all compared variables.

3.2.8 Calibration

The phenology of the model was set to meet the observed anthesis and maturity dates of the Control treatment. This was done to avoid any model bias from sources different than the O_3 stress effects. The maximum transpiration efficiency ($E_{TN,max}$) was calibrated with the use of an optimizer which selected the value that minimized AE between the end-of-season observed and simulated above-ground biomass in the Control treatment. Similarly, the rate of change of harvest index (dHI/dt) was selected by the optimizer to minimize AE between the observed and simulated grain yield of the Control treatment. The step for the runs of the optimizer was 0.1 for $E_{TN,max}$ and 0.0005 for dHI/dt. The ranges and values of the calibrated parameters are provided in Table B.2. All other parameter values were taken from *Droutsas et al.* (2019). The yield gap parameter (YGP) was set to one since O_3 was the only yield-limiting factor.

3.2.9 Sensitivity analysis

We performed a sensitivity analysis to test GLAM-ROC in a wide range of O_3 concentrations. The relative O_3 damage to yield was examined in comparison with the yield at the baseline O_3 concentration. In the meta-analysis of *Pleijel et al.* (2018), average [O_3] of charcoal-filtered air treatments was 13.3 ppb. We used the same baseline for direct comparison between the two studies. We modified all hourly O_3 concentrations in the Chronic and Episodic treatment by the appropriate value, such that the average [O_3] during the growing season was [13.3, 23.3, ..., 83.3 ppb]. We run GLAM-ROC at the different O_3 concentration levels by keeping all other environmental conditions constant. The relative O_3 damages to yield in the Chronic and Episodic treatment were calculated as percentage differences in yield from the baseline simulation.

3.3 Results

3.3.1 Evaluation of GLAM-ROC model skill

Exposure to O_3 significantly decreased the plant biomass and yield of KWS Bittern wheat in the experiments as well as the total evapotranspiration (TET) and WUE. All measured and simulated values of the compared variables and their percent error are shown in Table 3.4. The model reproduced the observed plant biomass response in both O_3 treatments (Fig. 3.5(a)). In the Chronic treatment, the percent error between the observed and simulated biomass at harvest was 5.02%. In the Episodic treatment, biomass was simulated to within 1% of observation. Thus, the model closely followed the effect of O_3 stress on wheat biomass in both durations of exposure by accounting for O_3-induced reductions in canopy ET and TE.

Table 3.4: Measured and simulated above-ground biomass (g m^{-2}), grain yield (g m^{-2}), harvest index (HI), total ET (TET) and WUE difference from control (%) as well as their percent error in Control, Chronic and Episodic O_3 treatment.

	Control			Chronic			Episodic		
	Measured	Simulated	Percent error (%)	Measured	Simulated	Percent error (%)	Measured	Simulated	Percent error (%)
Biomass	2643.1	2659.0	0.60	2075.1	1971.0	5.02	2169.5	2185.0	0.71
Yield	1114.8	1113.0	0.16	738.2	738.0	0.03	913.0	915.0	0.22
HI	0.422	0.419	0.71	0.356	0.374	5.06	0.420	0.419	0.24
TET difference from control (%)	-	-	-	-12.10	-14.54	20.17	-9.42	-10.14	7.64
WUE difference from control (%)	-	-	-	-9.98	-13.27	32.97	-9.27	-8.55	7.77

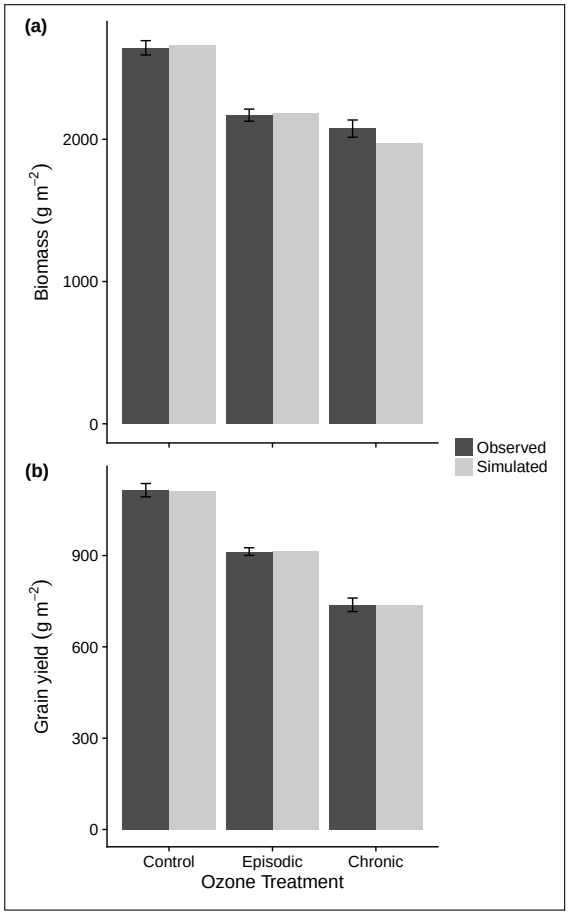

Figure 3.5: Observed (wheat variety KWS Bittern) and simulated (a) above-ground biomass and (b) grain yield at harvest in Control, Chronic and Episodic O_3 treatment. Error bars are standard errors of means in the observations.

Regarding the grain yield, GLAM-ROC accurately estimated the observed decreases in both the Chronic and Episodic treatment. Yield was simulated to within 1% of observation in both the Chronic and Episodic treatment. Reduction in HI was also noticed in the Chronic but not the Episodic treatment (Fig. 3.6). This was due to lack of O_3 fumigation during the grain filling period in the Episodic treatment. The model reproduced the observed plant response to HI in the Episodic treatment where the simulated value was within 1% of observation. In the Chronic treatment, HI was overestimated by 5.06%.

Finally, GLAM-ROC overestimated the O_3-induced reduction in TET in the Chronic treatment and the percent error was 20.17% (Fig. 3.7 (a)). The model skill was higher in the Episodic treatment where the percent error was 7.64%. WUE was significantly overestimated in the Chronic treatment, where the percent error was 32.97 % (Fig. 3.7 (b)). In the Episodic treatment, GLAM-ROC exhibited improved skill and the percent error for WUE was 7.77%.

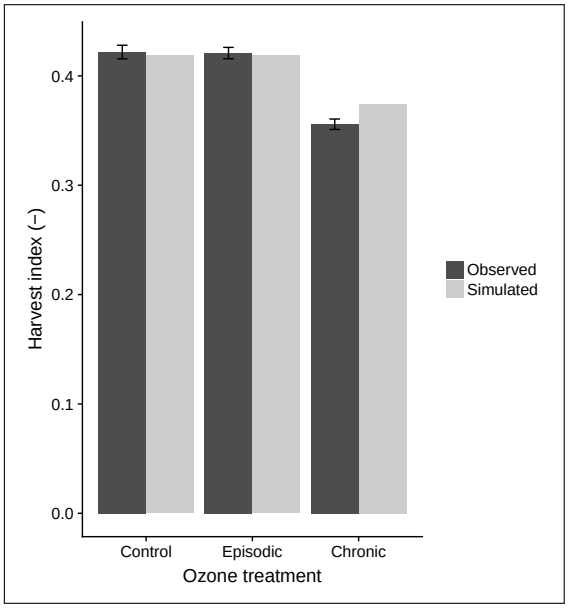

Figure 3.6: Observed (wheat variety KWS Bittern) and simulated harvest index in Control, Chronic and Episodic O_3 treatment. Error bars are standard errors of means in the observations.

3.3.2 Sensitivity of GLAM-ROC to different O_3 concentrations

Yield reduction was higher in the Chronic than the Episodic exposure in all O_3 concentrations (Fig. 3.8). In the Episodic treatment, yield reduced in an almost linear fashion for every 10 ppb increase in $[O_3]$ from the baseline. Using linear regression of the data points, yield loss was found to increase by 0.28% per ppb increase in $[O_3]$ (regression not shown). In the Chronic treatment, yield loss increased by 0.54% per ppb increase in $[O_3]$ (regression not shown), however the standard error (se) of the slope was 177.3% higher than the Episodic treatment (i.e. se of slope was 0.0366 in Chronic against 0.0132 in Episodic treatment). This means that in the Chronic treatment, the reduction in grain yield diverted substantially from the linear line depending on $[O_3]$. The highest yield loss was estimated when the difference from the baseline $[O_3]$ value increased from 30 to 40 ppb. In absolute numbers, the grain yield of wheat was most affected when $[O_3]$ increased from 43.3 to 53.3 ppb. Within that concentration range, the average damage to yield was 0.96% per ppb increase in $[O_3]$. In the Episodic treatment, the same $[O_3]$ range gave the highest damage to yield with 0.39% loss per ppb increase in $[O_3]$.

We also applied linear regression to all data points in the Chronic and Episodic treatment and compared the regression line to those developed in the meta-analysis of *Pleijel et al.* (2018) and *Broberg et al.* (2015) (Fig. 3.8). The three lines were in close agreement with each other and the slope of this study was -0.41 against -0.36 of *Pleijel et al.* (2018) and -0.47 of *Broberg et al.* (2015). Thus, the studies suggest 0.41%, 0.36% and 0.47% increase in wheat yield loss respectively per ppb increase in $[O_3]$ above the

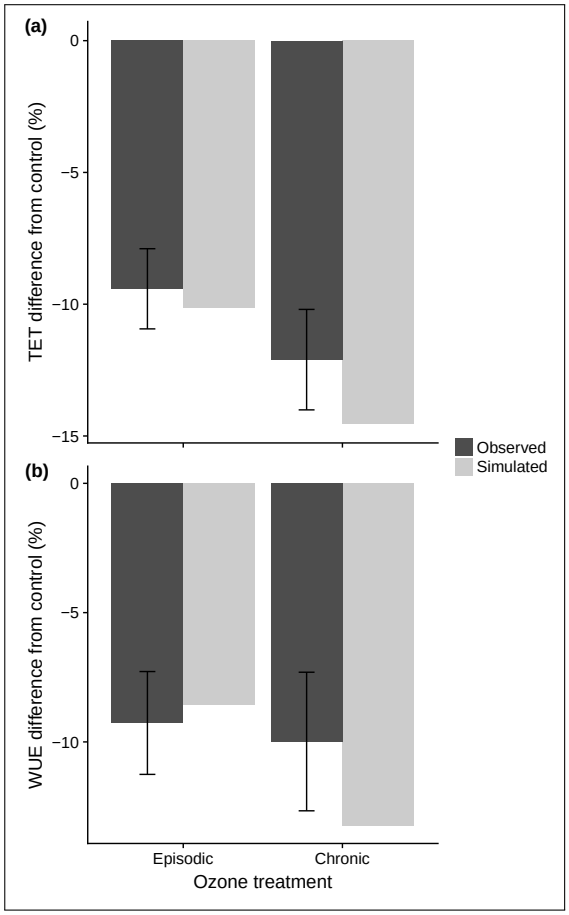

Figure 3.7: Observed (wheat variety KWS Bittern) and simulated difference from control in end-of season (a) total evapotranspiration (TET) and (b) water use efficiency (WUE) in Chronic and Episodic O_3 treatment. Error bars are standard errors of means in the observations.

baseline. However, it should be noted that the lower O_3 damage suggested by *Pleijel et al.* (2018) in comparison to *Broberg et al.* (2015) may be explained by that the former study used wheat yield data only from charcoal-filtered and non-filtered air treatments, whilst the latter study used also treatments with elevated O_3 levels. In addition, the meta-analysis of *Feng et al.* (2008) estimates that the grain yield of wheat is reduced by 17.5 and 29% at average $[O_3]$ of 43 and 72 ppb respectively. Both findings are in very close agreement with the regression line of our study which predicted the loss in grain yield with less than 3% difference from the reported values (Fig. 3.8). Overall, GLAM-ROC was in accordance with the existing meta-analysis studies and closely followed the measured effect of O_3 on the grain yield of wheat.

3.3.3 GLAM-ROC comparison with ozone exposure response function

A large number of studies estimate the regional or global effect of O_3 on crop productivity based on a statistical response function (SRF) between the relative crop yield

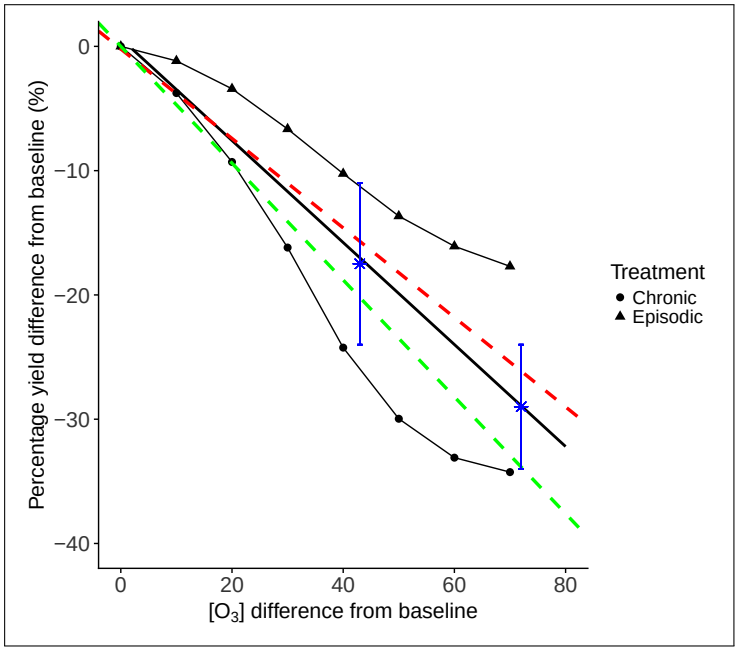

Figure 3.8: GLAM-ROC estimations of O_3-induced grain yield loss of wheat at different O_3 concentrations in Chronic (circles) and Episodic treatment (triangles) in comparison with baseline. Solid black line is linear regression of all data points in Chronic and Episodic treatment, red and green dashed lines are linear regressions in meta-analysis of *Pleijel et al.* (2018) and *Broberg et al.* (2015) respectively. Star data points are O_3-induced yield losses at 43 and 72 ppb [O_3] in meta-analysis of *Feng et al.* (2008) and error bars are 95% confidence intervals. The two star data points are presented using their absolute [O_3] value on x axis instead of the difference from baseline, since this was not reported.

and the level of O_3 exposure (e.g. *Hollaway et al.*, 2012; *Ghude et al.*, 2014; *Sharma et al.*, 2019). This formula assumes linear reduction in grain yield in relation to AOT40. The modelling methodology introduced in GLAM-ROC assumes non-linear O_3 effect on yield with increased exposure to the pollutant. The two methods were evaluated against the observed data for KWS Bittern wheat. In the SRF model, the function for wheat was taken from *Mills et al.* (2007). The AOT40 index was accumulated during Stages 2 and 3, since these days were the most O_3-sensitive (i.e. the last 68 days of the crop season).

In GLAM-ROC, the grain yield in the Chronic treatment was 80.7% of the Episodic, which was less than 1% different from the observed value (Fig. 3.9). In the SRF model, the Chronic: Episodic yield ratio was 0.35, underestimated by 56.5%. This was due to the overestimation of the O_3 damage to yield at a greater extent in the Chronic than the Episodic treatment. Nevertheless, no acclimation mechanism is considered in the SRF model and the O_3 damage to yield is linearly extrapolated as AOT40 increases. As a result, the observed non-linear plant response with increased exposure to O_3 stress affected the skill of the model. Thus, GLAM-ROC improved upon the SRF model in the estimation of the Chronic: Episodic yield ratio by accounting for the plant acclimation to chronic O_3 stress at variable duration of exposure.

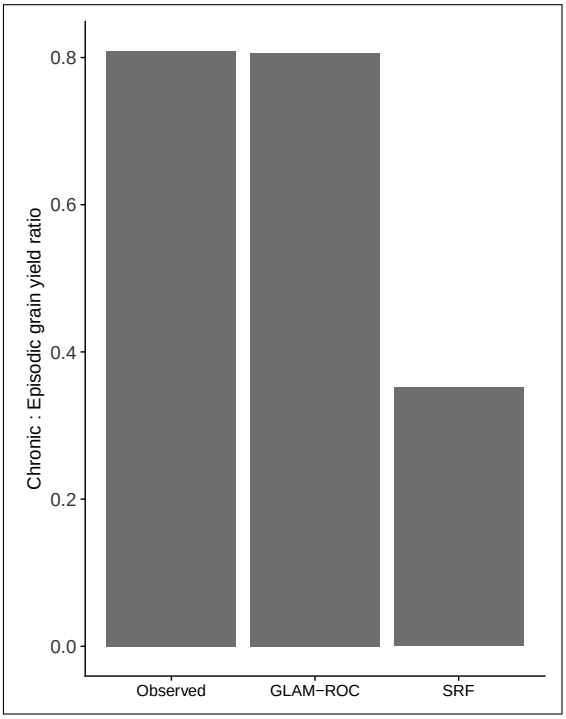

Figure 3.9: Observed and simulated grain yield in Chronic relative to Episodic treatment. SRF is statistical response function for wheat taken from *Mills et al.* (2007).

3.4 Discussion

We developed and evaluated the GLAM-ROC model to simulate the effect of O_3 on wheat growth and development. The model successfully reproduced the O_3-induced damage to wheat biomass and yield in both the Episodic and Chronic treatment. The plant biomass was simulated to within 6% of observation in both durations of exposure. Similarly, the simulated grain yield was less than 1% different from the measurements. The model also closely followed the observed effects of O_3 on HI, ET and WUE.

The modelling approach followed here is simpler than stomatal flux-based methods commonly used in crop models. Such method was avoided since it strongly depends on stomatal conductance, a trait which is highly complex (*Buckley*, 2017) and not simple to incorporate in process-based crop models. Difficulties may also be faced in crop models with complex O_3 schemes regarding their parameterization for large scale applications (*Emberson et al.*, 2018). GLAM is a large area crop model and unwarranted complexity should be avoided (*Challinor et al.*, 2018). In addition, our approach − even relying on an exposure-based methodology − overcomes some limitations of the statistical response function. This is due to relating AOT40 to the potential ET rate instead of using the index to estimate grain yield loss directly. ET and AOT40 have been previously seen to correlate significantly under well-watered conditions (*Jaudé et al.*, 2008; *VanLoocke et al.*, 2012). Nevertheless, the use of AOT40 disregards the effect of

O_3 stress on ET below 40 ppb. *Bernacchi et al.* (2011) and *VanLoocke et al.* (2012) exposed soybean plants to various O_3 concentrations and showed that the pollutant reduces canopy ET significantly for exposures above 40 ppb. Since wheat and soybean exhibit similar sensitivity to O_3 (*Mills et al.*, 2007), in our study we also related the reduction in canopy ET to the AOT40 index.

In GLAM-ROC, the O_3-induced decrease in ET is estimated in comparison with the same plant growing in optimal environment. Under water stress, the effect of O_3 on crop growth can be reduced due to decreased stomatal conductance and lower uptake of the pollutant by the leaves (*Khan and Soja*, 2003; *Feng et al.*, 2008). Both O_3 and drought reduce the daily canopy transpiration rate in the model, the minimum of which is considered as the actual transpiration (i.e. the effect of drought (*Challinor et al.*, 2004) and O_3 (this study) on ET are estimated independently). Thus, if limited soil water suppresses transpiration to a greater extend than O_3, there will be no additive effect of the pollutant on canopy ET. In other words, the O_3 damage to crop transpiration and growth decreases with higher levels of water stress in GLAM-ROC. The accuracy of this approach should be tested against experimental data with wheat exposed to both stressors simultaneously. In this study, GLAM-ROC was only evaluated for the effect of O_3 on well-watered wheat crops. Thus, the model can be currently used only in regions where adequate rainfall prevents water stress or where wheat is fully irrigated. Elevated CO_2 concentrations can also reduce stomatal conductance and protect against O_3 pollution (*Yadav et al.*, 2019). Currently, GLAM-ROC does not account for the effect of elevated CO_2 on crop growth and yield, thus it cannot be used for future environments with rising CO_2 concentrations (i.e. the model has to be calibrated each time for the given CO_2 level). Following the addition of the CO_2 fertilization mechanism, the interaction between elevated CO_2 and O_3 should be addressed to allow for the estimation of crop performance and yield under future climate change conditions.

GLAM-ROC uses the acclimation factor to simulate the plant adaptation to chronic O_3 stress. This was necessary for capturing the differences in water consumption and biomass productivity between the Chronic and Episodic treatment. The plants in the Chronic treatment exhibited higher values of water consumption than the Episodic during their common period of O_3 fumigation (i.e. at Stage 2). Nevertheless, only the plants in Chronic treatment were exposed to high O_3 during Stage 1. The lack of previous exposure to the stressor in the Episodic treatment increased the plant sensitivity at Stage 2, thus reducing the water consumption rates. This difference in plant behaviour could not be simulated without considering the effect of plant acclimation to chronic O_3 exposure. The acclimation factor was calculated according to the number of days of O_3 fumigation, thus modifying the plant sensitivity to O_3 at different durations of exposure. The same factor simulated the differences in biomass productivity between the two O_3 exposures through modifying the effect on TE. The SRF model does not account for the plant acclimation mechanism and overestimated the relative damage to

grain yield between the Chronic and Episodic treatment by 56.5%.

In GLAM-ROC, the acclimation factor was related to the 40 ppb threshold (Eq. 3.8, 3.9), which means that no plant acclimation was considered for exposure to O_3 below that level. This threshold was chosen since it is the most commonly used threshold for relating the O_3 exposure to loss in crop yield (e.g., *Fuhrer et al.*, 1997; *Mills et al.*, 2011; *Sharma et al.*, 2019). However, it is unclear if this is the optimal threshold for wheat acclimation to the pollutant or if it needs to be adjusted in the future. In our study, the O_3 concentrations in the chambers were either very low (below 10 ppb in the Control treatment) or significantly higher than 40 ppb during exposure to the pollutant in the Chronic and Episodic treatments. Thus, decreasing the acclimation threshold does not change the model results in comparison with the observations (Section 3.3.1). In addition, the sensitivity analysis (Section 3.3.2) indicates that this threshold is appropriate, since the model can be reliably used for simulating grain yield losses for O_3 exposure below 40 ppb. Nevertheless, since wheat performance is affected by O_3 below 40 ppb (*Pleijel*, 2011), the plant acclimation threshold may need to be reconsidered in the future.

The plant sensitivity to O_3 varies also according to the growth stage. O_3 did not exhibit significant effect on wheat from plant emergence to ZS 31, at least in terms of water consumption. Thus, the O_3 damage to wheat was simulated to initiate at ZS 31. On the other hand, the period from anthesis to the end of grain filling is the most O_3-sensitive for grain yield reduction (*Lee et al.*, 1988; *Pleijel et al.*, 1998; *Soja et al.*, 2000). The Episodic treatment was not fumigated with high O_3 after anthesis and HI was less than 1% different from the Control. In the Chronic treatment, HI was 14.3% lower than the Control due to high O_3 exposure during grain filling. GLAM-ROC was able to reproduce the O_3-induced reduction to yield by slowing down the daily rate of increase of HI (dHI/dt) based on the $[O_3]$ level. As a result, the model followed the observed decrease in HI and successfully simulated the O_3 impact on grain yield at maturity.

The development and evaluation of GLAM-ROC were based on controlled-environment chamber experiments where the environmental conditions cannot perfectly match the field. For instance, the plants were grown in pots instead of being rooted on the ground. Nevertheless, the meta-analysis of *Feng and Kobayashi* (2009) revealed no significant differences in the yield response to O_3 between pot and ground-rooted wheat plants. In addition, the daily O_3 concentration in the chambers did not match the diurnal variation experienced under ambient conditions (e.g. *Pawlak and Jarosławski*, 2015; *Wang et al.*, 2017). However, *Harmens et al.* (2018) exposed a modern wheat variety to various background O_3 concentrations and different peak O_3 episodes and showed that the relationship between the reduction in grain yield and the accumulated stomatal O_3 flux could be explained by the same slope irrespective of the temporal O_3 profile. Moreover, in our study the fumigation in the Chronic treatment lasted for the full crop cycle (i.e.

107 days) with an average concentration of 78.8 ppb, which can be unrealistic for most parts of the world. The highest frequency of O_3 pollution episodes (i.e. daily average 8-h $[O_3]$ of at least 75 ppb) in the summertime for the year 2000 was 38 days in North America (*Lei et al.*, 2012). The Episodic treatment was closer to these conditions with the total duration of plant O_3 exposure being 33 days. The real dynamics of surface O_3 in polluted regions are likely to be between the Episodic and Chronic treatments of this study. In addition, the average CO_2 concentration in the chambers was around 530 ppm and this concentration level was experienced in all treatments. For this reason, CO_2 was not accounted as an additional varying factor in the estimation of O_3 damage to wheat.

Our sensitivity analysis suggested 0.41% average yield loss per ppb increase in O_3 concentration above 13.3 ppb, which is directly comparable with existing meta-analysis studies (Fig. 3.8). In the Chronic treatment, the model estimated a 0.96% maximum damage to yield per ppb increase in O_3 concentration, which occured when $[O_3]$ was in the 43.3 - 53.3 ppb range. In the Episodic treatment, the same concentration range gave the maximum damage to yield per ppb increase in $[O_3]$, which was considerably lower at 0.39%. Overall, the yield loss per ppb increase in $[O_3]$ varied from 0.17% to 0.96%, depending on the treatment (i.e. Chronic vs. Episodic) and the $[O_3]$ level. Hence, the duration of exposure to O_3 stress is a significant factor influencing the effect of the pollutant on wheat productivity and yield. Longer duration of exposure to O_3 implies higher reduction in yield, however the relative damage may decrease as the duration increases. The non-linear grain yield vs. $[O_3]$ pattern can result from enhanced plant acclimation with increased duration exposure to the pollutant. Thus, we believe that the plant acclimation process should be taken into account for robust estimation of the chronic effect of O_3 on crop growth, productivity and yield.

3.5 Conclusion

Exposure to O_3 significantly decreased the wheat biomass and grain yield in the experiments. The GLAM-ROC crop model was developed and evaluated for the effect of O_3 on wheat growth and development. A statistical relationship was introduced to estimate the reduction in canopy evapotranspiration based on the O_3 exposure (i.e. AOT40 index). Decreases in transpiration efficiency and harvest index were also incorporated into the model according to the O_3 concentration. The model successfully reproduced the observed O_3 damage to biomass and yield of KWS Bittern wheat in both the Episodic and Chronic treatment. Accounting for the plant acclimation to chronic O_3 stress was necessary for good model skill. The acclimation process was empirically incorporated with the use of an acclimation factor based on the days of O_3 exposure. This allowed the simulation of plant adjustment to O_3 over time which reduced the relative damage to biomass and yield. The statistical response function

ignored the acclimation process and overestimated the Chronic: Episodic grain yield ratio. It is concluded that the plant acclimation to chronic O_3 stress is significant and should be taken into account for the estimation of the O_3 damage to wheat growth and productivity.

Acknowledgements

This work was supported by the UK N8 AgriFood Resilience Programme. I.D. gratefully acknowledges the Oatley PhD Scholarship and the Priestley International Centre for Climate for financial support. The experimental data is generated as a part of the Joint Programming Initiative on Agriculture, Food Security and Climate Change (FACCE-JPI) and funded by the FACCE-ERA-NET+project: ClimateCAF.

References

Ainsworth, E. A. (2017), Understanding and improving global crop response to ozone pollution, *The Plant Journal*, *90*(5), 886–897. 3.1

Arnold, S., D. Lombardozzi, J.-F. Lamarque, T. Richardson, L. Emmons, S. Tilmes, S. Sitch, G. Folberth, M. Hollaway, and M. Val Martin (2018), Simulated global climate response to tropospheric ozone-induced changes in plant transpiration, *Geophysical Research Letters*, *45*(23), 13–070. 3.2.6.1

Ashmore, M. (2005), Assessing the future global impacts of ozone on vegetation, *Plant, Cell & Environment*, *28*(8), 949–964. 3.1

Avnery, S., D. L. Mauzerall, J. Liu, and L. W. Horowitz (2011), Global crop yield reductions due to surface ozone exposure: 1. year 2000 crop production losses and economic damage, *Atmospheric Environment*, *45*(13), 2284–2296. 3.1

Barnes, J., D. Velissariou, A. Davison, and C. Holevas (1990), Comparative ozone sensitivity of old and modern greek cultivars of spring wheat, *New Phytologist*, *116*(4), 707–714. 3.1

Bernacchi, C. J., A. D. Leakey, B. A. Kimball, and D. R. Ort (2011), Growth of soybean at future tropospheric ozone concentrations decreases canopy evapotranspiration and soil water depletion, *Environmental pollution*, *159*(6), 1464–1472. 3.2.6.1, 3.4

Betzelberger, A. M., K. M. Gillespie, J. M. Mcgrath, R. P. Koester, R. L. Nelson, and E. A. Ainsworth (2010), Effects of chronic elevated ozone concentration on antioxidant capacity, photosynthesis and seed yield of 10 soybean cultivars, *Plant, Cell & Environment*, *33*(9), 1569–1581. 3.2.6.3

Broberg, M. C., Z. Feng, Y. Xin, and H. Pleijel (2015), Ozone effects on wheat grain quality–a summary, *Environmental pollution*, *197*, 203–213. (document), 3.3.2, 3.8

Bruce, T. J., M. C. Matthes, J. A. Napier, and J. A. Pickett (2007), Stressful memories of plants: evidence and possible mechanisms, *Plant Science*, *173*(6), 603–608. 3.1

Buckley, T. N. (2017), Modeling stomatal conductance, *Plant physiology*, pp. pp–01,772. 3.4

Buckley, T. N., and K. A. Mott (2013), Modelling stomatal conductance in response to environmental factors, *Plant, cell & environment*, *36*(9), 1691–1699. 3.1

Burney, J., and V. Ramanathan (2014), Recent climate and air pollution impacts on indian agriculture, *Proceedings of the National Academy of Sciences*, *111*(46), 16,319–16,324. 3.1

Challinor, A., T. Wheeler, P. Craufurd, J. Slingo, and D. Grimes (2004), Design and optimisation of a large-area process-based model for annual crops, *Agricultural and forest meteorology*, *124*(1-2), 99–120. 3.2.5, 3.4

Challinor, A. J., F. Ewert, S. Arnold, E. Simelton, and E. Fraser (2009), Crops and climate change: progress, trends, and challenges in simulating impacts and informing adaptation, *Journal of experimental botany*, *60*(10), 2775–2789. 3.1

Challinor, A. J., C. Müller, S. Asseng, C. Deva, K. J. Nicklin, D. Wallach, E. Vanuytrecht, S. Whitfield, J. Ramirez-Villegas, and A.-K. Koehler (2018), Improving the use of crop models for risk assessment and climate change adaptation, *Agricultural systems*, *159*, 296–306. 3.4

Chen, C. P., M. Frei, and M. Wissuwa (2011), The ozt8 locus in rice protects leaf carbon assimilation rate and photosynthetic capacity under ozone stress, *Plant, cell & environment*, *34*(7), 1141–1149. 3.1

Damour, G., T. Simonneau, H. Cochard, and L. Urban (2010), An overview of models of stomatal conductance at the leaf level, *Plant, Cell & Environment*, *33*(9), 1419–1438. 3.1

Droutsas, I., A. Challinor, M. Swiderski, and M. A. Semenov (2019), New modelling technique for improving crop model performance-application to the glam model, *Environmental Modelling & Software*, *118*, 187–200. 3.2.5, 3.2.8

Emberson, L., M. Ashmore, H. Cambridge, D. Simpson, and J.-P. Tuovinen (2000), Modelling stomatal ozone flux across europe, *Environmental Pollution*, *109*(3), 403–413. 3.1

Emberson, L., P. Büker, M. Ashmore, G. Mills, L. Jackson, M. Agrawal, M. Atikuzzaman, S. Cinderby, M. Engardt, C. Jamir, et al. (2009), A comparison of north american and asian exposure–response data for ozone effects on crop yields, *Atmospheric Environment*, *43*(12), 1945–1953. 3.1

Emberson, L. D., H. Pleijel, E. A. Ainsworth, M. Van den Berg, W. Ren, S. Osborne, G. Mills, D. Pandey, F. Dentener, P. Büker, et al. (2018), Ozone effects on crops and consideration in crop models, *European Journal of Agronomy*, *100*, 19–34. 3.4

Ewert, F., and J. R. Porter (2000), Ozone effects on wheat in relation to co2: modelling short-term and long-term responses of leaf photosynthesis and leaf duration, *Global Change Biology*, *6*(7), 735–750. 3.1

FAO, I., UNICEF, et al. (2017), Wfp, who (2017) the state of food security and nutrition in the world 2017, *Building Resilience for Peace and Food Security (Food and Agriculture Organization, Rome)*. 3.1

Farage, P., and S. P. Long (1999), The effects of o3 fumigation during leaf development on photosynthesis of wheat and pea: an in vivo analysis, *Photosynthesis Research*, *59*(1), 1–7. 3.1

Farage, P. K., S. P. Long, E. G. Lechner, and N. R. Baker (1991), The sequence of change within the photosynthetic apparatus of wheat following short-term exposure to ozone, *Plant Physiology*, *95*(2), 529–535. 3.1

Fatima, A., A. A. Singh, A. Mukherjee, M. Agrawal, and S. B. Agrawal (2019), Ascorbic acid and thiols as potential biomarkers of ozone tolerance in tropical wheat cultivars, *Ecotoxicology and environmental safety*, *171*, 701–708. 3.2.6.3

Feng, Z., and K. Kobayashi (2009), Assessing the impacts of current and future concentrations of surface ozone on crop yield with meta-analysis, *Atmospheric Environment*, *43*(8), 1510–1519. 3.4

Feng, Z., K. Kobayashi, and E. A. Ainsworth (2008), Impact of elevated ozone concentration on growth, physiology, and yield of wheat (triticum aestivum l.): a meta-analysis, *Global Change Biology*, *14*(11), 2696–2708. (document), 3.2.6.3, 3.3.2, 3.8, 3.4

Feng, Z., L. Wang, H. Pleijel, J. Zhu, and K. Kobayashi (2016), Differential effects of ozone on photosynthesis of winter wheat among cultivars depend on antioxidative enzymes rather than stomatal conductance, *Science of the Total Environment*, *572*, 404–411. 3.1

Fiscus, E. L., F. L. Booker, and K. O. Burkey (2005), Crop responses to ozone: uptake, modes of action, carbon assimilation and partitioning, *Plant, Cell & Environment*, *28*(8), 997–1011. 3.1

Frenck, G., L. van der Linden, T. N. Mikkelsen, H. Brix, and R. B. Jørgensen (2011), Increased [co2] does not compensate for negative effects on yield caused by higher temperature and [o3] in brassica napus l., *European Journal of Agronomy*, *35*(3), 127–134. 3.2.1

Fuhrer, J., L. Skärby, and M. R. Ashmore (1997), Critical levels for ozone effects on vegetation in europe, *Environmental pollution*, *97*(1-2), 91–106. 3.1, 3.4

Ghude, S. D., C. Jena, D. Chate, G. Beig, G. Pfister, R. Kumar, and V. Ramanathan (2014), Reductions in india's crop yield due to ozone, *Geophysical Research Letters*, *41*(15), 5685–5691. 3.3.3

Gillespie, K. M., A. Rogers, and E. A. Ainsworth (2011), Growth at elevated ozone or elevated carbon dioxide concentration alters antioxidant capacity and response to acute oxidative stress in soybean (glycine max), *Journal of Experimental Botany*, *62*(8), 2667–2678. 3.1

Gillespie, K. M., F. Xu, K. T. Richter, J. M. McGrath, R. C. MARKELZ, D. R. Ort, A. D. Leakey, and E. A. Ainsworth (2012), Greater antioxidant and respiratory metabolism in field-grown soybean exposed to elevated o3 under both ambient and elevated co2, *Plant, cell & environment*, *35*(1), 169–184. 3.1

Hansen, E. M., H. Hauggaard-Nielsen, M. Launay, P. Rose, and T. N. Mikkelsen (2019), The impact of ozone exposure, temperature and co2 on the growth and yield of three spring wheat varieties, *Environmental and Experimental Botany*, p. 103868. 3.2.1

Harmens, H., F. Hayes, G. Mills, K. Sharps, S. Osborne, and H. Pleijel (2018), Wheat yield responses to stomatal uptake of ozone: Peak vs rising background ozone conditions, *Atmospheric environment*, *173*, 1–5. 3.4

Heath, R. L. (1994), Possible mechanisms for the inhibition of photosynthesis by ozone, *Photosynthesis Research*, *39*(3), 439–451. 3.1

Heath, R. L., A. S. Lefohn, and R. C. Musselman (2009), Temporal processes that contribute to nonlinearity in vegetation responses to ozone exposure and dose, *Atmospheric Environment*, *43*(18), 2919–2928. 3.1

Held, A., H. Mooney, and J. N. Gorham (1991), Acclimation to ozone stress in radish: leaf demography and photosynthesis, *New phytologist*, *118*(3), 417–423. 3.1

Hollaway, M. J., S. Arnold, A. J. Challinor, and L. Emberson (2012), Intercontinental trans-boundary contributions to ozone-induced crop yield losses in the northern hemisphere, *Biogeosciences*, *9*(1), 271–292. 3.3.3

Ingvordsen, C. H., G. Backes, M. F. Lyngkjær, P. Peltonen-Sainio, J. D. Jensen, M. Jalli, A. Jahoor, M. Rasmussen, T. N. Mikkelsen, A. Stockmarr, et al. (2015), Significant decrease in yield under future climate conditions: Stability and production of 138 spring barley accessions, *European Journal of Agronomy*, *63*, 105–113. 3.2.1

Jaudé, M. B., N. Katerji, M. Mastrorilli, and G. Rana (2008), Analysis of the effect of ozone on soybean in the mediterranean region: I. the consequences on crop-water status, *European Journal of Agronomy*, *28*(4), 508–518. 3.4

Khan, S., and G. Soja (2003), Yield responses of wheat to ozone exposure as modified by drought-induced differences in ozone uptake, *Water, Air, and Soil Pollution*, *147*(1-4), 299–315. 3.4

Kollist, H., S. I. Zandalinas, S. Sengupta, M. Nuhkat, J. Kangasjärvi, and R. Mittler (2018), Rapid responses to abiotic stress: priming the landscape for the signal transduction network, *Trends in plant science*. 3.1

Lee, E. H., D. T. Tingey, and W. E. Hogsett (1988), Evaluation of ozone exposure indices in exposure-response modeling, *Environmental Pollution*, *53*(1-4), 43–62. 3.4

Lei, H., D. J. Wuebbles, and X.-Z. Liang (2012), Projected risk of high ozone episodes in 2050, *Atmospheric environment*, *59*, 567–577. 3.4

Li, X., J. Cai, F. Liu, T. Dai, W. Cao, and D. Jiang (2014), Cold priming drives the sub-cellular antioxidant systems to protect photosynthetic electron transport against subsequent low temperature stress in winter wheat, *Plant Physiology and Biochemistry*, *82*, 34–43. 3.2.6.1

Lombardozzi, D., S. Levis, G. Bonan, and J. Sparks (2012), Predicting photosynthesis and transpiration responses to ozone: decoupling modeled photosynthesis and stomatal conductance., *Biogeosciences Discussions*, *9*(4). 3.2.6.1

Marenco, A., H. Gouget, P. Nédélec, J.-P. Pagés, and F. Karcher (1994), Evidence of a long-term increase in tropospheric ozone from pic du midi data series: Consequences: Positive radiative forcing, *Journal of Geophysical Research: Atmospheres*, *99*(D8), 16,617–16,632. 3.2.6.3

Mauzerall, D. L., and X. Wang (2001), Protecting agricultural crops from the effects of tropospheric ozone exposure: reconciling science and standard setting in the united states, europe, and asia, *Annual Review of energy and the environment*, *26*(1), 237–268. 3.1

McGrath, J. M., A. M. Betzelberger, S. Wang, E. Shook, X.-G. Zhu, S. P. Long, and E. A. Ainsworth (2015), An analysis of ozone damage to historical maize and soybean yields in the united states, *Proceedings of the National Academy of Sciences*, *112*(46), 14,390–14,395. 3.1

Mikkelsen, T. N., and H. Ro-Poulsen (1994), Exposure of norway spruce to ozone increases the sensitivity of current year needles to photoinhibition and desiccation, *New Phytologist*, *128*(1), 153–163. 3.1

Mills, G., A. Buse, B. Gimeno, V. Bermejo, M. Holland, L. Emberson, and H. Pleijel (2007), A synthesis of aot40-based response functions and critical levels of ozone for agricultural and horticultural crops, *Atmospheric Environment*, *41*(12), 2630–2643. (document), 3.3.3, 3.9, 3.4

Mills, G., F. Hayes, D. Simpson, L. Emberson, D. Norris, H. Harmens, and P. Büker (2011), Evidence of widespread effects of ozone on crops and (semi-) natural vegetation in europe (1990–2006) in relation to aot40-and flux-based risk maps, *Global Change Biology*, *17*(1), 592–613. 3.4

Mills, G., K. Sharps, D. Simpson, H. Pleijel, M. Frei, K. Burkey, L. Emberson, J. Uddling, M. Broberg, Z. Feng, et al. (2018), Closing the global ozone yield gap: Quantification and cobenefits for multistress tolerance, *Global change biology*, *24*(10), 4869–4893. 3.1

Mulholland, B., J. Craigon, C. Black, J. Colls, J. Atherton, and G. Landon (1998), Effects of elevated co2 and o3 on the rate and duration of grain growth and harvest index in spring wheat (triticum aestivum l.), *Global Change Biology*, *4*(6), 627–635. 3.1

Musselman, R. C., A. S. Lefohn, W. J. Massman, and R. L. Heath (2006), A critical review and analysis of the use of exposure-and flux-based ozone indices for predicting vegetation effects, *Atmospheric Environment*, *40*(10), 1869–1888. 3.1

Pawlak, I., and J. Jarosławski (2015), The influence of selected meteorological parameters on the concentration of surface ozone in the central region of poland, *Atmosphere-Ocean*, *53*(1), 126–139. 3.4

Pleijel, H. (2011), Reduced ozone by air filtration consistently improved grain yield in wheat, *Environmental pollution*, *159*(4), 897–902. 3.4

Pleijel, H., H. Danielsson, J. Gelang, E. Sild, and G. Selldén (1998), Growth stage dependence of the grain yield response to ozone in spring wheat (triticum aestivum l.), *Agriculture, ecosystems & environment*, *70*(1), 61–68. 3.4

Pleijel, H., H. Danielsson, K. Ojanperä, L. De Temmerman, P. Högy, M. Badiani, and P. Karlsson (2004), Relationships between ozone exposure and yield loss in european wheat and potatoa comparison of concentration-and flux-based exposure indices, *Atmospheric Environment*, *38*(15), 2259–2269. 3.1

Pleijel, H., H. Danielsson, L. Emberson, M. Ashmore, and G. Mills (2007), Ozone risk assessment for agricultural crops in europe: Further development of stomatal flux and flux–response relationships for european wheat and potato, *Atmospheric Environment*, *41*(14), 3022–3040. 3.1

Pleijel, H., H. Danielsson, D. Simpson, and G. Mills (2014), Have ozone effects on carbon sequestration been overestimated? a new biomass response function for wheat, *Biogeosciences*, *11*(16), 4521–4528. 3.2.6.3

Pleijel, H., M. C. Broberg, J. Uddling, and G. Mills (2018), Current surface ozone concentrations significantly decrease wheat growth, yield and quality, *Science of the Total Environment*, *613*, 687–692. (document), 3.2.9, 3.3.2, 3.8

Schauberger, B., S. Rolinski, S. Schaphoff, and C. Müller (2019), Global historical soybean and wheat yield loss estimates from ozone pollution considering water and temperature as modifying effects, *Agricultural and Forest Meteorology*, *265*, 1–15. 3.1

Sharma, A., N. Ojha, A. Pozzer, G. Beig, and S. S. Gunthe (2019), Revisiting the crop yield loss in india attributable to ozone, *Atmospheric Environment: X*, *1*, 100,008. 3.3.3, 3.4

Sicard, P., A. Anav, A. D. Marco, and E. Paoletti (2017), Projected global ground-level ozone impacts on vegetation under different emission and climate scenarios, *Atmospheric Chemistry and Physics*, *17*(19), 12,177–12,196. 3.1

Soja, G., J. Barnes, M. Posch, K. Vandermeiren, H. Pleijel, and G. Mills (2000), Phenological weighting of ozone exposures in the calculation of critical levels for wheat, bean and plantain, *Environmental Pollution*, *109*(3), 517–524. 3.4

Tanou, G., V. Fotopoulos, and A. Molassiotis (2012), Priming against environmental challenges and proteomics in plants: update and agricultural perspectives, *Frontiers in Plant Science*, *3*, 216. 3.2.6.1

Temple, P. (1986), Stomatal conductance and transpirational responses of field-grown cotton to ozone, *Plant, Cell & Environment*, *9*(4), 315–321. 3.2.6.1

Tiedemann, A., and B. Pfähler (1994), Growth stage-dependent effects of ozone on the permeability for ions and non-electrolytes of wheat leaves in relation to the susceptibility to septoria nodorum berk., *Physiological and molecular plant pathology*, *45*(2), 153–167. 3.1

Van Goethem, T., L. Azevedo, R. Van Zelm, F. Hayes, M. Ashmore, and M. Huijbregts (2013), Plant species sensitivity distributions for ozone exposure, *Environmental pollution*, *178*, 1–6. 3.1

VanLoocke, A., A. M. Betzelberger, E. A. Ainsworth, and C. J. Bernacchi (2012), Rising ozone concentrations decrease soybean evapotranspiration and water use efficiency whilst increasing canopy temperature, *New Phytologist*, *195*(1), 164–171. 3.2.6.3, 3.4

Wang, W.-N., T.-H. Cheng, X.-F. Gu, H. Chen, H. Guo, Y. Wang, F.-W. Bao, S.-Y. Shi, B.-R. Xu, X. Zuo, et al. (2017), Assessing spatial and temporal patterns of observed ground-level ozone in china, *Scientific reports*, *7*(1), 3651. 3.4

Wang, X., M. Vignjevic, D. Jiang, S. Jacobsen, and B. Wollenweber (2014), Improved tolerance to drought stress after anthesis due to priming before anthesis in wheat (triticum aestivum l.) var. vinjett, *Journal of experimental botany*, *65*(22), 6441–6456. 3.2.6.1

Wilkinson, S., G. Mills, R. Illidge, and W. J. Davies (2012), How is ozone pollution reducing our food supply?, *Journal of Experimental Botany*, *63*(2), 527–536. 3.1

Yadav, A., A. Bhatia, S. Yadav, V. Kumar, and B. Singh (2019), The effects of elevated co2 and elevated o3 exposure on plant growth, yield and quality of grains of two wheat cultivars grown in north india, *Heliyon*, *5*(8), e02,317. 3.4

Chapter 4

Use of a crop model to estimate the effect of ozone pollution on wheat in India

I. Droutsas[1,2], A. J. Challinor[1,2], S. R. Arnold[1,2], C. Deva[1,2] and S.T. Turnock[3]

[1] *Institute for Climate and Atmospheric Science, School of Earth and Environment, University of Leeds, LS2 9JT Leeds, UK*

[2] *Priestley International Centre for Climate, University of Leeds, LS2 9JT Leeds, UK*

[3] *Met Office Hadley Centre, Fitzroy Road, Exeter, Devon, United Kingdom*

Abstract

Ozone has been shown to have a significantly negative impact on wheat yields. India is one of the countries with the highest levels of surface ozone pollution due to various anthropogenic activities which emit air pollutants into the atmosphere. Wheat is a major crop in India during the Rabi season, a period which coincides with high ground-level ozone concentrations. Process-based crop modelling approaches can be used to quantify the effect of ozone on crop yield. Mills et al. 2018 used a stomatal flux model to estimate a mean 12.2% wheat yield loss in India due to ozone pollution for the years 2010-2012. Here, we used a process-based crop model, GLAM-ROC, to suggest a higher mean ozone effect (16.2%) on wheat yield in India for the years 1980-2009. We also showed that the ozone damage to yield exhibits large state-to-state variation as well as significant spatial differences in each state. For instance, in Uttar Pradesh, the state with the highest share of total wheat production, the ozone-induced yield loss varied between 5.7 and 27.6% for the year 2000. Reduction in the levels of ozone pollution can lead to significant decrease in wheat yield loss, with 25, 50 and 75% decrease in ozone lowering yield damage from 16.2% to 11.8, 4.9 and 1.3% respectively. Overall, our

results show that ozone stress causes significant wheat yield loss in India, the effect of the pollutant exhibits considerable spatial variation and effective regulation is needed to reduce the levels of ozone and increase wheat productivity in the future.

4.1 Introduction

Surface ozone (O_3) is an important air pollutant globally causing significant damage to crop production (*Van Dingenen et al.*, 2009; *Avnery et al.*, 2011). O_3 interacts with vegetation by being taken up by the leaves of the plants throught the stomatal pores, which are openings on the surface of the leaves used for gas exchange. In polluted regions of the world, O_3 diffuses into the leaves together with CO_2 and causes negative effects on plant growth, development and productivity (*Ainsworth et al.*, 2020).

Exposure to chronic O_3 concentration decreases leaf photosynthesis (*Pell et al.*, 1992) as well as stomatal conductance and transpiration (*Temple*, 1986; *Lombardozzi et al.*, 2013) and accelerates the rate of leaf senescence (*Pell et al.*, 1997; *Osborne et al.*, 2019). As a result, the plant biomass is reduced as well as the photosynthate allocation to the grain, leading to lower productivity and loss in grain yield (*Wilkinson et al.*, 2012). The negative effects of O_3 on plants depend upon the concentration level of the pollutant, the time and duration of exposure (*Heath et al.*, 2009), the plant sensitivity (*Van Goethem et al.*, 2013) and the stage of plant development (*Tiedemann and Pfähler*, 1994; *Mulholland et al.*, 1998).

Wheat exhibits high sensitivity to O_3 as demonstrated repeatedly in various experimental studies (e.g., *Heagle et al.*, 1979; *Farage et al.*, 1991; *Hansen et al.*, 2019). Enhanced concentrations of the pollutant reduce the crop's yield and alter the nutritional properties of the grains (*Broberg et al.*, 2015). In India, during the rabi season, 58% of the crop area is used for the cultivation of wheat (*Rao et al.*, 2015), which is typically sown in November-December and harvested in February-March. The country also faces high O_3 pollution levels, with the Indo-Gangetic plain being one of the hotspots (*Ghude et al.*, 2008), as well as the 'breadbasket' of India. During the months from February to June, high temperatures and increased solar radiation favour the photochemical production of O_3 (*Deb Roy et al.*, 2009). This period also coincides with the later stages of wheat development, which are the most O_3-sensitive for grain yield loss (*Lee et al.*, 1988; *Pleijel et al.*, 1998). Given that India is the second largest producer of wheat globally (*Mottaleb et al.*, 2019), the effect of O_3 pollution on wheat is a crucial issue of food security in the country.

During the recent years, studies have demonstrated the deleterious effect of O_3 on wheat productivity in India. Most studies to date are empirical and used a statistical response function to relate the grain yield loss to the AOT40 index (i.e. Accumulated ozone exposure above a threshold of 40 ppbv). *Sinha et al.* (2015) estimated 27-41% reduction in wheat yield in the states of Punjab and Haryana for the years 2012-2013,

using O_3 data from a measurement site. *Lal et al.* (2017) expanded this analysis to a wide network of O_3 observation sites and estimated 4.2-15% annual yield loss due to O_3. *Van Dingenen et al.* (2009) and *Avnery et al.* (2011) estimated up to 28 and 30% average wheat yield loss respectively for the year 2000. *Burney and Ramanathan* (2014) developed a statistical regression model and suggested that O_3 and black carbon (BC) have caused around 33% wheat yield loss in India for the year 2010.

There is a large range of results in the above studies and some more process-based approaches have emerged recently to increase the confidence in the estimations. These methods improve upon the statistical approaches by explicitly accounting for the plant/environment interactions on crop growth and development during the whole crop season (*Emberson et al.*, 2018). *Mills et al.* (2018) used a stomatal flux model to account for the plant O_3 uptake and estimated a mean 12.2% wheat yield loss in India due to O_3 pollution for the years 2010-2012. Another recent method is taking a process-based crop model as a starting point. In this study, we apply the GLAM-ROC crop model (Chapter 3), to estimate the effect of O_3 pollution on wheat yield in India over a long time period (growing seasons 1980-2009). Our analysis considers all the main wheat-growing areas in the country and accounts for over 90% of the total wheat production. In addition, we estimate the spatial differences in the effect of O_3 between the states of India as well as between the different parts of each state. Finally, we assess the potential decreases in wheat yield loss due to different levels of reduction in surface O_3 pollution.

4.2 Materials and Methods

4.2.1 Climate, ozone and crop data

Daily meteorological data were obtained from the AgMerra climate series (*Ruane et al.*, 2015). We used maximum and minimum temperature (°C) and solar radiation ($MJ/m^2/day$) for the years 1980-2010 in horizontal resolution of 0.25° x 0.25°. Hourly surface ozone concentrations were obtained from the UKESM1 model, which was developed and evaluated in *Sellar et al.* (2019). The predecessor of this model, HadGEM2-ES, was evaluated for surface ozone concentrations over India in *Hakim et al.* (2019). UKESM1 considers 360 days in the simulations, in the form of 12 months $\times$ 30 days $month^{-1}$. In order to ensure consistency with the climate data, we duplicated all hourly ozone values on the last day of all months with 31 days and erased all ozone concentrations from the 29^{th} and 30^{th} of February. Ozone was provided in 1.25° x 1.875° horizontal resolution and was converted into 0.25° x 0.25° grids using the bilinear interpolation method of the Climate Data Operator (CDO) software (*Schulzweida*, 2019). We also considered three different levels of reduction in O_3 pollution: 25, 50 and 75%. For each reduction level, we multiplied all hourly O_3 concentrations by the

respective value to derive the decreased O_3 concentrations.

Historical wheat yield data were obtained from the ICRISAT district-level database (*ICRISAT*, 2015), where wheat yields were calculated from area and production information during the growing seasons of years 1980-2009. The following six states were considered in our analysis: Haryana, Madhya Pradesh, Uttar Pradesh, Punjab, Rajasthan and Bihar. We focused on these six states since they accounted for at least 90% of the total wheat production in each year. The wheat yield data were converted from districts to 0.25° x 0.25° resolution grids using the 'raster' package (*Hijmans et al.*, 2015) of Rv3.4.1 (*Team*, 2017). In order to remove the impact of technology on historical wheat productivity, the yield data were also detrended using the smoothing spline methodology of the R package 'dplR' (*Bunn et al.*, 2019).

4.2.2 Crop model

The GLAM-ROC (GLAM - Relative Ozone Concentrations) crop model was used to estimate the O_3-induced damage to wheat grain yield in India. GLAM-ROC is the version of the GLAM-Parti crop model (Chapter 2), which incorporates the effect of ground-level O_3 pollution on crop growth and development (Chapter 3). The model was developed based on the General Large Area Model for annual crops (GLAM) (*Challinor et al.*, 2004), which is a relatively simple model designed to operate on the spatial scale of climate models (*Challinor et al.*, 2003).

GLAM-ROC uses transpiration efficiency to simulate crop growth and allometric relationships for partitioning the crop biomass to the plant compartments. The daily potential evapotranspiration is calculated by the Priestley-Taylor approach and is partitioned into potential evaporation and potential transpiration. The actual transpiration is computed from the potential transpiration rate by taking into account the soil water content. The transpiration is multiplied by the transpiration efficiency to return the daily biomass growth. In this study, the canopy SLA was determined according to the daily maximum temperature events accumulated during the crop growing season (*Droutsas et al.*, 2019). This equation was chosen since it was designed for high temperature environments similar the ones encountered in India. In addition, given that over 90% of wheat in India is irrigated (*Koehler et al.*, 2013), fully irrigated conditions were considered for the model runs.

4.2.3 Ozone concentrations and metrics

GLAM-ROC requires daily mean O_3 concentration and the AOT40 index (Accumulated ozone exposure above a threshold of 40 ppbv) for the model runs (Chapter 3). Both metrics are calculated for the 16 hours with the highest O_3 concentration in each day

(i.e. the daylight hours). AOT40 is computed as follows:

$$AOT40 = \sum_{i=1}^{n} DOE40_i \tag{4.1}$$

where n is the number of days in the growing season, i is the day index and DOE40 is the daily O_3 exposure (ppmh) defined as:

$$DOE40 = \sum_{j=1}^{16} max([O_3]_j - 40ppb, 0) \cdot 0.001\ ppmh\ ppbh^{-1} \tag{4.2}$$

where $[O_3]$ is the one-hour mean O_3 concentration (ppb) and j is the hour index.

Fig. 4.1 shows the spatial average and maximum value of the mean O_3 concentrations (16-hour) during the wheat growing season (November - April) for the six states considered in this study. The spatially averaged mean O_3 concentrations exhibit an increasing trend in the states of Bihar, Madhya Pradesh and Rajastan and decreasing in Haryana, Punjab and Uttar Pradesh. The spatial maximum of the mean O_3 concentrations is increasing in all states, with Bihar exhibiting the highest and Punjab the lowest rate of change over time. This shows that the mean O_3 concentrations do not exhibit a consistent trend in all states for the November to April time period, however, the O_3 pollution episodes have increased in magnitude in all states over time.

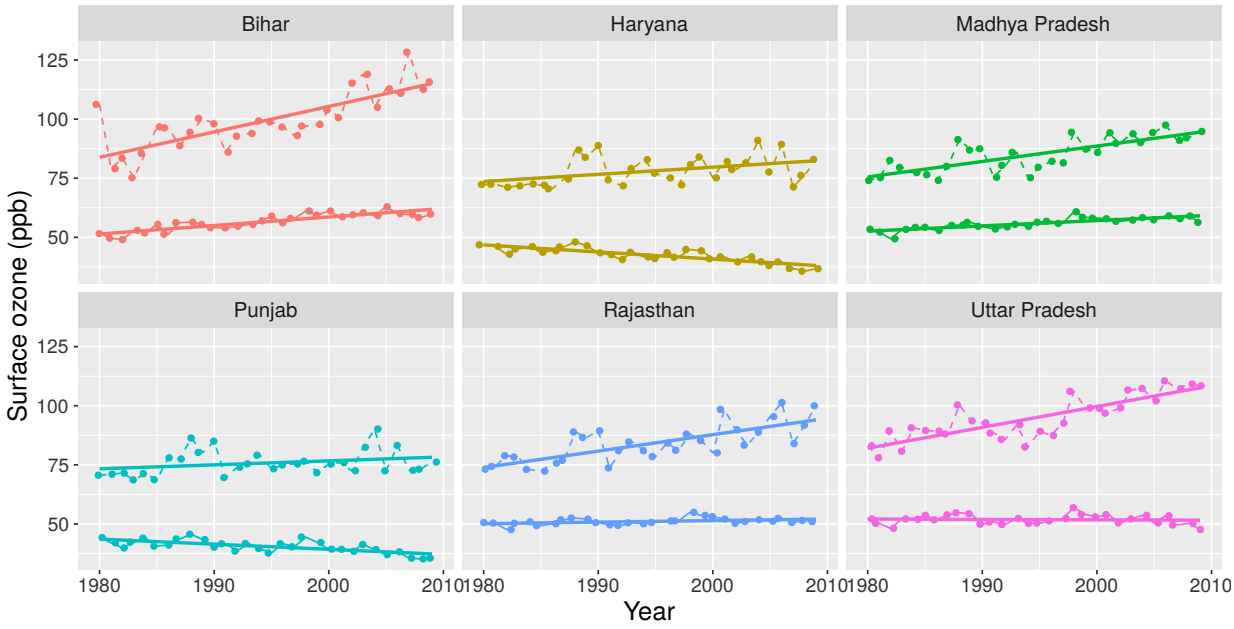

Figure 4.1: UKESM1 model estimations of spatial average (solid lines) and maximum value (dashed lines) of the 16-h mean O_3 concentration in the states of Bihar, Haryana, Madhya Pradesh, Punjab, Rajasthan and Uttar Pradesh during the wheat growing season (November - April) for the years 1980-2010.

4.2.4 Performance metrics

For the calibration and evaluation of the model performance, we used the root mean square error (RMSE), the normalized root mean square error (nRMSE) and the mean percent difference (MPD) as follows:

$$RMSE = \sqrt{\frac{\sum_{i=1}^{n}(P_i - O_i)^2}{n}} \tag{4.3}$$

$$nRMSE = \frac{RMSE}{\overline{O}} * 100 \tag{4.4}$$

$$MPD = \frac{\sum_{i=1}^{n}(\frac{|O_i - P_i|}{O_i})}{n} * 100 \tag{4.5}$$

where P_i and O_i are the estimated and observed values respectively, $\bar{O}$ is the mean of observations and n equals the number of observations.

4.2.5 Model calibration

For the calibration of the GLAM-ROC model, the yield gap parameter (YGP) was used to minimize the RMSE between the observed and simulated grain yield in each grid cell included in the analysis on the first year of the simulations (i.e. growing year 1980). YGP is in the [0-1] range and accounts for all parameters that influence crop yield and are not explicitly simulated by the model (e.g. limited soil nutrients, pests, diseases, non-optimal management). It (YGP) is multiplied with the simulated grain yield at maturity to reduce production from the attainable to the actual level. Moreover, the values of normalized transpiration efficiency (E_T), maximum transpiration efficiency ($E_{TN,max}$) and the rate of change of harvest index (dHI/dt) are provided in Table C.1. All other parameter values are taken from Chapter 3. Irrigated wheat is usually sown around mid-November (*Prasad and Nagarajan*, 2004), thus the 15th of November was chosen as the planting date for the model runs.

4.2.6 GLAM-ROC estimation of ozone effect on wheat

The O_3-induced damage to wheat yield was estimated by running GLAM-ROC with the parameterization used for the model evaluation, but ignoring the effect of O_3 stress on wheat growth and development. The relative yield loss (RYL) from O_3 pollution was defined as follows:

$$RYL = (1 - \frac{Y_{oz}}{Y_c}) * 100 \tag{4.6}$$

where Y_{oz} and Y_c are the simulated grain yields with and without the O_3 effect respectively.

4.3 Results

4.3.1 Evaluation of GLAM-ROC model performance

The modelled yield times series were compared against the observations for the wheat growing seasons 1980 - 2009 (Fig. C.1). The values of the metrics used for the model evaluation are presented in Table 4.1. Across the six states, RMSE for yield ranged from 148.0 kg ha^{-1} in Madhya Pradesh to 324.3 kg ha^{-1} in Haryana. When RMSE was normalized by the observed mean yield, the lowest error was observed in Punjab with 9.6%. Haryana, Madhya Pradesh and Uttar Pradesh exhibited an error less than 15%, whilst Bihar and Rajasthan showed nRMSE of 17.2 and 21.9% respectively. The lowest MDP was observed in Punjab (7.7%). Bihar, Haryana, Madhya Pradesh and Uttar Pradesh exhibited MDP lower than 15%, whilst in Rajasthan MPD was less that 20%. We followed the ranking of *Hammad et al.* (2018) (i.e. in their study, the CSM-CERES-Maize Model was evaluated for maize growth and yield in Pakistan) and considered the GLAM-ROC model simulations as very good in Punjab (i.e. nRMSE and MDP $< 10\%$) and good in all other states (i.e. nRMSE and MDP $< 20\%$). Only in Rajastan, nRMSE was higher than 20% (21.9%).

Table 4.1: Root mean square error (RMSE), normalized root mean square error (nRMSE) and mean percent difference (MPD) between observed and simulated (GLAM-ROC) average wheat yields in the states of Bihar, Haryana, Madhya Pradesh, Punjab, Rajasthan and Uttar Pradesh for the growing seasons 1980-2009.

RMSE	nRMSE	MPD	State
223.6	17.2	13.9	Bihar
324.3	13.9	10.5	Haryana
148.0	14.8	10.9	Madhya Pradesh
262.5	9.6	7.7	Punjab
311.3	21.9	19.5	Rajasthan
233.7	14.8	11.3	Uttar Pradesh

Overall, the above results demonstrate that the model was suitable for simulating wheat yields in India during the growing seasons 1980-2009. The model comparison to observations is summarized in Fig. 4.2.

4.3.2 Historical effects of ozone on wheat yield in India (1980 - 2010)

4.3.2.1 Simulated state-level ozone damage to wheat yield

GLAM-ROC suggested a mean 16.2 $\pm$ 1.7% O_3-induced wheat yield loss during the wheat growing seasons 1980 - 2009 (Table 4.2, Fig. C.2). This effect varies considerably between the six states with Bihar exhibiting the largest RYL (18.9%) and Punjab the lowest (9.8%). Madhya Pradesh, Uttar Pradesh, Rajastan and Haryana exhibit 18.5, 15.5, 15.3, and 10.5% damage to wheat yield respectively due to O_3 pollution. In all

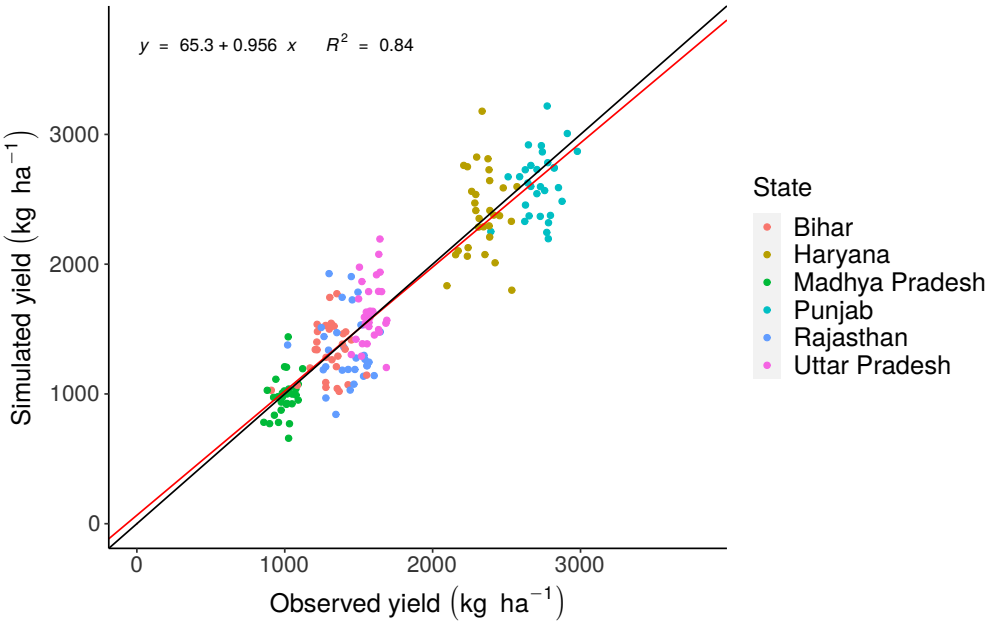

Figure 4.2: Simulated (GLAM-ROC) versus observed average wheat yield in the states of Bihar, Haryana, Madhya Pradesh, Punjab, Rajasthan and Uttar Pradesh during the growing seasons 1980-2009. The solid black line is the 1:1 line and the solid red line is the linear regression between simulated and observed yield.

states, the effect of O_3 does not vary strongly between the years, with the standard deviation (sd) being less than 4% (Table 4.2).

In addition, Uttar Pradesh, Madhya Pradesh, Rajastan and Bihar show an increasing trend of RYL over time, whilst in Haryana and Punjab the trend is declining (Fig. C.2). The highest RYL trend is seen in Bihar, where the increase in surface O_3 leads to an added yield loss of 0.24% each year. On the contrary, the largest decreasing trend in RYL is in Haryana, where the reduced O_3 concentrations lower the damage of the pollutant to wheat yield by an average 0.08% annually.

Table 4.2: Average wheat Relative Yield Loss (RYL) and standard deviation (sd) in the states of Bihar, Haryana, Madhya Pradesh, Punjab, Rajasthan and Uttar Pradesh during the growing seasons 1980-2009.

RYL	sd	State
18.9	3.1	Bihar
10.5	1.9	Haryana
18.5	2.2	Madhya Pradesh
9.8	1.7	Punjab
15.3	1.8	Rajasthan
15.5	1.9	Uttar Pradesh
16.2	1.7	Average

4.3.2.2 Ozone damage to wheat yield at grid level

Fig. 4.3 and C.3B illustrate the large variation in RYL between the different grids of each state, with the year 2000 taken as example. In Uttar Pradesh, the state with the highest share of total wheat production, the mean RYL is 17.6%, whilst the minimum and maximum values are 5.7 and 27.6% respectively. Large differences exist in all other states, with RYL ranging from 5.8 - 13.6% in Punjab, 6.5 - 14.5% in Haryana, 8.8 - 24.4% in Rajastan, 15.1 - 25.7% in Madhya Pradesh and 17.0 - 27.4% in Bihar. The large variability in RYL reveals that the effect of O_3 on wheat yield depends upon the area where wheat is cultivated in each state.

In Punjab and Haryana, the states with the lowest O_3 levels (Fig. 4.1), the parts with the highest O_3 damage to yield are those in close vicinity to the state of Rajastan (Fig. C.3A). Similarly, in Uttar Pradesh, the largest O_3-induced yield losses are experienced in the Southeast part which is close to Bihar and Madhya Pradesh (i.e. the two states with the highest O_3 concentrations; Fig. 4.1). Rajastan faces high O_3 pollution as well as RYL in the central and south parts, whilst Madhya Pradesh and Bihar exhibit the highest O_3 levels, the largest damage to wheat yield and the lowest spatial variation in comparison with all other states. Overall, the O_3 damage to wheat yield strongly depends upon the area where wheat is cultivated in each state, with the regions belonging to or neighbouring the most pollutant states exhibiting the highest effect of O_3 pollution on yield.

When all grids are taken together, the average O_3 damage to wheat yield for the year 2000 is 19.0% (Fig. 4.3; red dashed line), which is similar to the mean effect of the pollutant in the states of Uttar Pradesh, and Rajastan. In Madhya Pradesh and Bihar, the O_3-induced yield losses are higher than the average, whilst in Haryana and Punjab they are considerably lower. Nevertheless, the latter two states exhibit low impact on RYL, since they include low number of grid cells due to their small size.

4.3.3 Avoided yield losses from reduction in ozone pollution

We used GLAM-ROC to estimate the reduction in wheat yield loss due to three different levels of reduction in O_3 pollution: 25, 50 and 75%. Fig. 4.4 illustrates the large avoided yield damage, where the mean yield loss of 16.2% under the current O_3 level is reduced to 11.8, 4.9 and 1.3% accordingly for O_3 decreases of 25, 50 and 75% respectively. In other words, the O_3 damage to wheat yield lowers by 27.2, 70 and 92% for O_3 reductions of 25, 50 and 75% respectively. Similarly, the maximum RYL is 19.2%, which decreases to 15.7, 6.0 and 2.1% for the same O_3 reductions. The largest avoided yield losses are seen for O_3 decrease from 25 to 50% in comparison with the current level (Fig. 4.4). Significant RYL decrease is also seen for O_3 reduction from 0 to 25% and 50 to 75%. Above 75% there is limited yield benefit since RYL is already very low (1.3%).

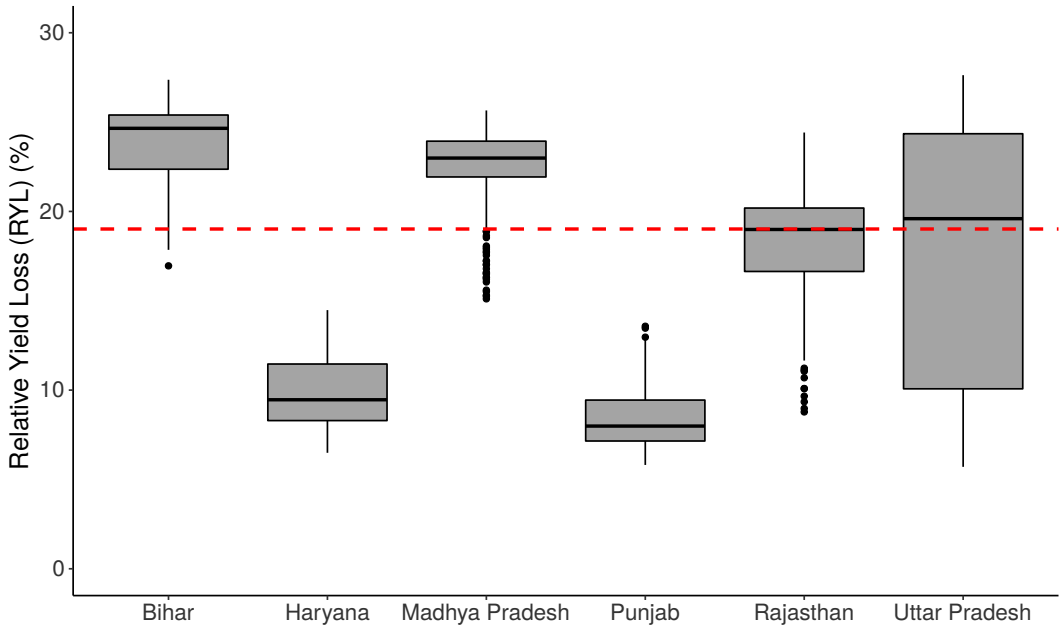

Figure 4.3: Boxplots of Relative Yield Loss (RYL) for wheat in the states of Bihar, Haryana, Madhya Pradesh, Punjab, Rajasthan and Uttar Pradesh for the year 2000. Red dashed line is the average RYL of all grids in the six states.

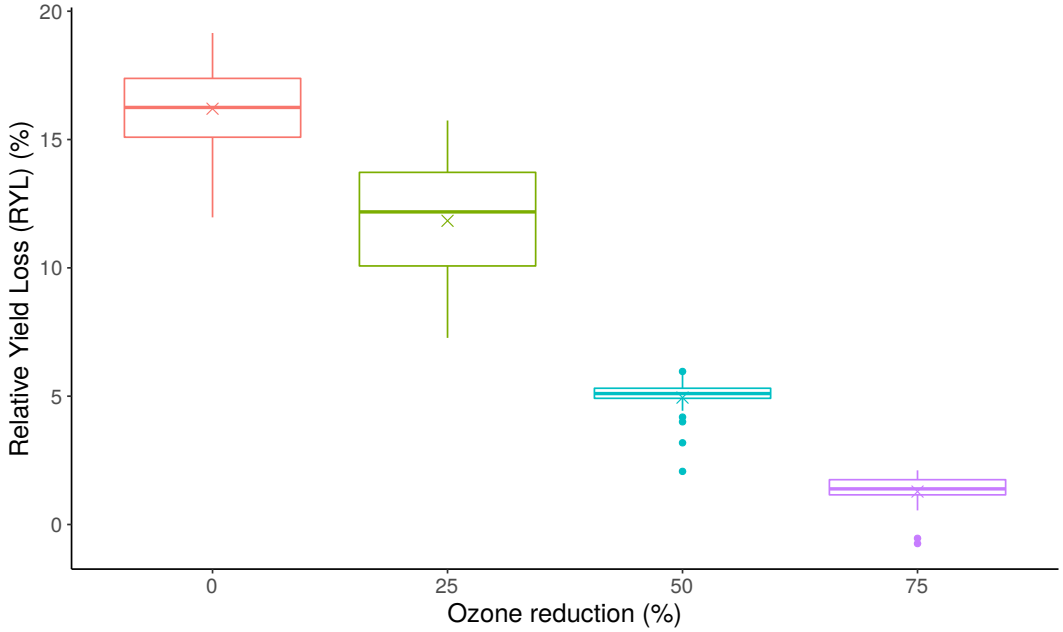

Figure 4.4: Boxplots of wheat relative yield loss (RYL) in India due to 0, 25, 50 and 75% decrease in ground-level ozone pollution during the growing seasons 1980-2009. The states considered in the analysis are Bihar, Haryana, Madhya Pradesh, Punjab, Rajasthan and Uttar Pradesh. Horizontal line is median and 'x' symbol is the mean value.

4.4 Discussion

GLAM-ROC suggests that ground-level O_3 pollution is significantly lowering the productivity of the wheat crop in India. The six major wheat-producing states in the

country are all experiencing enhanced surface O_3 levels during the wheat growing season, causing a mean grain yield loss of 16.2%. Thus, India loses the equivalent of one wheat harvest every six years due to O_3 pollution. Only for the year 2000, wheat exposure to O_3 caused 19% grain yield damage which corresponds to loss of 15.99 million tons in wheat production. This translates to an economic loss of about 3.36 billion USD in the country.

Our estimations are relatively higher than *Mills et al.* (2018), which used a stomatal O_3 flux model to suggest that O_3 pollution causes 12.2% wheat yield loss in India for the years 2010-2012. In their study, Uttar Pradesh and Bihar face the highest O_3-induced yield damage, around 12.5 - 17.5%. In our study, Bihar and Uttar Pradesh rank 1st and 3rd regarding the O_3 damage to wheat yield, with 18.9 and 15.5% yield losses respectively. In addition, our estimates are lower than *Sharma et al.* (2019), who used a statistical yield response function to suggest that O_3 pollution has caused 21% average yield loss in India for the years 2014-2015. All the above findings are considerably lower than the 33% wheat yield loss due to air pollution suggested by *Burney and Ramanathan* (2014). However, in their study, the impact of black carbon was also taken into account for their estimations.

Our results reveal that there is large spatial variability in the effect of O_3 on wheat yield, depending on the area where the crop is cultivated. For instance, in Uttar Pradesh, the state with the highest share of wheat production in the country, the O_3 damage to yield varied from 4.3 to 26.2% for the year 2000. This is due to the large contrast in the levels of surface O_3, with the Southeast part of the state exhibiting significantly higher pollution levels than the Northwest (Fig. C.3B). This large variation in O_3 drives the spatial differences in wheat yield response to the pollutant. Madhya Pradesh and Bihar exhibit the highest O_3 levels in our analysis with the lowest spatial variation leading to high yield losses in almost all parts of the state. On the contrary, Punjab and Haryana exhibit the lowest O_3 and RYL levels, with the levels of the pollutant being higher in their south parts neighbouring Rajasthan which leads to enhanced yield losses.

The spatial variability in the response of wheat yield to O_3 may partially explain the large differences in the estimations of *Sinha et al.* (2015) and *Lal et al.* (2017). The former study used O_3 observations from a specific site in Punjab and estimated up to 41% wheat yield losses due to the pollutant for the years 2012-2013. The latter study used O_3 data from 17 independent sites and suggested up to 15% average wheat yield damage due to O_3. Despite that the two studies used different methodologies for the calculation of the O_3 effect on wheat yield, our results show that the spatial differences in surface O3 pollution play an important role on the estimations. Thus, the effect of O_3 on wheat yield in a state cannot be assessed based on the level of the pollutant at a specific site. The use of O_3 data from multiple sites can improve the estimation of the average O_3 damage to wheat yield in India significantly.

GLAM-ROC suggested significant reductions in wheat yield loss due to decrease in the level of surface O_3 pollution. Reduced O_3 concentrations of 25% could avoid up to 18.2% wheat yield damage in the six states of our analysis. Halving O_3 and 75% reduction in the concentrations of the pollutant can decrease RYL by up to 68.8 and 89.1% respectively. This clearly shows the importance of regulating the emissions of air pollutants for increasing wheat productivity and improving food security in India. It is important to note that the yield benefit decreases for O_3 reductions above 50% in comparison with the current level. This is due to the low O_3 phytotoxicity below a certain level (40 ppb for wheat, (*Mills et al.*, 2007)). At 75% reduction in O_3 pollution, the RYL is already low (1.3%), which means that further O_3 decrease does not lead to significant yield gain. In addition, the highest relative yield gain was observed when the reduction in O_3 concentration was between 25 to 50% in comparison with the current level of the pollutant. This suggests that reducing O_3 by up to 25 and 50% can have a very significant, positive effect on wheat productivity in India.

4.5 Conclusion

Surface O_3 pollution threatens food security in India. The six main wheat-producing states in the country face significant wheat yield losses due to enhanced levels of surface O_3 concentration during the crops growing season. Our analysis suggests an average annual yield loss of 16.2% due to O_3, which varies from 9.8% in Punjab to 18.9% in Bihar. The effect of the pollutant on wheat yield is relatively stable over time with low inter-annual variability. However, there is significant spatial variation, with some areas facing up to five times higher O_3-induced yield losses than others into the same state. Reduction in the levels of O_3 can increase wheat yields significantly, with 25 and 50% decrease in the concentrations of the pollutant lowering the yield damage by up to 18.2 and 68.8% respectively. Hence, effective regulation for the reduction of surface O_3 in India can provide a significant mechanism for future increases in wheat grain yield.

Acknowledgements

This work was supported by the UK N8 AgriFood Resilience Programme. I.D. gratefully acknowledges the Oatley PhD Scholarship and the Priestley International Centre for Climate for the financial support.

References

Ainsworth, E. A., P. Lemonnier, and J. M. Wedow (2020), The influence of rising tropospheric carbon dioxide and ozone on plant productivity, *Plant Biology*, *22*, 5–11. 4.1

Avnery, S., D. L. Mauzerall, J. Liu, and L. W. Horowitz (2011), Global crop yield reductions due to surface ozone exposure: 1. year 2000 crop production losses and economic damage, *Atmospheric Environment*, *45*(13), 2284–2296. 4.1

Broberg, M. C., Z. Feng, Y. Xin, and H. Pleijel (2015), Ozone effects on wheat grain quality–a summary, *Environmental Pollution*, *197*, 203–213. 4.1

Bunn, A., M. Korpela, F. Biondi, F. Campelo, P. Mrian, F. Qeadan, and C. Zang (2019), *dplR: Dendrochronology Program Library in R*, r package version 1.7.0. 4.2.1

Burney, J., and V. Ramanathan (2014), Recent climate and air pollution impacts on indian agriculture, *Proceedings of the National Academy of Sciences*, *111*(46), 16,319–16,324. 4.1, 4.4

Challinor, A., J. Slingo, T. Wheeler, P. Craufurd, and D. Grimes (2003), Toward a combined seasonal weather and crop productivity forecasting system: determination of the working spatial scale, *Journal of Applied Meteorology*, *42*(2), 175–192. 4.2.2

Challinor, A., T. Wheeler, P. Craufurd, J. Slingo, and D. Grimes (2004), Design and optimisation of a large-area process-based model for annual crops, *Agricultural and forest meteorology*, *124*(1-2), 99–120. 4.2.2

Deb Roy, S., G. Beig, and S. D. Ghude (2009), Exposure-plant response of ambient ozone over the tropical indian region, *Atmospheric Chemistry and Physics*, *9*(14), 5253–5260. 4.1

Droutsas, I., A. Challinor, M. Swiderski, and M. A. Semenov (2019), New modelling technique for improving crop model performance-application to the glam model, *Environmental Modelling & Software*, *118*, 187–200. 4.2.2

Emberson, L. D., H. Pleijel, E. A. Ainsworth, M. Van den Berg, W. Ren, S. Osborne, G. Mills, D. Pandey, F. Dentener, P. Büker, et al. (2018), Ozone effects on crops and consideration in crop models, *European journal of agronomy*, *100*, 19–34. 4.1

Farage, P. K., S. P. Long, E. G. Lechner, and N. R. Baker (1991), The sequence of change within the photosynthetic apparatus of wheat following short-term exposure to ozone, *Plant Physiology*, *95*(2), 529–535. 4.1

Ghude, S. D., S. Fadnavis, G. Beig, S. Polade, and R. Van Der A (2008), Detection of surface emission hot spots, trends, and seasonal cycle from satellite-retrieved no2 over india, *Journal of Geophysical Research: Atmospheres*, *113*(D20). 4.1

Hakim, Z. Q., S. Archer-Nicholls, G. Beig, G. A. Folberth, K. Sudo, N. Abraham, S. Ghude, D. Henze, and A. Archibald (2019), Evaluation of tropospheric ozone and ozone precursors in simulations from the htapii and ccmi model intercomparisons–a focus on the indian subcontinent. 4.2.1

Hammad, H. M., F. Abbas, A. Ahmad, W. Farhad, J. Anothai, and G. Hoogenboom (2018), Predicting water and nitrogen requirements for maize under semi-arid conditions using the csm-ceres-maize model, *European Journal of Agronomy*, *100*, 56–66. 4.3.1

Hansen, E. M., H. Hauggaard-Nielsen, M. Launay, P. Rose, and T. N. Mikkelsen (2019), The impact of ozone exposure, temperature and co2 on the growth and yield of three spring wheat varieties, *Environmental and Experimental Botany*, *168*, 103,868. 4.1

Heagle, A. S., S. Spencer, and M. B. Letchworth (1979), Yield response of winter wheat to chronic doses of ozone, *Canadian Journal of Botany*, *57*(19), 1999–2005. 4.1

Heath, R. L., A. S. Lefohn, and R. C. Musselman (2009), Temporal processes that contribute to nonlinearity in vegetation responses to ozone exposure and dose, *Atmospheric Environment*, *43*(18), 2919–2928. 4.1

Hijmans, R. J., J. Van Etten, J. Cheng, M. Mattiuzzi, M. Sumner, J. A. Greenberg, O. P. Lamigueiro, A. Bevan, E. B. Racine, A. Shortridge, et al. (2015), Package raster, *R package*. 4.2.1

ICRISAT (2015), Meso level data for India: 1966-2011, collected and compiled under the project on Village Dynamics in South Asia. 4.2.1

Koehler, A.-K., A. J. Challinor, E. Hawkins, and S. Asseng (2013), Influences of increasing temperature on indian wheat: quantifying limits to predictability, *Environmental Research Letters*, *8*(3), 034,016. 4.2.2

Lal, S., S. Venkataramani, M. Naja, J. C. Kuniyal, T. K. Mandal, P. K. Bhuyan, K. M. Kumari, S. N. Tripathi, U. Sarkar, T. Das, et al. (2017), Loss of crop yields in india due to surface ozone: An estimation based on a network of observations, *Environmental Science and Pollution Research*, *24*(26), 20,972–20,981. 4.1, 4.4

Lee, E. H., D. T. Tingey, and W. E. Hogsett (1988), Evaluation of ozone exposure indices in exposure-response modeling, *Environmental Pollution*, *53*(1-4), 43–62. 4.1

Lombardozzi, D., J. Sparks, and G. Bonan (2013), Integrating o 3 influences on terrestrial processes: photosynthetic and stomatal response data available for regional and global modeling, *Biogeosciences*, *10*(11), 6815–6831. 4.1

Mills, G., A. Buse, B. Gimeno, V. Bermejo, M. Holland, L. Emberson, and H. Pleijel (2007), A synthesis of aot40-based response functions and critical levels of ozone for agricultural and horticultural crops, *Atmospheric Environment*, *41*(12), 2630–2643. 4.4

Mills, G., K. Sharps, D. Simpson, H. Pleijel, M. Broberg, J. Uddling, F. Jaramillo, W. J. Davies, F. Dentener, M. Van den Berg, et al. (2018), Ozone pollution will compromise efforts to increase global wheat production, *Global change biology*, *24*(8), 3560–3574. 4.1, 4.4

Mottaleb, K. A., P. K. Singh, K. Sonder, G. Kruseman, and O. Erenstein (2019), Averting wheat blast by implementing a wheat holiday: In search of alternative crops in west bengal, india, *PloS one*, *14*(2). 4.1

Mulholland, B., J. Craigon, C. Black, J. Colls, J. Atherton, and G. Landon (1998), Effects of elevated co2 and o3 on the rate and duration of grain growth and harvest index in spring wheat (triticum aestivum l.), *Global Change Biology*, *4*(6), 627–635. 4.1

Osborne, S., D. Pandey, G. Mills, F. Hayes, H. Harmens, D. Gillies, P. Büker, and L. Emberson (2019), New insights into leaf physiological responses to ozone for use in crop modelling, *Plants*, *8*(4), 84. 4.1

Pell, E., N. Eckardt, and A. Enyedi (1992), Timing of ozone stress and resulting status of ribulose bisphosphate carboxylase/oxygenase and associated net photosynthesis, *New Phytologist*, *120*(3), 397–405. 4.1

Pell, E. J., C. D. Schlagnhaufer, and R. N. Arteca (1997), Ozone-induced oxidative stress: mechanisms of action and reaction, *Physiologia Plantarum*, *100*(2), 264–273. 4.1

Pleijel, H., H. Danielsson, J. Gelang, E. Sild, and G. Selldén (1998), Growth stage dependence of the grain yield response to ozone in spring wheat (triticum aestivum l.), *Agriculture, ecosystems & environment*, *70*(1), 61–68. 4.1

Prasad, R., and S. Nagarajan (2004), Rice-wheat cropping system-food security and sustainability, *CURRENT SCIENCE-BANGALORE-*, *87*, 1334–1335. 4.2.5

Rao, B. B., P. S. Chowdary, V. Sandeep, V. Pramod, and V. Rao (2015), Spatial analysis of the sensitivity of wheat yields to temperature in india, *Agricultural and forest meteorology*, *200*, 192–202. 4.1

Ruane, A. C., R. Goldberg, and J. Chryssanthacopoulos (2015), Climate forcing datasets for agricultural modeling: Merged products for gap-filling and historical climate series estimation, *Agricultural and Forest Meteorology*, *200*, 233–248. 4.2.1

Schulzweida, U. (2019), Cdo user guide, doi:10.5281/zenodo.3539275. 4.2.1

Sellar, A. A., C. G. Jones, J. Mulcahy, Y. Tang, A. Yool, A. Wiltshire, F. M. O'connor, M. Stringer, R. Hill, J. Palmieri, et al. (2019), Ukesm1: Description and evaluation of the uk earth system model, *Journal of Advances in Modeling Earth Systems*. 4.2.1

Sharma, A., N. Ojha, A. Pozzer, G. Beig, and S. S. Gunthe (2019), Revisiting the crop yield loss in india attributable to ozone, *Atmospheric Environment: X*, *1*, 100,008. 4.4

Sinha, B., K. S. Sangwan, Y. Maurya, V. Kumar, C. Sarkar, B. Chandra, and V. Sinha (2015), Assessment of crop yield losses in punjab and haryana using two years of continuous in-situ ozone measurements., *Atmospheric Chemistry & Physics Discussions*, *15*(2). 4.1, 4.4

Team, R. C. (2017), R: A language and environment for statistical com-puting, *R Foundation for Statistical Computing, Vienna, Austria. URL https://www. R-project. org*. 4.2.1

Temple, P. (1986), Stomatal conductance and transpirational responses of field-grown cotton to ozone, *Plant, Cell & Environment*, *9*(4), 315–321. 4.1

Tiedemann, A., and B. Pfähler (1994), Growth stage-dependent effects of ozone on the permeability for ions and non-electrolytes of wheat leaves in relation to the susceptibility to septoria nodorum berk., *Physiological and molecular plant pathology*, *45*(2), 153–167. 4.1

Van Dingenen, R., F. J. Dentener, F. Raes, M. C. Krol, L. Emberson, and J. Cofala (2009), The global impact of ozone on agricultural crop yields under current and future air quality legislation, *Atmospheric Environment*, *43*(3), 604–618. 4.1

Van Goethem, T., L. Azevedo, R. Van Zelm, F. Hayes, M. Ashmore, and M. Huijbregts (2013), Plant species sensitivity distributions for ozone exposure, *Environmental pollution*, *178*, 1–6. 4.1

Wilkinson, S., G. Mills, R. Illidge, and W. J. Davies (2012), How is ozone pollution reducing our food supply?, *Journal of Experimental Botany*, *63*(2), 527–536. 4.1

Chapter 5

Discussion and conclusion

5.1 Summary

Agricultural systems are complex environments where there are interactions between crops and the weather; atmosphere (e.g. CO_2 level, air pollution); soil quality; land availability; human decisions (e.g. planting date, crop management); socio-economic factors (human labour availability, fertilizers, pesticides); environmental resources (e.g. available water for irrigation); technological and scientific advancements (e.g. agricultural machinery, new cultivars); and other ecological aspects (e.g. plant pests, diseases, weeds). Large-area crop models mainly focus on the influence of weather (short-term) and the climate (long-term) on crop productivity, whilst they may also take into account the condition of the soil, the changes in land use patterns and basic management information (e.g. planting date, amount of fertilizer application). Other above-mentioned interactions are usually not included due to the difficulty in their quantification, such as the influence of technology and scientific progress on crop yield, the effects of pests, weeds and deseases and various socio-economic factors such as the level of human labour and the available capital.

The evaluation of crop models is usually performed against experimental studies with plants exposed to certain environmental conditions and management practices. If the model exhibits good skill in the simulation of plant growth, development and yield, there is increased confidence that it can be reliably used for large-area applications, at least when similar weather conditions apply. Recent studies, however, reveal that crop models often exhibit limited skill in their simulations, especially under stress conditions (e.g., *Asseng et al.*, 2015; *Li et al.*, 2015; *Maiorano et al.*, 2017). These studies show that the effects of water and temperature stress are not always adequately simulated, due to the difficulty in modelling complex plant biological processes in extreme environments. Future climate variability and change are expected to increase the frequency of heat and drought extremes, thus, improving the representation of these events in the crop models is a vital step toward robust estimations of the effect of climate change on crop

production.

5.2 Discussion

One of the main factors that drive the performance of a crop model is the complexity. If the model is too simple for the purpose of its use, the predictions are poor; the same happens if it is too complex. Agricultural environments exhibit high complexity and the crop models often become increasingly complex to include more processes and interactions affecting crop yield (e.g. drought, heat, nitrogen, salinity or ozone stress) (*Sinclair and Seligman*, 1996). The role of the model structure is very important to support the added complexity and avoid model inconsistencies. A problematic model structure limits the impact of further model development with the addition of new processes and interactions and increases the error in the simulations. Thus, an appropriate level of complexity should be combined with a robust model structure to improve the model performance (*Passioura*, 1996).

A simple example of a model structure which requires improvement is given in the GLAM crop model, where in each time step the first calculated state variable is the leaf area index (LAI) based on a maximum leaf area growth (Fig. 5.1). The value of LAI is then used to estimate the potential level of canopy transpiration. If there is not enough water in the soil, the canopy transpiration is reduced from a maximum to an actual (water-stressed) value, which in turn reduces the growth of the above-ground biomass under the transpiration efficiency approach. The issue here is that on the same time step, LAI is calculated for optimal growth conditions, whilst the total biomass corresponds to water stress conditions (Fig. 5.1). For this reason, a water stress factor is calculated as fraction of the actual to potential transpiration and is applied to reduce the growth of leaf area on the next time step. In addition, an optional subroutine (named SLA control) is usually applied to adjust LAI to the value of biomass.

The model structure outlined above creates two problems. The first issue is the time-step limitation, where the model is unable to synchronize LAI and biomass on the same time-step if the SLA control is not used. It should be mentioned that this is not a problem encountered only in GLAM, but may be faced in every crop model that uses sequential method for solving the equations (after three years of investigation in the literature, I could not find a process-based crop model in use which solves all equations simultaneously). The second issue is the model over-parameterization, where for the estimation of the water-stressed LAI, GLAM firstly uses the maximum growth of leaf area (dL/dt_{max}; 1st parameter), then the drought stress factor on LAI (WSFAC; 2nd parameter) and then the SLA control, where the value of SLA is given as input (3rd parameter) (Fig. 5.1). The SLA subroutine is also inconsistent with the reality since it ignores the mass of stems (i.e. in the model: SLA = LAI/(Biomass - Yield)). In

this thesis, the above issues had to be addressed before further increasing the model complexity with the inclusion of the impact of air pollution into the crop model.

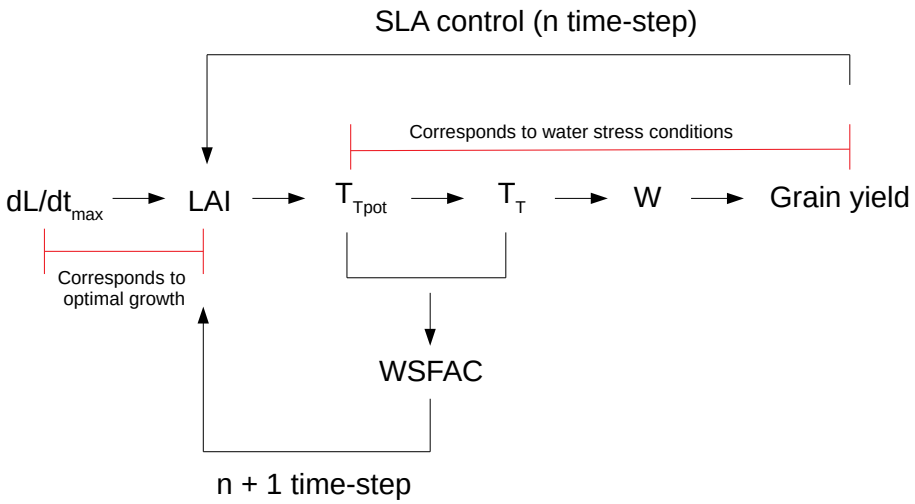

Figure 5.1: GLAM model structure on typical n day after crop emergence. dL/dt_{max} is maximum leaf area growth, LAI is leaf area index, T_{Tpot} is potential canopy transpiration, T_T is actual canopy transpiration, W is above-ground biomass and WSFAC is water stress factor.

The incorporation of SEMAC into GLAM introduces a new model version, GLAM-Parti, which addresses the above-mentioned issues in the crop model structure. The simultaneous equation modelling approach implemented into GLAM-Parti removes the time-step limitation in the update of state variables, since all equations are solved as a system and no interactions are missed. In addition, the parameters previously used for the estimation of LAI are removed (i.e. in GLAM-Parti there is no SLA control, dL/dt_{max} and WSFAC acting on LAI). Instead, LAI is an emergent property of the simultaneous solution of the system of equations (Fig. 2.6). For the development of GLAM-Parti, two more major modifications were implemented. An allometric relationship is introduced to express the mass of stems as function of the leaf mass and the canopy SLA is parameterized as function of the maximum temperature events accumulated during the crop growing season.

In Chapter 2, GLAM-Parti improves upon GLAM in the comparison of wheat exposed to different levels of drought stress. The RMSE of GLAM-Parti is reduced by at least 44, 66 and 41% for LAI, biomass and grain yield respectively in comparison with GLAM in the early, late and full drought treatments (Table 2.1). The improvement in model performance is both due to the model modifications and the simultaneous solution of the model equations. Restructuring GLAM-Parti to solve the equations sequentially resulted in an RMSE increase of 25.2% for LAI, 28.6% for biomass and 7.9% for yield in the four water stress treatments (Fig. 2.12). In addition, the use of

allometric relationship for partitioning the wheat biomass between leaves and stems allows to easily shift the allocation of carbon to favour the mass of stems over the leaf mass under water stress. This is an important property of GLAM-Parti, since the modelling of assimilate allocation is complex and consists of an ongoing issue in crop models (*Boote et al.*, 2013). Overall, the SEMAC methodology demonstrated significant contribution on the performance of GLAM, providing with a robust model structure, improved internal consistency, reduced parameterization requirements and increased skill in the simulation of plant growth, development and yield for wheat under water stress conditions. Hence, GLAM-Parti closely followed the observed reduction in leaf and overall wheat growth, the acceleration of leaf senescence and the decrease in grain yield induced by drought in the experiments (Fig. 2.8 - 2.10).

In Chapter 3, GLAM-Parti was further parameterized for the effect of O_3 pollution on wheat growth, development and productivity. The derived model, GLAM-ROC, was tested against experimental data with wheat exposed to enhanced levels of O_3 at variable duration of exposure to the pollutant. The model exhibited high skill in the simulation of both the chronic and the episodic exposure to O_3 and the biomass and grain yield were less than 6% and 1% different from the observations respectively (Fig. 3.5). An important novelty in the development of the O_3 subroutine was the inclusion of an acclimation process to modify the canopy response to O_3 with increased duration of exposure to the pollutant. The plant acclimation to O_3 has already been reported in the literature (e.g., *Held et al.*, 1991; *Gillespie et al.*, 2011), however, to my knowledge, the mechanism of plant acclimation to chronic O_3 exposure is not incorporated into any crop model up to date. One reason may be that the crop models are usually evaluated for the crop response to different O_3 concentration levels but not in variable duration of exposure to the pollutant. The mechanism of plant acclimation to O_3 is also significant for future crop yield projections, since climate change can increase surface O_3, especially in highly polluted regions of the world (*Doherty et al.*, 2013).

GLAM-ROC was compared with a commonly used statistical response function (SRF), a model where the O_3-induced damage to grain yield is determined according to the level of exposure to the pollutant (i.e. the AOT40 index) through a linear relationship (*Mills et al.*, 2007). SRF assumes that plants exposed to 'x' times higher O_3 than other identical plants, will also face 'x' times higher reduction in yield. This was not confirmed in our study, since the plants in the chronic treatment exhibited lower impact per ppmh of AOT40 in comparison with the same plants in the episodic treatment. As a result, the ratio of chronic:episodic grain yield was underestimated by 56.5% in the SRF formula (Fig. 3.9). On the contrary, GLAM-ROC successfully followed the observed chronic:episodic grain yield ratio (less than 1% different from observation) (Fig. 3.9) by incorporating the acclimation mechanism to reduce the effect of O_3 with increased duration of plant exposure to the pollutant.

The grain filling period is the most O_3-sensitive for grain yield loss due to the adverse

effect of the stressor on the allocation of carbon to the grains (*Fuhrer and Booker*, 2003). GLAM-ROC successfully reproduced the observed plant response to O_3 by reducing the harvest index when exposure to the pollutant was experienced during grain filling. The crop growth was also reduced through modifications of transpiration (i.e. canopy water loss) and transpiration efficiency (i.e. biomass produced per unit of water transpired). In Chapter 3, GLAM-ROC exhibited high skill in the simulations based on the introduction of an O_3-reduction mechanism on crop growth, the modification in the partitioning of biomass to the grains and the plant acclimation process for variable plant exposure to O_3. Models which do not incorporate the acclimation mechanism may increase the error in the simulations of O_3 damage to wheat yield under chronic plant exposure to the pollutant.

India faces high levels of surface O_3 pollution with negative impact on wheat productivity. In Chapter 4, GLAM-ROC was applied to estimate the effect of O_3 stress on wheat yield in India during a long historical time period (1980-2009). The model suggested that the six main wheat-producing states in India are all considerably affected by the pollutant. The O_3-induced damage to yield was found to vary spatially according to the concentration level of the pollutant in the different states of the country. The largest O_3-induced reductions in wheat grain yield are experienced in Bihar (18.9%), followed by Madhya Pradesh (18.5%), Uttar Pradesh (15.5%) and Rajasthan (15.3%). Haryana and Punjab exhibited lower effects with 10.5 and 9.8% loss in grain yield from O_3 pollution respectively. Reduction in the level of O_3 leads to significant decrease in the damage to grain yield, with 25, 50 and 75% decrease in O_3 concentration reducing yield losses by 27.2, 70 and 92% respectively. Surface O_3 is the major air pollutant affecting crop yields at national level (*Ainsworth et al.*, 2012), thus effective legislation is needed to reduce the levels of the pollutant and improve wheat productivity in India.

5.3 Limitations and future work

The SEMAC methodology provides with a new modelling opportunity for the simulation of crop growth, development and yield. A main limitation of the methodology is the model parameterization. In each time step, three major processes are included into the approach which need careful consideration. These are the accumulation of new biomass based on the radiation or transpiration efficiency approach, the partitioning of biomass into the plant compartments through allometric relationships and the evolution of canopy SLA. The first two aspects affect the accuracy of the model to simulate the aboveground biomass and the masses of the different organs (e.g. leaves, stems, grains). The third aspect (i.e. the SLA) affects the simulation of both the leaf mass and LAI.

The challenge in the parameterization is to account for all interactions between the factors that affect the crop performance (as described in the first paragraph of

the Discussion) and estimate their combined effect on these three processes. As a simplified example, one could argue that under any given environment and management practice, crop growth, development and yield can be accurately simulated if the slopes and intercepts of the three graphs in Fig. 5.2 can be correctly estimated. In other words, SEMAC incorporates all the uncertainties of the cropping system into these three processes (i.e. daily crop growth, development and canopy SLA), which makes it difficult to define the slopes and intercepts of the relationships in Fig. 5.2.

In the future, the model parameterization can be improved either with traditional crop modelling methods (i.e. through collection of experimental data - model comparison with observations - improvement in model parameterization) or with novel approaches, such as the use of machine learning for the determination of the unknown parameters. The ultimate goal is to develop a robust parameterization of these three processes (i.e. daily growth, development and canopy SLA) in order to improve the representation of crop performance in the simulations. This will lead to a model capable of accurate predictions of crop yield by accounting for the climatic factors and management conditions, the soil quality and the technological and scientific advancements.

Regarding the effect of O_3 pollution on wheat, GLAM-ROC should be evaluated for the interaction between O_3 and drought. Dry areas are hotspots of ozone pollution, such as the Mediterranean, the Middle East and the Southwestern United States (*Hodnebrog et al.*, 2012; *Lelieveld et al.*, 2009; *Wise and Comrie*, 2005) and the crops in these regions may not always be fully irrigated. In wheat, water stress causes stomatal closure, which reduces the uptake of the pollutant, the canopy transpiration and the O_3 damage to grain yield (*Khan and Soja*, 2003). In GLAM-ROC, both O_3 and drought decrease the daily canopy transpiration rate, the minimum of which is considered as the actual transpiration. The validity of this approach should be tested against experimental data with wheat exposed to both stressors simultaneously. In crop modelling, the interaction between O_3 and drought consists of an ongoing issue and previous model development studies which incorporate the O_3 damage into DSSAT-NWheat (*Guarin et al.*, 2019) and AFRCWHEAT2 (*Ewert and Porter*, 2000) did not evaluate the models against experimental data with plants exposed to a combination of both stressors. *Schauberger et al.* (2019) tested the LPJmL model against various experiments with wheat and soybean exposed to O_3 stress and few of them included a combination of O_3 and drought. Nevertheless, the authors did not separate the results for single (i.e. O_3 and combined (i.e. O_3 and drought) stress environments, which makes it difficult to evaluate the model performance in each case.

O_3 interacts with CO_2 with important implications for climate change. Elevated CO_2 concentrations reduce stomatal conductance and can protect against O_3 pollution *Yadav et al.* (2019). Hence, the role of CO_2 should not be ignored for future projections of the impact of surface O_3 pollution on wheat productivity. In GLAM-ROC, the

mechanism of CO_2 fertilisation on crop photosynthesis and growth should be added into the model. *Reyenga et al.* (1999) suggests a formula which increases radiation use efficiency according to the level of temperature and CO_2 concentration. Following the addition of this process, the interaction between elevated CO_2 and O_3 should be modelled to allow the estimation of crop growth and yield under future climate change projections.

Wheat exposure to O_3 pollution affects the nutritional properties of the grains. The meta-analysis of *Broberg et al.* (2015) showed that when the wheat crop is exposed to enhanced O_3 levels, the grain protein yield decreases significantly, meaning that less amount of protein is produced per unit area. This can have important implications for human nutrition, especially in developing countries where people rely more strongly on plant protein than in developed regions (*Henchion et al.*, 2017). For instance, in India, up to 70% of the daily protein intake comes from cereals, especially in rural areas (*Swaminathan et al.*, 2012). At the same time, the Indian population suffers from protein deficiency in their diet (*Rampal*, 2018), which has been found to link to several health issues such as reduced growth, stunting and wasting (*Golden*, 1985). Thus, reducing O_3 pollution can increase wheat protein yield and the daily intake of the nutrient for people in India.

GLAM-ROC does not simulate any traits of grain quality. Ongoing GLAM development attempts to incorporate a soil nitrogen subroutine into the model. This can consist of the first step in the simulation of the uptake of nitrogen by the plants and the partitioning of the nutrient to the different compartments, including the grains. The pattern of nitrogen partitioning may be modified according to the magnitude and the duration of the O_3 pollution event. Grain nitrogen can be converted into protein (*Mariotti et al.*, 2008), hence the model will be able to simulate alterations in the amount of grain protein according to the plant exposure to O_3. The simulation of other grain nutrients is not well understood (e.g. K, P, Mg, Zn, Fe) and most crop models do not yet incorporate algorithms for their estimation (*Nuttall et al.*, 2017). Future model development should focus more strongly on the effect of the environmental conditions on grain quality, since both climate change and air pollution exhibit significant impact on the nutritional composition of the wheat grains (*Myers et al.*, 2014; *Broberg et al.*, 2015).

In Chapter 4, GLAM-ROC was the single model applied for the estimation of the O_3 damage to wheat yield in India. All models contain errors and multi-model ensembles are particularly useful for the reduction of the uncertainty in the output. The median of the crop model ensemble has been seen to be a better predictor than any single crop model due to compensating for errors of the individual models and providing with higher consistency in the predictions (*Martre et al.*, 2015; *Asseng et al.*, 2015; *Challinor et al.*, 2018). AgMIP-Ozone is an initiative which started recently and attempts to evaluate the O_3 algorithms in the crop models which simulate O_3 damage. It would be very

interesting to compare GLAM-ROC with other models in the response of wheat to O_3 stress. This would provide a great opportunity for further assessing the model skill, learning from other modelling groups and improving the simulated processes.

In conclusion, SEMAC is a novel crop modelling technique which can be mainly applied in crop models of medium complexity (based on transpiration or radiation use efficiency approaches). The implementation of SEMAC into GLAM revealed significant improvement in model skill and good predictive power for wheat under drought and O_3 stress environments. The GLAM-ROC model can be used by scientists for the estimation of the effect of surface ozone pollution on wheat yield and assist in desicion-making for the regulation of anthropogenic emissions of air pollutants to increase wheat productivity. Similarly, GLAM-Parti can be used to estimate the impact of drought on wheat yield in large-area applications. The simplicity of SEMAC allows to further extend the model to incorporate more stresses into the simulations. This is an important property of the methodology, since crops in the field are exposed to various stress conditions during their growing season. Finally, following necessary parameterizations, GLAM-Parti can be used to estimate the impact on wheat of stresses such as heat and limited soil nitrogen.

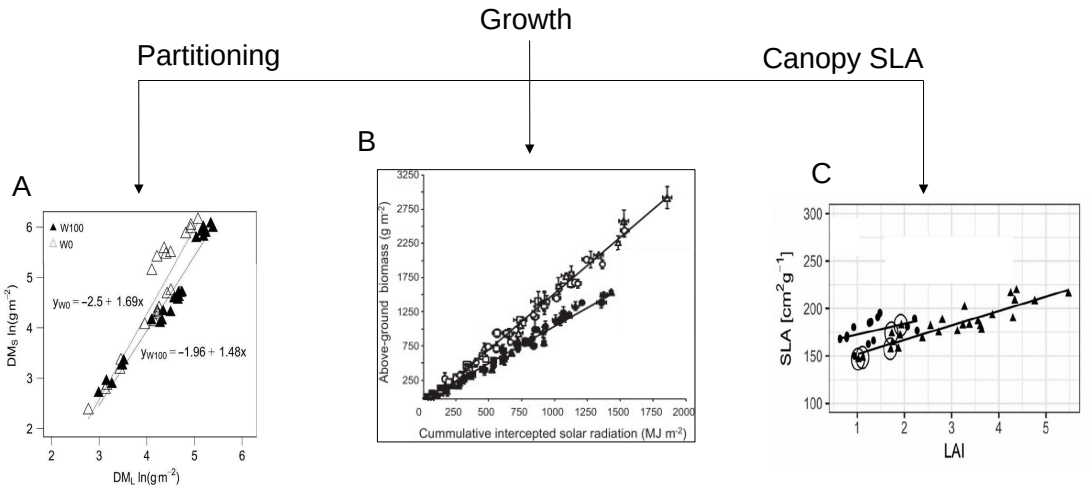

Figure 5.2: Sources of uncertainty in GLAM-Parti. Fig. A illustrates stem-leaf mass partitioning (taken from *Ratjen et al.* (2016)), Fig. B illustrates the determination of RUE as slope of above-ground biomass vs. cumulative intercepted radiation (taken from *Sandaña et al.* (2012)) and Fig. C illustrates canopy SLA vs. LAI (taken from *Ratjen et al.* (2018)).

References

Ainsworth, E. A., C. R. Yendrek, S. Sitch, W. J. Collins, and L. D. Emberson (2012), The effects of tropospheric ozone on net primary productivity and implications for climate change, *Annual review of plant biology*, *63*, 637–661. 5.2

Asseng, S., F. Ewert, P. Martre, R. P. Rötter, D. B. Lobell, D. Cammarano, B. A. Kimball, M. J. Ottman, G. Wall, J. W. White, et al. (2015), Rising temperatures reduce global wheat production, *Nature climate change*, *5*(2), 143. 5.1, 5.3

Boote, K. J., J. W. Jones, J. W. White, S. Asseng, and J. I. Lizaso (2013), Putting mechanisms into crop production models, *Plant, cell & environment*, *36*(9), 1658–1672. 5.2

Broberg, M. C., Z. Feng, Y. Xin, and H. Pleijel (2015), Ozone effects on wheat grain quality–a summary, *Environmental Pollution*, *197*, 203–213. 5.3

Challinor, A. J., C. Müller, S. Asseng, C. Deva, K. J. Nicklin, D. Wallach, E. Vanuytrecht, S. Whitfield, J. Ramirez-Villegas, and A.-K. Koehler (2018), Improving the use of crop models for risk assessment and climate change adaptation, *Agricultural systems*, *159*, 296–306. 5.3

Doherty, R., O. Wild, D. Shindell, G. Zeng, I. MacKenzie, W. Collins, A. M. Fiore, D. Stevenson, F. Dentener, M. Schultz, et al. (2013), Impacts of climate change on surface ozone and intercontinental ozone pollution: A multi-model study, *Journal of Geophysical Research: Atmospheres*, *118*(9), 3744–3763. 5.2

Ewert, F., and J. R. Porter (2000), Ozone effects on wheat in relation to co2: modelling short-term and long-term responses of leaf photosynthesis and leaf duration, *Global Change Biology*, *6*(7), 735–750. 5.3

Fuhrer, J., and F. Booker (2003), Ecological issues related to ozone: agricultural issues, *Environment international*, *29*(2-3), 141–154. 5.2

Gillespie, K. M., A. Rogers, and E. A. Ainsworth (2011), Growth at elevated ozone or elevated carbon dioxide concentration alters antioxidant capacity and response to acute oxidative stress in soybean (glycine max), *Journal of Experimental Botany*, *62*(8), 2667–2678. 5.2

Golden, M. H. (1985), The consequences of protein deficiency in man and its relationship to the features of kwashiorkor, *Nutritional adaptation in man*, pp. 169–185. 5.3

Guarin, J. R., B. Kassie, A. M. Mashaheet, K. Burkey, and S. Asseng (2019), Modeling the effects of tropospheric ozone on wheat growth and yield, *European Journal of Agronomy*, *105*, 13–23. 5.3

Held, A., H. Mooney, and J. N. Gorham (1991), Acclimation to ozone stress in radish: leaf demography and photosynthesis, *New phytologist*, *118*(3), 417–423. 5.2

Henchion, M., M. Hayes, A. M. Mullen, M. Fenelon, and B. Tiwari (2017), Future protein supply and demand: strategies and factors influencing a sustainable equilibrium, *Foods*, *6*(7), 53. 5.3

Hodnebrog, Ø., S. Solberg, F. Stordal, T. M. Svendby, D. Simpson, M. Gauss, A. Hilboll, G. Pfister, S. Turquety, A. Richter, et al. (2012), Impact of forest fires, biogenic emissions and high temperatures on the elevated eastern mediterranean ozone levels during the hot summer of 2007, *Atmospheric Chemistry and Physics*, *12*(18), 8727–8750. 5.3

Khan, S., and G. Soja (2003), Yield responses of wheat to ozone exposure as modified by drought-induced differences in ozone uptake, *Water, Air, and Soil Pollution*, *147*(1-4), 299–315. 5.3

Lelieveld, J., P. Hoor, P. Jöckel, A. Pozzer, P. Hadjinicolaou, J.-P. Cammas, and S. Beirle (2009), Severe ozone air pollution in the persian gulf region., *Atmospheric Chemistry & Physics*, *9*(4). 5.3

Li, T., T. Hasegawa, X. Yin, Y. Zhu, K. Boote, M. Adam, S. Bregaglio, S. Buis, R. Confalonieri, T. Fumoto, et al. (2015), Uncertainties in predicting rice yield by current crop models under a wide range of climatic conditions, *Global change biology*, *21*(3), 1328–1341. 5.1

Maiorano, A., P. Martre, S. Asseng, F. Ewert, C. Müller, R. P. Rötter, A. C. Ruane, M. A. Semenov, D. Wallach, E. Wang, et al. (2017), Crop model improvement reduces the uncertainty of the response to temperature of multi-model ensembles, *Field Crops Research*, *202*, 5–20. 5.1

Mariotti, F., D. Tomé, and P. P. Mirand (2008), Converting nitrogen into proteinbeyond 6.25 and jones' factors, *Critical reviews in food science and nutrition*, *48*(2), 177–184. 5.3

Martre, P., D. Wallach, S. Asseng, F. Ewert, J. W. Jones, R. P. Rötter, K. J. Boote, A. C. Ruane, P. J. Thorburn, D. Cammarano, et al. (2015), Multimodel ensembles of wheat growth: many models are better than one, *Global change biology*, *21*(2), 911–925. 5.3

Mills, G., A. Buse, B. Gimeno, V. Bermejo, M. Holland, L. Emberson, and H. Pleijel (2007), A synthesis of aot40-based response functions and critical levels of ozone for agricultural and horticultural crops, *Atmospheric Environment*, *41*(12), 2630–2643. 5.2

Myers, S. S., A. Zanobetti, I. Kloog, P. Huybers, A. D. Leakey, A. J. Bloom, E. Carlisle, L. H. Dietterich, G. Fitzgerald, T. Hasegawa, et al. (2014), Increasing co 2 threatens human nutrition, *Nature*, *510*(7503), 139–142. 5.3

Nuttall, J., G. O'Leary, J. Panozzo, C. Walker, K. Barlow, and G. Fitzgerald (2017), Models of grain quality in wheata review, *Field crops research*, *202*, 136–145. 5.3

Passioura, J. B. (1996), Simulation models: science, snake oil, education, or engineering?, *Agronomy Journal*, *88*(5), 690–694. 5.2

Rampal, P. (2018), An analysis of protein consumption in india through plant and animal sources, *Food and nutrition bulletin*, *39*(4), 564–580. 5.3

Ratjen, A., D. Neukam, and H. Kage (2016), A simple drought-sensitive model for leaf: Stem partitioning of wheat, *Journal of agronomy and crop science*, *202*(4), 300–308. (document), 5.2

Ratjen, A., G. Lemaire, H. Kage, D. Plénet, and E. Justes (2018), Key variables for simulating leaf area and n status: biomass based relations versus phenology driven approaches, *European journal of agronomy*, *100*, 110–117. (document), 5.2

Reyenga, P. J., S. M. Howden, H. Meinke, and G. M. McKeon (1999), Modelling global change impacts on wheat cropping in south-east queensland, australia, *Environmental modelling & software*, *14*(4), 297–306. 5.3

Sandaña, P., M. Ramírez, and D. Pinochet (2012), Radiation interception and radiation use efficiency of wheat and pea under different p availabilities, *Field crops research*, *127*, 44–50. (document), 5.2

Schauberger, B., S. Rolinski, S. Schaphoff, and C. Müller (2019), Global historical soybean and wheat yield loss estimates from ozone pollution considering water and temperature as modifying effects, *Agricultural and forest meteorology*, *265*, 1–15. 5.3

Sinclair, T. R., and N. G. Seligman (1996), Crop modeling: from infancy to maturity, *Agronomy Journal*, *88*(5), 698–704. 5.2

Swaminathan, S., M. Vaz, and A. V. Kurpad (2012), Protein intakes in india, *British Journal of Nutrition*, *108*(S2), S50–S58. 5.3

Wise, E. K., and A. C. Comrie (2005), Meteorologically adjusted urban air quality trends in the southwestern united states, *Atmospheric Environment*, *39*(16), 2969–2980. 5.3

Yadav, A., A. Bhatia, S. Yadav, V. Kumar, and B. Singh (2019), The effects of elevated co2 and elevated o3 exposure on plant growth, yield and quality of grains of two wheat cultivars grown in north india, *Heliyon*, *5*(8), e02,317. 5.3

Appendix A

Supporting information for Chapter 2

The equations of potential evapotranspiration (E^{T}_{pot}), potential transpiration (T_T) and biomass growth (dW/dt) are taken from *Challinor et al.* (2004).
Potential evapotranspiration:

$$\begin{aligned} E^{T}_{pot} &= \frac{\alpha}{\lambda} \cdot \frac{\Delta(R_N - G)}{\Delta + \gamma} \\ &= \frac{\alpha}{\lambda} \cdot \frac{\Delta(R_N - C_G \cdot R_N \cdot e^{-kLAI})}{\Delta + \gamma} \\ &= \frac{\alpha \cdot \Delta \cdot R_N}{\lambda \cdot (\Delta + \gamma)} \cdot (1 - C_G e^{-kLAI}) \end{aligned} \tag{A.1}$$

Eq. A.1 can be used to express potential transpiration as:

$$\begin{aligned} T_T &= E^{T}_{pot} \cdot (1 - e^{-kLAI}) \\ &= \frac{\alpha \cdot \Delta \cdot R_N}{\lambda \cdot (\Delta + \gamma)} \cdot (1 - C_G \cdot e^{-kLAI})(1 - e^{-kLAI}) \end{aligned} \tag{A.2}$$

Eq. A.2 can be used to describe biomass growth (dW/dt) as:

$$\begin{aligned} \frac{dW}{dt} &= TE \cdot T_T \\ &= TE \cdot \frac{\alpha \cdot \Delta \cdot R_N}{\lambda \cdot (\Delta + \gamma)} \cdot (1 - C_G \cdot e^{-kLAI}) \cdot (1 - e^{-kLAI}) \end{aligned} \tag{A.3}$$

Eq. A.3 consists of the dW/dt term in Eq. 2.11. The C_G, k, γ and λ are constants and the α, Δ, R_N, TE are dependent on the environmental conditions. After calculating the environmental dependence, the dW/dt becomes a function of LAI. Detailed description of all parameters and equations is provided in *Challinor et al.* (2004).

Table A.1: Values and units of calibrated parameters for GLAM, GLAM-Parti and GLAM-Parti$_{seq}$

Parameter	Unit	Range	GLAM value	GLAM-Parti value	GLAM-Parti$_{seq}$ value	Source
E_T	Pa	[3.5 6]	3.5	3.5	3.5	*Sanai et al.* (2010)
$E_{TN,max}$	g kg^{-1}	[5 9]	5	5.6	5.8	*Sanai et al.* (2010)
Post anthesis RUE	g MJ^{-1} PAR	[1.2 - 2.0]	2.0	2.0	2.0	*Calderini et al.* (1997)
$(dL/dt)_{max}$	m^2 m^{-2} d^{-1}	[0.06 0.28]	0.18	0.09 [a]	0.095 [a]	*Sanai et al.* (2010), *Jamieson et al.* (1995)
dHI/dt	d^{-1}	[0.0064 0.0137]	0.01	0.009	0.009	*Moot et al.* (1996)

[a] $(dL/dt)_{max}$ is used only after anthesis when SEMAC stops and the model runs under the GLAM approach.

References

Calderini, D. F., M. F. Dreccer, and G. A. Slafer (1997), Consequences of breeding on biomass, radiation interception and radiation-use efficiency in wheat, *Field Crops Research*, *52*(3), 271–281. A.1

Challinor, A., T. Wheeler, P. Craufurd, J. Slingo, and D. Grimes (2004), Design and optimisation of a large-area process-based model for annual crops, *Agricultural and forest meteorology*, *124*(1-2), 99–120. A, A

Jamieson, P., R. Martin, and G. Francis (1995), Drought influences on grain yield of barley, wheat, and maize, *New Zealand journal of crop and horticultural science*, *23*(1), 55–66. A.1

Moot, D., P. Jamieson, A. Henderson, M. Ford, and J. Porter (1996), Rate of change in harvest index during grain-filling of wheat, *The Journal of Agricultural Science*, *126*(4), 387–395. A.1

Sanai, L., T. Wheeler, A. Challinor, L. Erda, X. Yinlong, and J. Hui (2010), Simulating the impacts of global warming on wheat in china using a large area crop model, *Journal of Meteorological Research*, *24*(1), 123–135. A.1

Appendix B

Supporting information for Chapter 3

B.0.1 SLA function in GLAM-Parti

In *Ratjen et al.* (2018) the canopy SLA for wheat was expressed as function of LAI (Fig B.1). The suggested relationship is the following:

$$SLA = \begin{cases} 161.3 + 11.3 \cdot LAI & DVS < 32 \\ 137 + 15.1 \cdot LAI & DVS \geq 32 \end{cases} \tag{B.1}$$

For GLAM-Parti, the major limitation of the above piecewise function is the lack of continuity on the first day when DVS reaches 32 (i.e. Zadoks stage 32). In Fig. B.1, this day is shown in point (LAI1, SLA1). In order to deal with this discontinuity, the slope and intercept of Eq. B.1 were modified above DVS = 32 as:

$$SLA = \begin{cases} 161.3 + 11.3 \cdot LAI & DVS < 32 \\ z + y \cdot LAI & DVS \geq 32 \end{cases} \tag{B.2}$$

where y and z were determined using points (LAI1, SLA1) and (6, 227.6). The second point is the solution of Eq. B.1 for LAI = 6 and DVS $\geq$ 32. Based on the two points, y and z were calculated as:

$$y = (SLA1 - 227.6)/(LAI1 - 6) \tag{B.3}$$

$$z = 227.6 - 6 \cdot y \tag{B.4}$$

Eq. B.2 is used in GLAM-Parti to express SLA as function of LAI and graphical illustration is shown in Fig. B.1 (b).

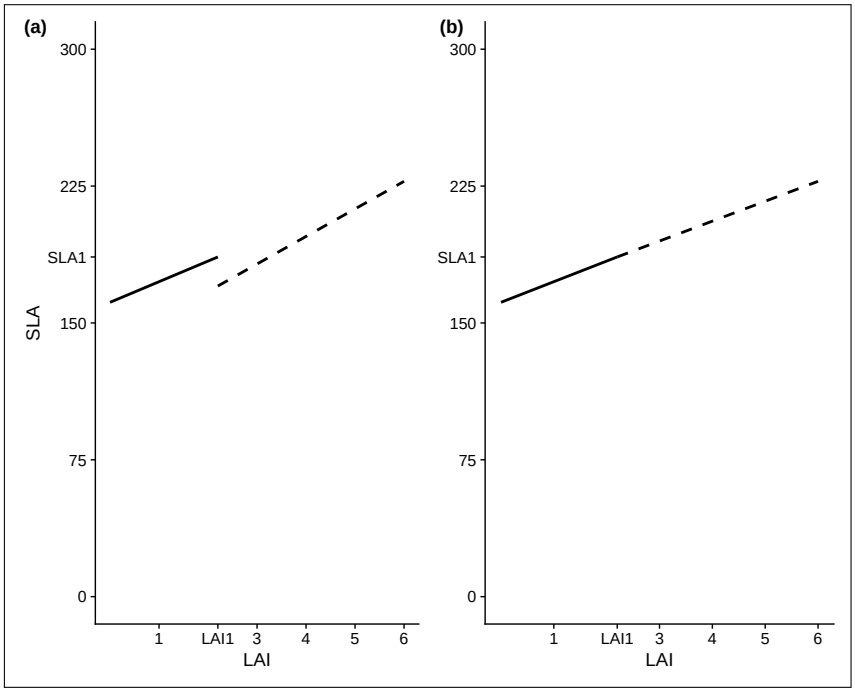

Figure B.1: Canopy SLA as function of LAI (a) in *Ratjen et al.* (2018) (b) in this study. Point (LAI1, SLA1) is when DVS reaches 32.

B.0.2 Expanding GLAM-Parti approach after anthesis

In GLAM-Parti, the above-ground biomass (W_n) consists of leaves, stems, ears and grains as follows:

$$W_n = M_L + M_S + M_E + M_G \tag{B.5}$$

where M_L is leaf, M_S is stem, M_E is the non-grain ear mass and M_G is the grain mass. M_E is expressed as function of M_S as follows:

$$M_E = C_E \cdot TT_n/TT_{fl} \cdot M_S \tag{B.6}$$

where TT_n is the thermal time elapsed from terminal spikelet initiation (TS) until day n after TS and TT_{fl} is the thermal time requirement from TS to anthesis. C_E expresses the ratio of ear: stem mass at anthesis, which is set to 0.5 for modern wheat varieties (*Siddique et al.*, 1989). M_G is expressed as function of W_n using the harvest index (HI) as follows:

$$M_G = HI \cdot W_n \tag{B.7}$$

Eq. B.6, B.7 can be combined to describe Eq. B.5 as:

$$W_n = (1/(1 - HI)) \cdot (M_L + (1 + C_E * TT_n/TT_{fl}) * M_S) \tag{B.8}$$

Eq. B.8 can be further manipulated to express W_n as function of leaf area change. M_L is expressed as:

$$M_L = LAI/SLA + M_{YL} \tag{B.9}$$

where LAI is green leaf area index, SLA is canopy specific leaf area and M_{YL} is the mass of yellow leaves. LAI can be expanded as:

$$LAI_n = LAI_{n-1} + dL \tag{B.10}$$

where LAI_n is the value of LAI at any given n day, LAI_{n-1} is LAI of the previous day and dL is the leaf area change between the two consecutive days. The mass of stems (M_S) is expressed with an allometric relationship according to M_L as:

$$M_S = h \cdot M_L^g \tag{B.11}$$

where g, h are allometric coefficients. Eq. B.2, B.9, B.10, B.11 can be combined to express Eq. B.8 as:

$$W_n = (1/(1-HI))\cdot(\frac{LAI_{n-1}+dL}{z+y\cdot(LAI_{n-1}+dL)}+M_{YL}+(1+C_E\cdot TT_n/TT_{fl})\cdot h(\frac{LAI_{n-1}+dL}{z+y\cdot(LAI_{n-1}+dL)}+M_{YL})^g) \tag{B.12}$$

where the slope and intercept of Eq. B.2 (y, z) vary before and after DVS = 32. Eq. B.12 expresses W_n as function of the leaf area change (dL) and is used for the implementation of the SEMAC methodology during the full crop cycle in GLAM-Parti. A detailed description of the SEMAC approach is given in *Droutsas et al.* (2019).

Moreover, the model was parametrerized to account for the canopy leaf mass loss which mainly occurs during the period of rapid leaf senescence after anthesis. Whenever a negative value of leaf area change (dL) was estimated, the mass of yellow leaves (M_{YL}) was updated as:

$$M_{YL(n)} = M_{YL(n-1)} + C_{yl} * (|dL|/SLA) \tag{B.13}$$

where $M_{YL(n)}$ is the mass of yellow leaves on the n day of the crop cycle, $M_{YL(n-1)}$ is the mass of yellow leaves on the previous day (n-1), SLA is the canopy specific leaf area and C_{yl} is the ratio of yellow:green leaf mass which was set to 0.68 to account for the leaf mass loss due to the remobilization of dry mass (*Borrell et al.*, 1989).

B.0.3 O_3 effect on evapotranspiration in GLAM-ROC

The statistical formula for the expression of percentage change in cumulative evapotranspiration (pCET) according to effective AOT40 (efAOT40) is given below (Fig. 3.3 (b)):

$$pCET = -0.021 + 0.018 \cdot efAOT40 - 0.000356 \cdot efAOT40^2 \tag{B.14}$$

where at any given n day of the growing season, pCET between the Control and O_3 treatments is defined as:

$$pCET_n = \frac{CET_{AA_n} - CET_{oz_n}}{CET_{oz_n}} = \frac{CET_{AA_n}}{CET_{oz_n}} - 1 = \frac{CET_{AA_n}}{CET_{oz_{n-1}} + ET_{oz_n}} - 1 \quad \text{(B.15)}$$

where CET_{AA} and CET_{oz} are the cumulative evapotranspiration of the control and O_3 treatment respectively. The substitution of Eq. B.15 into B.14 and solving for ET_{oz} gives:

$$ET_{oz_n} = \frac{CET_{AA_n}}{0.979 + 0.018 \cdot efAOT40 - 0.000365 \cdot efAOT40^2} - CET_{oz_{n-1}} \quad \text{(B.16)}$$

Eq. B.16 is used in GLAM-ROC to calculate the O_3-induced decrease in ET (ET_{oz}) in comparison with the same plant growing under optimal conditions.

Table B.1: Slope and intercept of O_3-induced reduction in transpiration efficiency (TE) and rate of change in harvest index (dHI/dt) relative to Control.

TE reduction factor		dHI/dt reduction factor	
c1	d1	c2	d2
-0.0029	1.029	-0.00145	1.0145

Table B.2: Values and units of GLAM-ROC calibrated parameters.

Parameter	Unit	Range	GLAM-ROC value	Source
$E_{TN,max}$	g kg^{-1}	[3 - 10.6][a]	9.3	*Christy et al.* (2018)
dHI/dt	day^{-1}	[0.0064 - 0.0137]	0.0135	*Moot et al.* (1996)

[a] Average CO_2 concentration in the chambers was around 530 ppm (see Table 3.1). The upper boundary of $E_{TN,max}$ was multiplied by 1.18 to account for the CO_2 fetilization effect on TE (*Reyenga et al.*, 1999).

References

Borrell, A. K., L. Incoll, R. J. Simpson, and M. J. Dalling (1989), Partitioning of dry matter and the deposition and use of stem reserves in a semi-dwarf wheat crop, *Annals of Botany*, *63*(5), 527–539. B.0.2

Christy, B., S. Tausz-Posch, M. Tausz, R. Richards, G. Rebetzke, A. Condon, T. McLean, G. Fitzgerald, M. Bourgault, and G. O'leary (2018), Benefits of increasing transpiration efficiency in wheat under elevated co 2 for rainfed regions, *Global change biology*, *24*(5), 1965–1977. B.2

Droutsas, I., A. Challinor, M. Swiderski, and M. A. Semenov (2019), New modelling technique for improving crop model performance-application to the glam model, *Environmental Modelling & Software*, *118*, 187–200. B.0.2

Moot, D., P. Jamieson, A. Henderson, M. Ford, and J. Porter (1996), Rate of change in harvest index during grain-filling of wheat, *The Journal of Agricultural Science*, *126*(4), 387–395. B.2

Ratjen, A., G. Lemaire, H. Kage, D. Plénet, and E. Justes (2018), Key variables for simulating leaf area and n status: biomass based relations versus phenology driven approaches, *European journal of agronomy*, *100*, 110–117. (document), B.0.1, B.1

Reyenga, P. J., S. M. Howden, H. Meinke, and G. M. McKeon (1999), Modelling global change impacts on wheat cropping in south-east queensland, australia, *Environmental modelling & software*, *14*(4), 297–306. B.2

Siddique, K., E. Kirby, and M. Perry (1989), Ear: stem ratio in old and modern wheat varieties; relationship with improvement in number of grains per ear and yield, *Field crops research*, *21*(1), 59–78. B.0.2

Appendix C

Supporting information for Chapter 4

Table C.1: Values and units of GLAM-ROC calibrated parameters.

Parameter	Unit	GLAM-ROC value	Source
E_T	Pa	3.5	*Droutsas et al.* (2019)
$E_{TN,max}$	g kg^{-1}	9.0	*Christy et al.* (2018)
dHI/dt	d^{-1}	0.01	*Moot et al.* (1996)

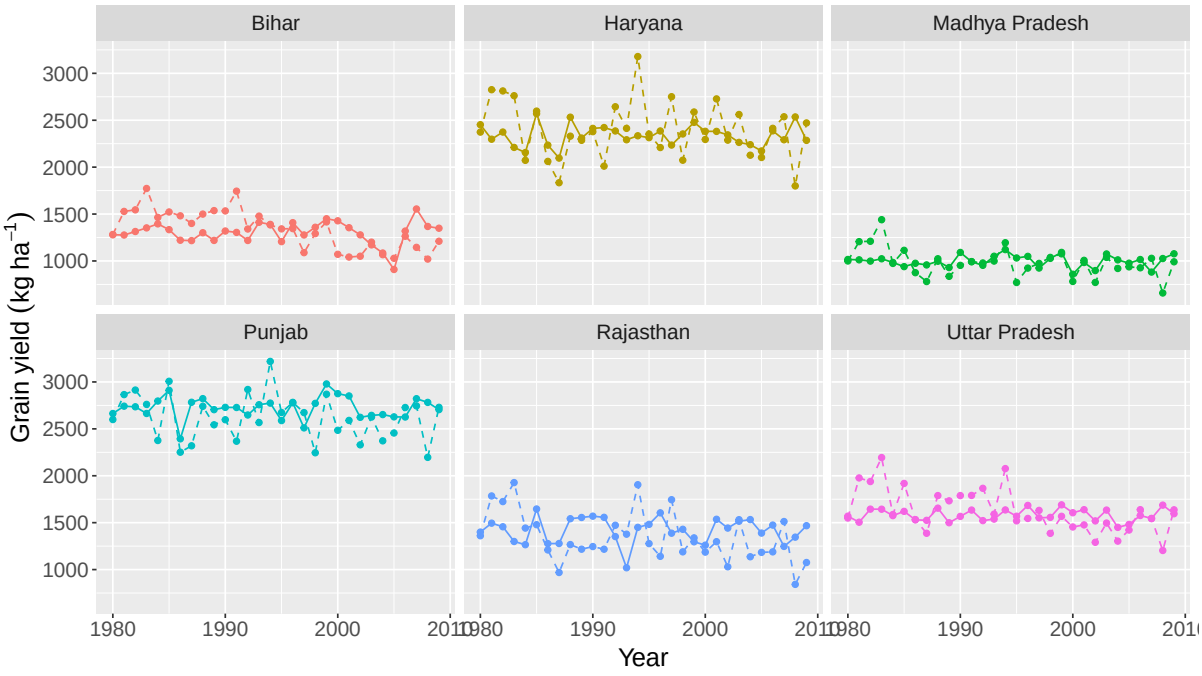

Figure C.1: Observed (solid lines) and simulated (GLAM-ROC; dashed lines) average wheat grain yields in the states of Bihar, Haryana, Madhya Pradesh, Punjab, Rajasthan and Uttar Pradesh during the growing seasons 1980 - 2009.

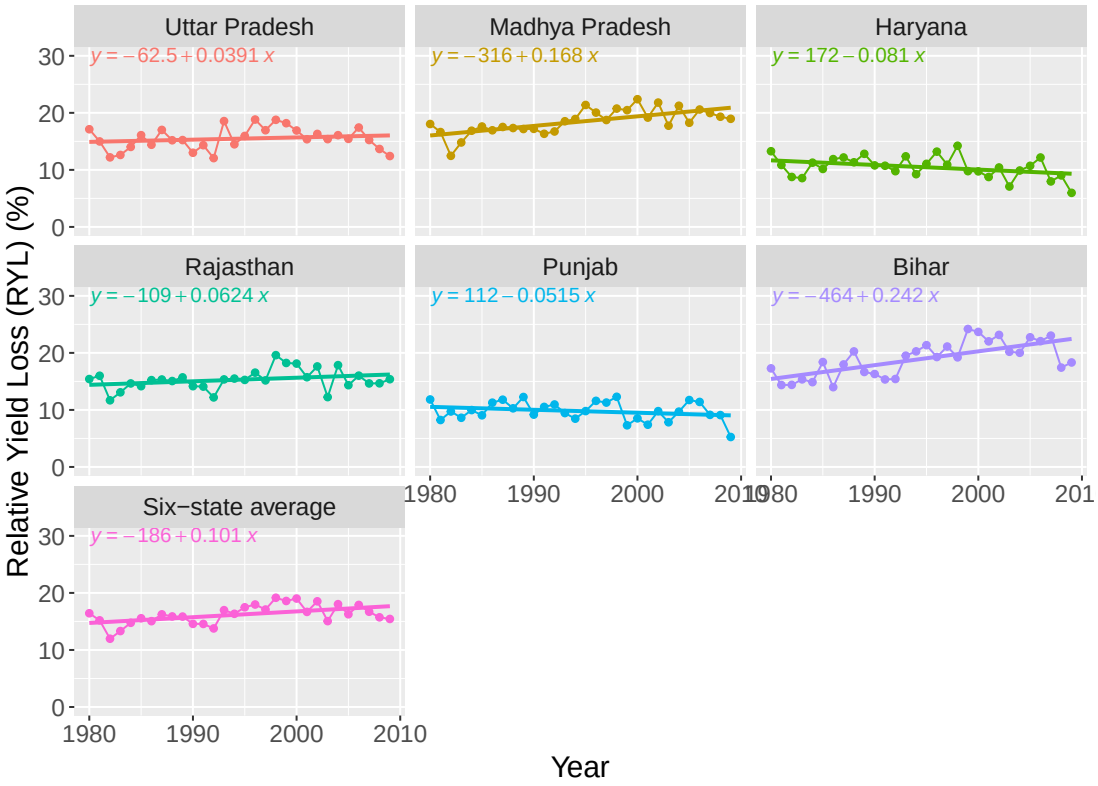

Figure C.2: Average wheat Relative Yield Loss (RYL) in the states of Bihar, Haryana, Madhya Pradesh, Punjab, Rajasthan and Uttar Pradesh as well as the six-state average during the growing seasons 1980 - 2009.

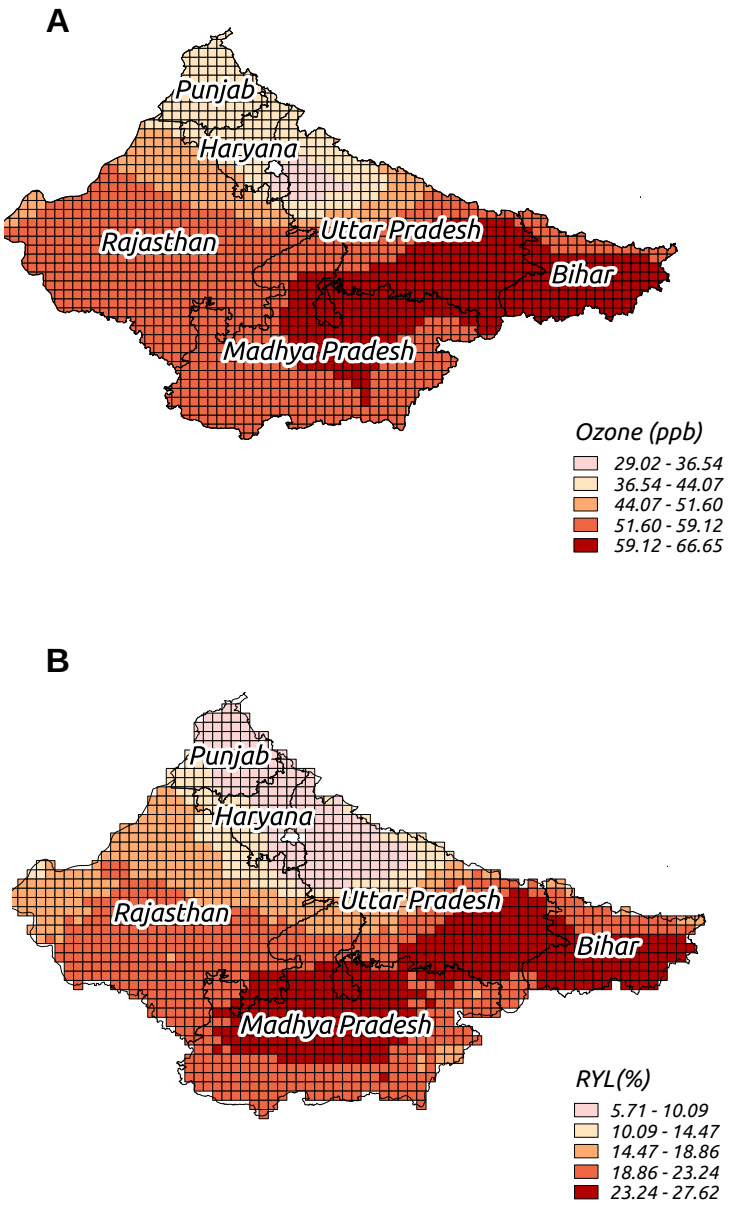

Figure C.3: A) 16-h mean ozone concentration for the November to April time period and B) Relative Yield Loss (RYL) in the states of Bihar, Haryana, Madhya Pradesh, Punjab, Rajasthan and Uttar Pradesh for the year 2000.

References

Christy, B., S. Tausz-Posch, M. Tausz, R. Richards, G. Rebetzke, A. Condon, T. McLean, G. Fitzgerald, M. Bourgault, and G. O'leary (2018), Benefits of increasing transpiration efficiency in wheat under elevated co 2 for rainfed regions, *Global change biology*, *24*(5), 1965–1977. C.1

Droutsas, I., A. Challinor, M. Swiderski, and M. A. Semenov (2019), New modelling technique for improving crop model performance-application to the glam model, *Environmental Modelling & Software*, *118*, 187–200. C.1

Moot, D., P. Jamieson, A. Henderson, M. Ford, and J. Porter (1996), Rate of change in harvest index during grain-filling of wheat, *The Journal of Agricultural Science*, *126*(4), 387–395. C.1